Defense Nuclear Agency
Alexandria, VA 22310-3398

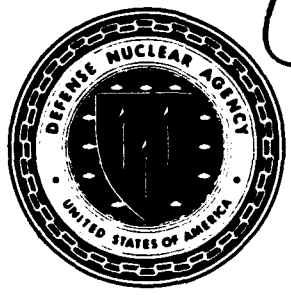

DNA-TR-91-89

Evaluation of In-Structure Shock Prediction Techniques for Buried RC Structures

Richard C. Dove
USAE Waterways Experiment Station
Structures Laboratory
3909 Halls Ferry Road
Vicksburg, MS 39180-6199

March 1992

Technical Report

CONTRACT No. DNA MIPR-90-600

Approved for public release; distribution is unlimited.

Destroy this report when it is no longer needed. Do not return to sender.

PLEASE NOTIFY THE DEFENSE NUCLEAR AGENCY, ATTN: CSTI, 6801 TELEGRAPH ROAD, ALEXANDRIA, VA 22310-3398, IF YOUR ADDRESS IS INCORRECT, IF YOU WISH IT DELETED FROM THE DISTRIBUTION LIST, OR IF THE ADDRESSEE IS NO LONGER EMPLOYED BY YOUR ORGANIZATION.

DISTRIBUTION LIST UPDATE

This mailer is provided to enable DNA to maintain current distribution lists for reports. We would appreciate your providing the requested information.

☐ Add the individual listed to your distribution list.

☐ Delete the cited organization/individual.

☐ Change of address.

NOTE:
Please return the mailing label from the document so that any additions, changes, corrections or deletions can be made more easily.

NAME: _____

ORGANIZATION: _____

OLD ADDRESS	CURRENT ADDRESS
_____	_____
_____	_____
_____	_____

TELEPHONE NUMBER: ( ) _____

SUBJECT AREA(s) OF INTEREST:

_____	_____
_____	_____
_____	_____

DNA OR OTHER GOVERNMENT CONTRACT NUMBER: _____

CERTIFICATION OF NEED-TO-KNOW BY GOVERNMENT SPONSOR (if other than DNA):

SPONSORING ORGANIZATION: _____

CONTRACTING OFFICER OR REPRESENTATIVE: _____

SIGNATURE: _____

CUT HERE AND RETURN

Director
Defense Nuclear Agency
ATTN: TITL
Washington, DC 20305-1000

Director
Defense Nuclear Agency
ATTN: TITL
Washington, DC 20305-1000

REPORT DOCUMENTATION PAGE

Form Approved OMB No. 0704-0188

1. AGENCY USE ONLY (Leave blank)	2. REPORT DATE	3. REPORT TYPE AND DATES COVERED
	920301	Technical 891001 – 910331

4. TITLE AND SUBTITLE
Evaluation of In-Structure Shock Prediction Techniques for Buried RC Structures

5. FUNDING NUMBERS
C - DNA MIPR-90-600

6. AUTHOR(S)
Richard C. Dove

7. PERFORMING ORGANIZATION NAME(S) AND ADDRESS(ES)
USAE Waterways Experiment Station
Structures Laboratory
3909 Halls Ferry Road
Vicksburg, MS 39180-6199

8. PERFORMING ORGANIZATION REPORT NUMBER
SL-91

9. SPONSORING/MONITORING AGENCY NAME(S) AND ADDRESS(ES)
Defense Nuclear Agency
6801 Telegraph Road
Alexandria, VA 22310-3398
SPSD/Giltrud

Headquarters
U.S. Army Corps of Engineers
20 Massachusetts Avenue, NW
Washington, DC 20314-1000

10. SPONSORING/MONITORING AGENCY REPORT NUMBER
DNA-TR-91-89

11. SUPPLEMENTARY NOTES
N/A

12a. DISTRIBUTION/AVAILABILITY STATEMENT
Approved for public release; distribution is unlimited.

12b. DISTRIBUTION CODE

13. ABSTRACT *(Maximum 200 words)*

A survey was conducted of available dynamic test data and current in-structure shock analysis techniques. Simplified semiempirical, single-degree-of-freedom, and two-dimensional (2-D) finite-element, in-structure shock analyses of buried reinforced concrete structures were conducted. Analysis results were compared to test data. An evaluation of the analysis techniques was completed, and a technique was selected for further development as an in-structure shock analysis tool.

The technique selected for further development, based on this evaluation, is the explicit 2-D finite-element program ISSV3. Extensive comparisons of the results of the in-structure shock analysis of the test configurations, using the available methods, show ISSV3 to be fast, accurate, and easy to use.

14. SUBJECT TERMS			15. NUMBER OF PAGES
Buried Structures	Finite Element Analysis	Shock Spectra	150
Dynamic Structures	Internal shock	Structure Response	16. PRICE CODE
Explosion Effects	Reinforced Concrete	Vibration	

17. SECURITY CLASSIFICATION OF REPORT	18. SECURITY CLASSIFICATION OF THIS PAGE	19. SECURITY CLASSIFICATION OF ABSTRACT	20. LIMITATION OF ABSTRACT
UNCLASSIFIED	UNCLASSIFIED	UNCLASSIFIED	SAR

CLASSIFIED BY:

N/A since Unclassified.

DECLASSIFY ON:

N/A since Unclassified.

PREFACE

The research reported herein was conducted under the joint sponsorship of the Defense Nuclear Agency, Task Code RS/RC, Work Unit 00224, and Headquarters, US Army Corps of Engineers, Project No. AT40, Work Unit HS-007.

The analysis contained herein was conducted at the US Army Engineer Waterways Experiment Station (WES) by members of the staff of the Structural Mechanics Division (SMD), Structures Laboratory (SL). This work was accomplished during the period October 1989 through March 1991 under the general supervision of Messrs. Bryant Mather, Chief, SL; and James T. Ballard, Assistant Chief, SL; and under the direct supervision of Dr. Jimmy P. Balsara, Chief, SMD. The Principal Investigator for this project and the author of this report was Mr. Richard C. Dove, SMD.

Acknowledgment is made to Drs. Jimmy P. Balsara and C. Dean Norman, SMD, SL, who provided guidance and constructive criticism throughout this study, and Ms. Pamela G. Hayes, SMD, for the provision of the CONWEB test data. Acknowledgment is also made of Mr. Scott D. Campbell, JAYCOR, Vicksburg, MS, for his assistance with the STABLE program, and Mr. Tom Slawson, ARA Inc., Southern Division, Vicksburg, for his assistance with the ISSV3 program.

COL Larry B. Fulton, EN, was the Commander and Director of WES during this study and the preparation of this report. Dr. Robert W. Whalin was Technical Director.

CONVERSION TABLE

Non-SI units of measurement used in this report can be converted to SI (metric) units as follows:

Multiply	By	To Obtain
degrees	0.01745	radians
cubic feet	0.02831685	cubic metres
inches	25.4	millimetres
feet	0.3048	metres
feet per second (fps)	0.3048	metres per second
inches per second (ips)	3.6576	metres per second
pounds (mass)	0.45359237	kilograms
pounds (mass) per cubic foot (pcf)	16.0179	kilograms per cubic metre
pounds (force) per square inch (psi)	0.006894757	megapascals
pounds (force) square seconds per inch	175.1265	kilograms
pounds (force) per inch	175.1265	newtons per metre

TABLE OF CONTENTS

TABLE OF CONTENTS (Continued)

LIST OF ILLUSTRATIONS

LIST OF TABLES

SECTION 1
INTRODUCTION

1.1 BACKGROUND.

The analysis of buried structures designed to resist blast loading is a continuing problem in the area of engineering mechanics. The complex structural dynamics of the problem, coupled with the uncertainties of soil structure interaction, make this a most difficult challenge. Even if the structure itself is designed to survive the expected dynamic loads, the shock environment inside may be severe enough to harm personnel or equipment. A thorough understanding of the expected shock environment is therefore needed to design ways to reduce this damage. The present simplified methods for the analysis of this type of problem are only directly applicable to very simple structures and are thought to yield very conservative results for more complex structures. As a result, large amounts of money are now being spent to mitigate shock levels which may be unrealistically high. This program of study was prompted by the hope that a relatively simple, fast, and accurate analysis procedure could be found, which will give realistic estimations of in-structure shock for complex buried reinforced concrete structures.

1.2 OBJECTIVE.

The objective of this study was to conduct and evaluate in-structure shock calculations for buried reinforced concrete structures under dynamic loads from buried conventional explosives. Of primary importance was the evaluation of two-dimensional (2-D) finite-element analysis techniques applied to this complex three-dimensional problem. Two personal computer (PC) based, 2-D finite-element programs, were evaluated for application to this problem.

1.3 SCOPE.

This study included simplified semi-empirical, single-degree-of-freedom (SDOF), and 2-D finite-element, in-structure shock analyses of buried reinforced concrete structures. A literature search was conducted to obtain available data to assist in the evaluation of these calculations.

The project began with an analysis of the existing data base of in-structure shock tests. A recent series of four dynamic tests conducted by the

US Army Engineer Waterways Experiment Station (WES), Structures Laboratory, Structural Mechanics Division, were selected as having the best data currently available [1]. In-structure shock calculations were performed to model these tests, using current simplified techniques. Results were compared to the test data. Two (2-D) finite-element analysis programs were selected as possible in-structure shock calculation tools. These programs were also used to conduct several analyses of the test series. These results were also compared to the test data and to the simplified analysis results.

There were three simplified analysis techniques used in this study. The first was the semi-empirical in-structure shock calculation procedures outlined in the US Army TM5 855-1 [2]. This technique yields average in-structure shock motions for the entire structure. An SDOF analysis of the wall closest to the explosion using the US Army Engineer Wall Analysis Code (WAC) [3] was the second simplified technique examined. In this analysis the mass and the resistance of the wall was replaced by an equivalent SDOF system and the in-structure shock motions of the wall were calculated. The third simplified technique was an SDOF analysis, in which the mass of the entire structure was lumped together at a point and the soil behind it replaced by a simple spring. This rigid-body SDOF analysis gave the overall motions of the structure as a whole. These SDOF analyses were done on PC-based programs developed at WES.

The 2-D finite-element analyses were accomplished using two PC-based beam element finite-element analysis programs, STABLE and ISSV3. STABLE is an implicit finite-element program for the dynamic analysis of frames subjected to blast and ground shock loadings [4]. This program is in the public domain and was written by JAYCOR, Vicksburg, MS, for the US Army Engineer District, Omaha. ISSV3 is a 2-D lumped parameter model, explicit, nonlinear, finite-element code written by Applied Research Associates, Southern Division, Vicksburg, MS [5]. This program was written for WES in conjunction with this project under the direction of the author, and is also in the public domain. The process of modeling this problem necessitated the inclusion of structure-media interaction (SMI) for the development of loads for the structural analysis. The development of this SMI load was carefully evaluated. Data analysis included the examination of soil pressure, deflection, velocity, and acceleration data and the generation of shock spectra.

1.4 INTRODUCTORY CONCEPTS.

The shock environment inside of a dynamically loaded structure is a complex phenomenon. The amplitude, shape, and duration of the acceleration, velocity, and deflection-time histories greatly influence the response of internal systems that may be damaged by the shock environment. To simplify the design and analysis of internal systems against in-structure shock, a shock spectrum is generated to characterize the shock environment inside the structure. A shock spectrum is a plot of the maximum response of an SDOF system in which the base is driven by the in-structure shock environment. As can be seen in Figure 1 the response of an SDOF system is dependent on the natural frequency of the system determined by the mass and spring stiffness, the damping ratio, and the motion driving the system. Given the motion and damping parameters the maximum response is calculated by means of the Duhamel integral [6] for a range of natural frequencies, and a shock spectra generated. For many shock spectra the natural frequency of the SDOF system is on the abscissa, while on the ordinate the maximum response, such as peak spectral acceleration, pseudo-velocity, or relative displacement, appears. Peak spectral acceleration and pseudo-velocity are terms that closely approximate the actual acceleration and velocity of the SDOF system while the relative displacement is the actual value. Thus, for a given internal system, such as a piece of equipment, all that is needed to define its maximum response to a shock environment is the natural frequency of the piece of equipment. All the shock spectra generated in the analysis in this study assumed no damping.

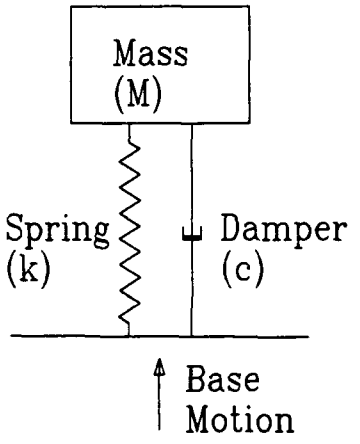

Figure 1. Single-Degree-of-Freedom System.

The shock spectra, which were generated in this study, are a little more complex in that they are plotted on tripartite paper. There are simple direct relationships between the maximum spectral acceleration, pseudo-velocity, and relative displacement that allow these quantities to appear on the same plot.

The log of the natural frequency of the SDOF system appears on the abscissa of these plots. There are three ordinates, one measuring the log of pseudo-velocity on the left scale, the second the log of the relative displacement on a scale at 45 degrees from the vertical measuring from the lower right corner to the upper left corner, and the third, also at 45 degrees from the vertical, measuring the log of the spectral acceleration from the lower left corner to the upper right corner. Numerous examples of shock spectra can be found throughout this report. At times in the report spectral acceleration and pseudo-velocity are referred to simply as acceleration and velocity. The prefix is implied whenever shock spectra are being discussed.

In discussing shock spectra, reference is sometimes made to the constant deflection, velocity or acceleration portion of the plot. In the low frequencies, the shock spectra of most SDOF systems tend to follow the deflection scale progressing at a 45 degree angle upward to the right, in the intermediate frequency region the curves tend to be horizontal with a constant velocity, while in higher frequencies the curve follows the acceleration scale downward to the right. These characteristics are often used to generate approximate shock spectra with straight lines for each portion of the graph. Shock spectra are covered well in the references [6], [7], and [8] and these are good references for anyone interested in exploring the subject to greater depth.

Before going into calculation of in-structure shock and hence shock spectra, the important concept of Hopkinson or cube-root scaling should be introduced. Most parameters in the field of explosion effects are presented as scaled by the cube root of the explosive weight. This scaling relates blast properties from an explosion of one energy level to that of an explosion of a second energy level. The energy is directly related to the weight of the explosive. This method is widely covered in the literature [9]. The distance from a bomb is scaled by dividing by the cube root of the explosive weight (TNT equivalent). Such a scaled distance is often referred to as Lambda. For a given Lambda, a similar blast environment will result from different explosive weights. Pressures and velocities will be identical, and time and impulse are scaled by the cube root of the explosive weight. Thus, when a parameter is given in a scaled form, it can be applied to any explosive charge size simply by multiplying by the cube root of the charge weight. For this

reason, most such parameters are given in the scaled form. The application of cube-root scaling was used throughout this analysis in the development of free-field loads.

SECTION 2
RELATED TEST DATA

2.1 LITERATURE SEARCH.

An extensive literature search was conducted to obtain available data to assist in the evaluation of in-structure shock calculations. It was obvious that much of the data available on the subject of dynamic response of buried concrete structures were not directly applicable to this effort. Most of the tests focused on plane wave type loadings and were also largely concerned with structural response, not in-structure shock response. Also, most of the data was in some way restricted from open publication. There was one notable exception, a series of well-controlled tests were conducted that included in-structure shock response of buried concrete structures to conventional explosive loadings which has been published in the open literature. This exception was the CONWEB test series.

2.2 CONWEB TEST SERIES.

The US Army Engineer Waterways Experiment Station conducted the CONWEB tests, a series of four backfill effects tests during the period of March through May 1989. The test procedures are covered extensively by Hayes [1] and [10]. The analyses contained in these two references were focused solely on the effects of backfill variation and structure media interaction on the structural response of a buried test wall. In the course of this test series, a large amount of structural acceleration data was recorded. These data, along with records of free-field acceleration, free-field soil stress, and interface stress, present a golden opportunity for the evaluation of in-structure shock calculation techniques. For this reason, this test series was selected as the primary focus of the in-structure shock analyses contained in this report. The following is a brief description of the CONWEB test series.

The four tests in the CONWEB test series were conducted to determine the response of buried reinforced concrete walls to localized dynamic loads in various backfill materials (Table 1). The first two tests were conducted in a clay backfill with two different test walls, the second test having a stiffer test wall than the first. This clay was characterized by a low shear strength and a low seismic velocity. The third test was conducted with a flexible wall

Table 1. CONWEB backfill soil properties.

Test	Unit Weight (γ) lb/ft^3	Seismic Velocity (c) ft/sec	Attenuation Coefficient (n or η)
CONWEB 1	122.5	1100	2.125
CONWEB 2	123.7	1100	2.125
CONWEB 3	116.4	1000	3.000
CONWEB 4	120	3000	1.500

in a sand backfill with a high shear strength and low seismic velocity. The fourth test was conducted with a flexible wall in a clay backfill with low shear strength and a high seismic velocity. Figure 2 through Figure 5 show the test structure, backfill properties, and the properties of the surrounding in-situ soil for each of the four tests. Table 1 shows the backfill properties which were used for all the analyses in this investigation.

The source of the localized dynamic loads in each of these tests was a cylindrical explosive charge. This charge contained 15.4 pounds of C4 explosives in a closed steel case 27 inches long with an inside diameter of 3.548 inches and a thickness of 0.166 inch. The charge was oriented vertically in CONWEB 1, 3, and 4, and horizontally in CONWEB 2.

Table 2. CONWEB structural material properties.

Test Component	f'_c (psi)	Steel Yield (psi)
CONWEB 1 Test Wall	6095	67424
CONWEB 2 Test Wall	6398	67424
CONWEB 3 CONWEB 4 Test Walls	5855	67424
Reaction Structure	6398	67424

The test article consisted of a reusable reaction structure supporting the test wall. The test wall was bolted to the heavily reinforced concrete reaction structure, forming a relatively rigid joint. Dimensions and gage layout of the reaction structure are shown in Figure 6. Test walls for CONWEB 1, 3, and 4 had a length-to-thickness

(L/t) ratio of 10 while the L/t ratio of the wall in CONWEB 2 was 5. The designs of the test walls are shown in Figure 7 and Figure 8, and the test wall gage layout is shown in Figure 9. Material properties are presented in Table 2.

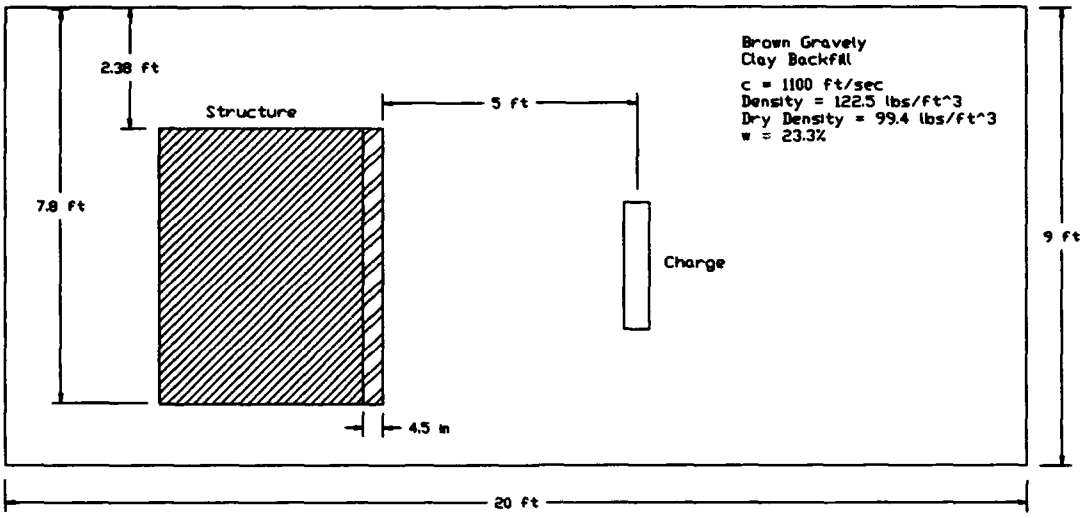

Figure 2. Section through CONWEB 1 test bed, showing backfill properties.

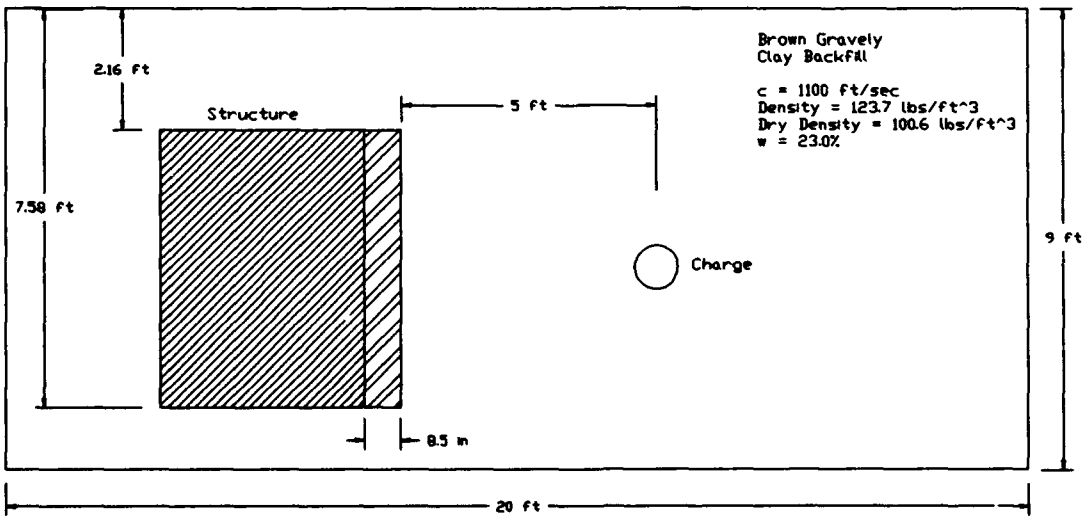

Figure 3. Section through CONWEB 2 test bed, showing backfill properties.

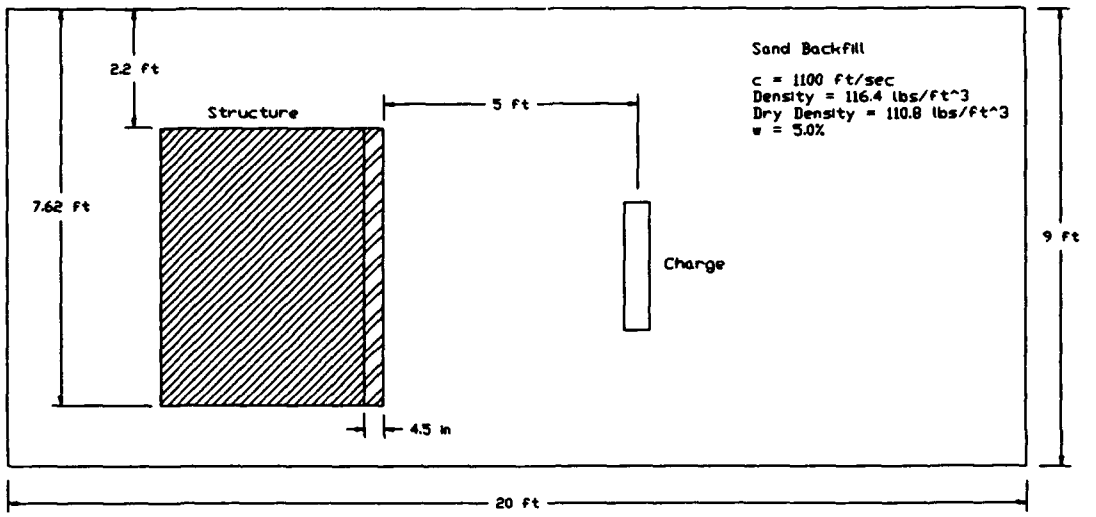

Figure 4. Section through CONWEB 3 test bed, showing backfill properties.

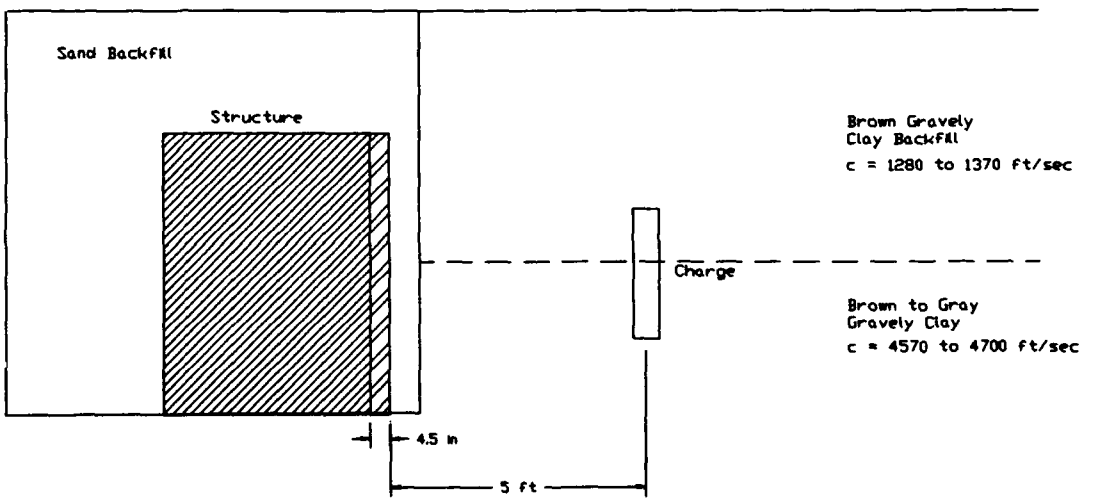

Figure 5. Section through CONWEB 4 test bed, showing in-situ soil properties.

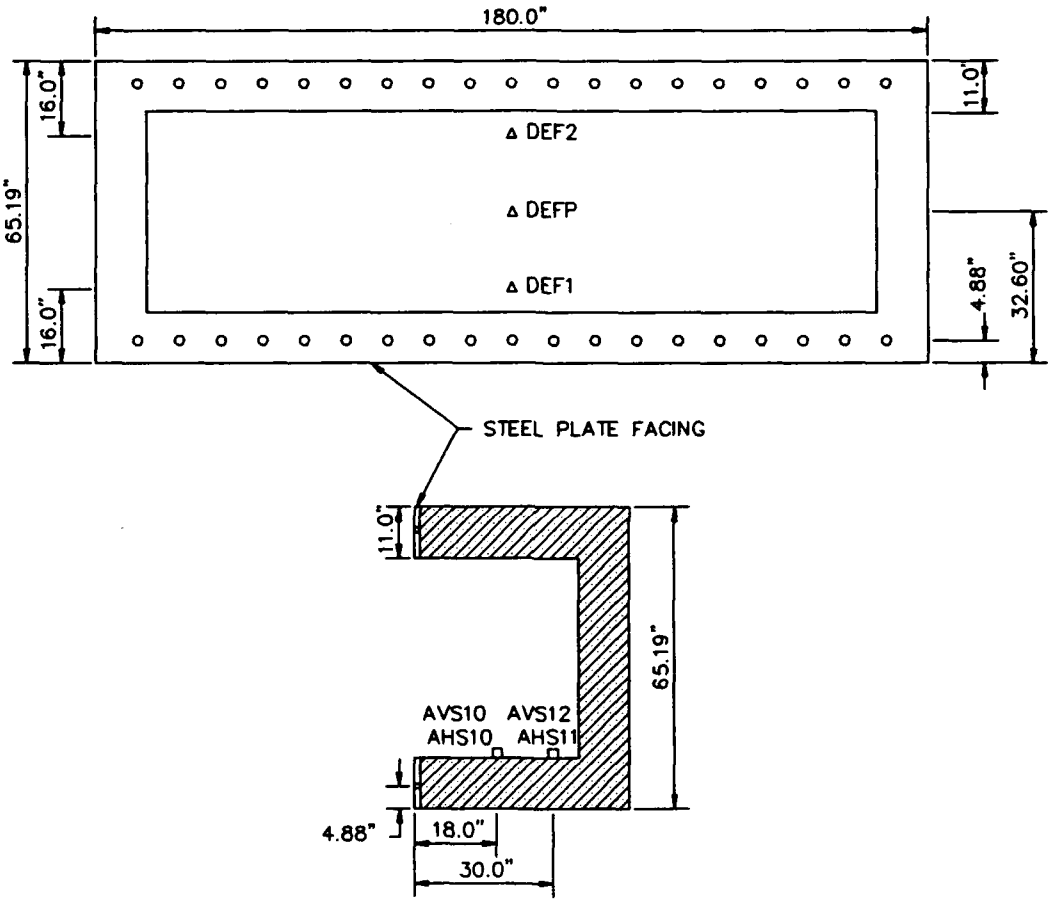

Figure 6. Reaction structure dimensions and gage layout.

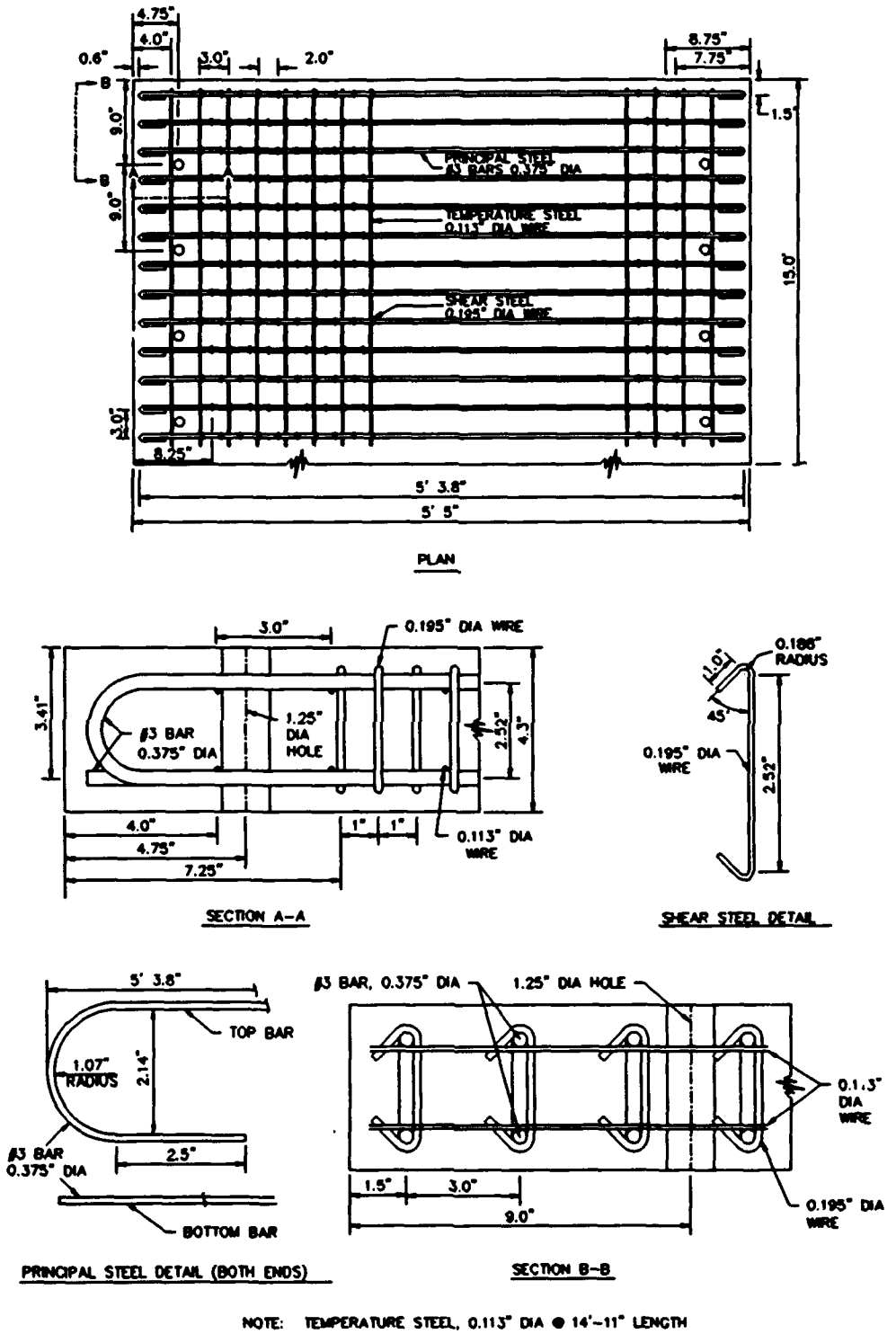

Figure 7. CONWEB 1, 3, and 4 test wall design.

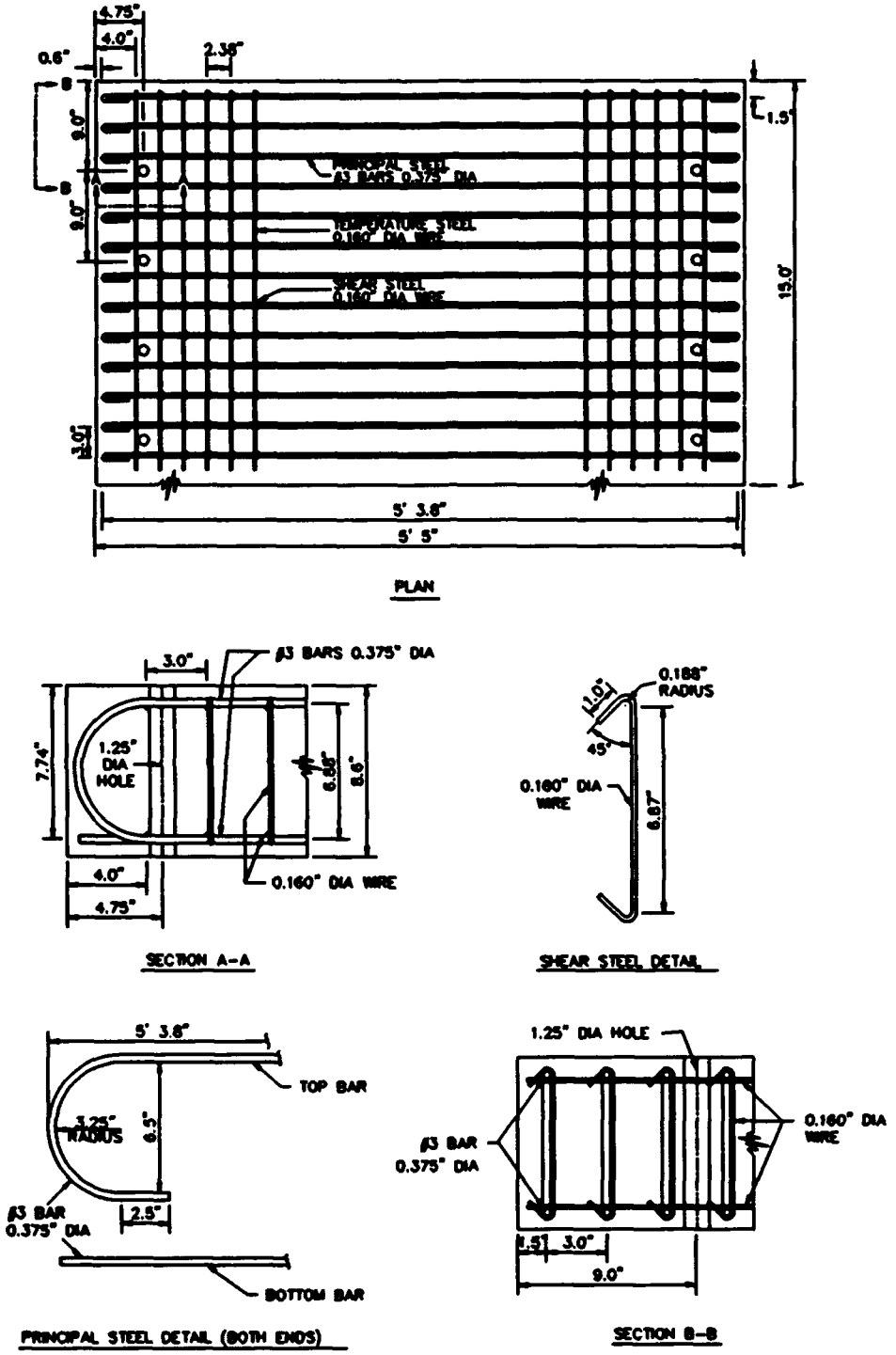

Figure 8. CONWEB 2, test wall design.

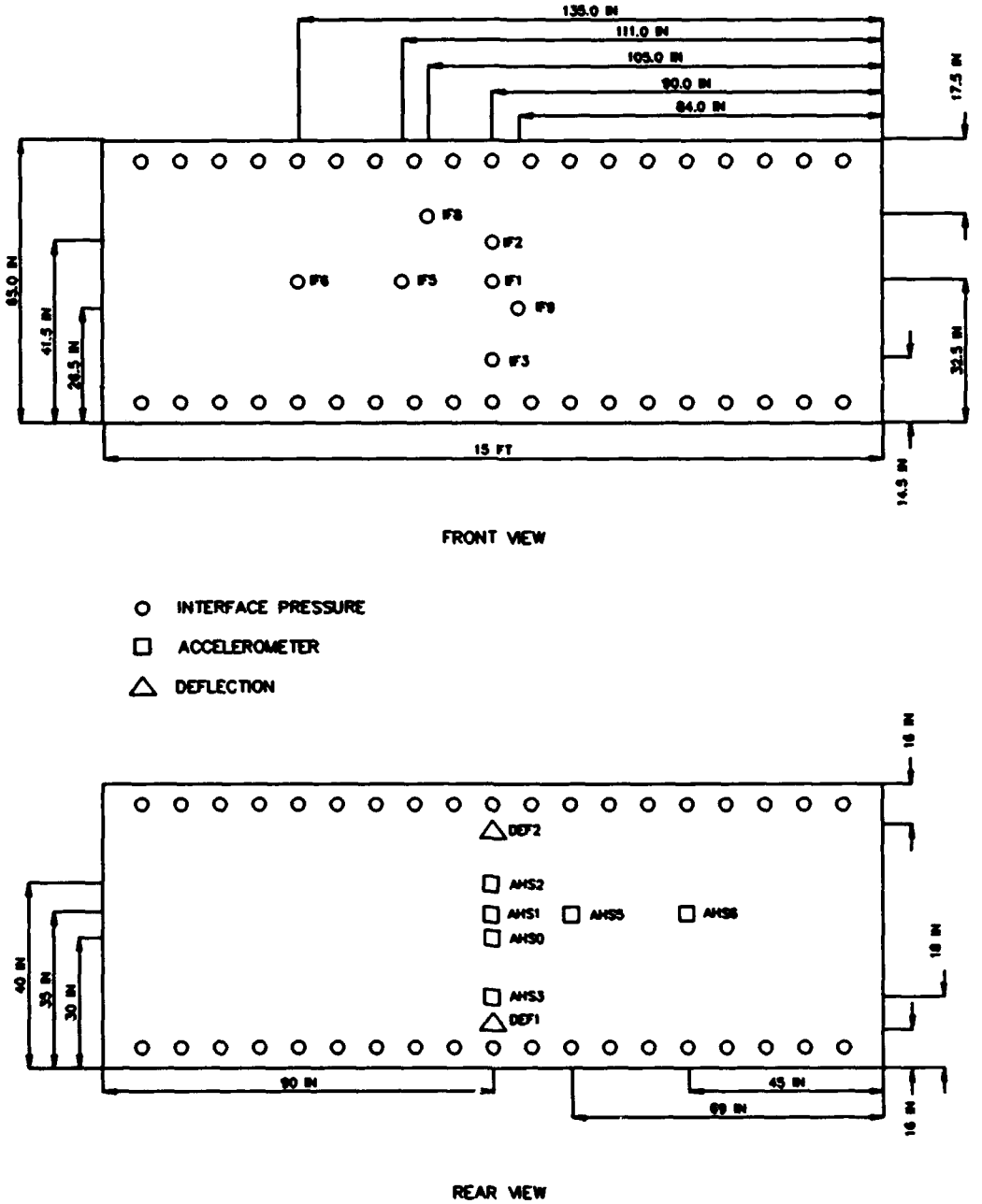

Figure 9. CONWEB test wall instrumentation.

SECTION 3
SIMPLIFIED ANALYSIS TECHNIQUES

3.1 TM5 855-1 IN-STRUCTURE SHOCK PROCEDURE.

A current method for the calculation of in-structure shock is the semi-empirical procedure in the Army Technical Manual (TM) 5 855-1 [2]. The procedure begins with the calculation of the average free-field accelerations, velocities, and deflections. Correction factors are then applied to convert these free-field values to in-structure shock values. The following is a brief explanation of the method. Later, the procedure will be applied to the CONWEB test series.

The most important parameters controlling the free-field motion are: the source of the ground shock, the mechanical properties of the free-field, and the range (distance) to the point of interest. The source of the ground shock is determined by the size and depth of burial of the bomb.

There are many types of explosives used in bombs, each having very different characteristics. In order to simplify analysis, the weight of explosive is converted to an equivalent TNT weight using equivalency factors. Unfortunately, these conversion factors were originally generated for free air (above ground) explosions and in low pressure ranges. Application of these factors to belowground explosions is therefore open to criticism. This is, however, common practice and is the best available approach.

After conversion to an equivalent TNT charge weight, the affect of depth of burial must also be taken into account. It is obvious that a bomb, which is barely penetrating into the soil, will not be as effective in transmitting energy into ground shock as would a bomb that is fully buried. A ground shock coupling factor is used to account for this phenomenon. This single factor is applied to all ground shock parameters and is simply the ratio of the shallower buried bomb's parameters to that of a fully buried bomb, as shown in Equation (1). The shock parameters in question are: pressure (P), velocity (V), deflection (d), impulse (I), and acceleration (a).

$$f = \frac{(P, V, d, I, a)\ near\ surface}{(P, V, d, I, a)\ contained} \qquad (1)$$

The propagation of shock through soil is a complex problem, dependent on a large number of variables. At the present time, the TM5 855-1 procedure for the calculation of free-field motions contains only two explicit variables for the characterization of the soil. These variables are the seismic velocity (c) and the attenuation coefficient (n). Seismic velocity, c, is used as an index of soil properties for ground shock prediction, providing an indication of the soil stiffness (M) and mass density (ρ), as shown in Equation (2). The

$$c=\sqrt{\frac{M}{\rho}} \tag{2}$$

value of c is also strongly dependent on the degree of saturation of a cohesive soil. In general, the higher the value of c, the better the soil is at transmitting shock. The reverse is true for the attenuation coefficient, n, which is a measure of the energy used in the irreversible crushing of the soil voids. A high value of n indicates a soil that will quickly attenuate a shock with distance. The characterization of a soil with only two parameters is an extreme simplification and should be used with great caution.

$$aW^{\frac{1}{3}}=50fc\left(\frac{R}{W^{\frac{1}{3}}}\right)^{(-n-1)} \tag{3}$$

$$V=160f\left(\frac{R}{W^{\frac{1}{3}}}\right)^{-n} \tag{4}$$

$$\frac{d}{W^{\frac{1}{3}}}=500\frac{f}{c}\left(\frac{R}{W^{\frac{1}{3}}}\right)^{(-n+1)} \tag{5}$$

The final parameter used in the TM5 855-1 procedure for the calculation of free-field motion is the range (R) or distance of the bomb from the point of interest. As would be expected, ground shock and free-field motions decrease with increasing range. The free-field peak acceleration (a) in g's, peak particle velocity (V) in ft/sec, and peak displacement (d) in feet can now be calculated using Equations (3), (4) and (5). The weapon yield (W) is in pounds TNT equivalent, coupling factor (f) and attenuation coefficient (n)

as defined above, seismic velocity (c) in ft/sec, and range (R) in feet. Note that Hopkinson's, cube-root scaling was used extensively in the development of these equations.

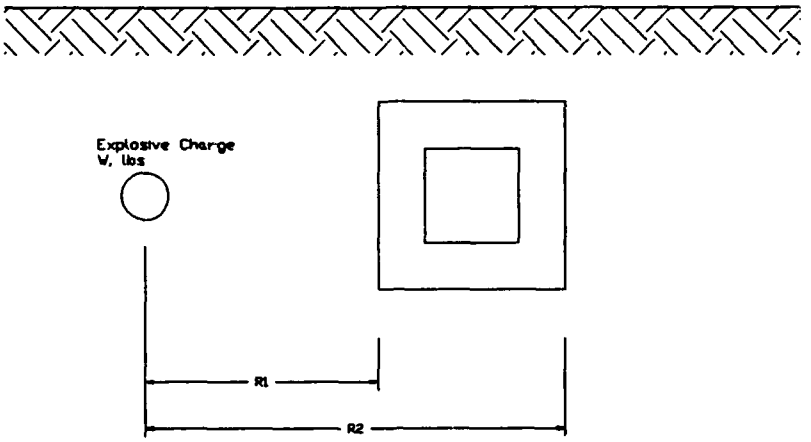

Figure 10. Average free-field motion configuration for side burst load case.

This brings us now to the actual calculation of in-structure shock. Figure 10 shows the general configuration of the side burst loading of a rectangular structure. The two ranges, R_1 and R_2, are the distance in feet from the front and the back of the structure, respectively. These two ranges, along with the parameters discussed above, are all that is required for the calculation of the average acceleration across the structure. Equations (6), (7), and (8) are used to calculate the average acceleration, velocity, and deflection across the structure. These equations were developed by integrating the acceleration-range relationship in Equation (3) across the structure and finding a uniform acceleration that yields the same integral across this range.

$$A_{avg}W^{\frac{1}{3}} = \frac{50fcW^{\frac{(n+1)}{3}}(R_1^{-n}-R_2^{-n})}{n(R_2-R_1)} \qquad (6)$$

$$V_{avg} = \frac{160 f W^{\left(\frac{n}{3}\right)} \left(R_1^{-n+1} - R_2^{-n+1}\right)}{(n-1)(R_2 - R_1)} \tag{7}$$

$$\frac{d_{avg}}{W^{\frac{1}{3}}} = \frac{500 f W^{\frac{(n-1)}{3}} \left(R_1^{-n+2} - R_2^{-n+2}\right)}{c(n-2)(R_2 - R_1)} \tag{8}$$

Given the average free-field motions calculated above, the next step is to modify these values, applying empirical factors to produce an approximation of in-structure shock motions. A reduction factor (RF) is calculated based on the geometry of the structure, wall height or width, structure length, and range. A nomograph is used to find this empirical relationship. This reduction factor is applied to accelerations and velocities. These values are taken as an approximation of the accelerations, velocities, and deflections, which would be measured inside the structure during an event under these conditions.

The final step in the TM5-855-1 in-structure shock analysis procedure is the generation of a shock spectrum. As discussed above, a shock spectrum is a very useful tool for the analysis of the dynamic response of equipment and other subsystems inside a structure. Generation of shock spectrum is simply a matter of multiplying the above in-structure motions by empirical amplification factors. These factors are 1.2, 1.5, and 1.6 for displacement, velocity, and accelerations, respectively. Response values are plotted on the tripartite shock spectrum curves as the maximum relative displacement, maximum pseudovelocity, and maximum acceleration. These shock spectra can be directly compared to information on the response of equipment inside the structure. Equipment response is often presented as a shock spectrum which gives recommended limits on equipment motion. Overlaying the structural shock spectrum on these equipment fragility curves allows an estimate of expected damage and the need for shock isolation.

3.2 TM5 855-1 CONWEB CALCULATIONS.

Table 3 shows the values used for the calculation of average free-field motions for CONWEB tests 1, 2, 3, and 4. These values were input into Equations (6), (7), and (8). Table 4 shows the average in-structure motions

Table 3. CONWEB TM5 855-1 free-field response parameters.

Test	W lbs,	f	n	c ft/sec	R_1 ft	R_2 ft	RF
CONWEB 1	19.71	1.0	2.125	1100	5.0	9.717	.48
CONWEB 2	19.71	1.0	2.25	1000	5.0	9.717	.48
CONWEB 3	19.17	1.0	3.0	1000	5.0	9.717	.48
CONWEB 4	19.71	1.0	1.5	3000	5.0	9.717	.48

and spectral values for each test. The shock spectrum values are shown plotted against shock spectra generated from test data in Figure 11, Figure 12, Figure 13, and Figure 14.

The TM5 855-1 procedure yielded very good results for CONWEB 1 and 2 and

Table 4. CONWEB TM5 855-1 average in-structure response and spectral values.

Test	A g	V in./sec	D in.	1.6A g	1.5V in./sec	1.2D in.
CONWEB 1	539	114	4.98	862	170.0	5.98
CONWEB 2	439	110	1.80	702	166	2.16
CONWEB 3	614	110	1.29	983	166	1.54
CONWEB 4	2549	219	3.32	4078	328	3.98

gave a conservative estimate of response for CONWEB 3. The relatively good results of these calculations are not surprising, as the procedure was developed from tests on simple box structures similar to the CONWEB test articles. Figure 14 shows that CONWEB 4 was underpredicted according to gage ASH10 and overpredicted for gage ASH11. If gage ASH10 is correct and CONWEB 4 was underpredicted, this could demonstrate a problem often seen in dynamic structural analysis, the problem of calculating the response of structures in high seismic velocity clay. However, another explanation could be the

variability in the testing itself. CONWEB 4 was an in-situ test in which the soil was excavated and the structure was placed in the excavation. Difficulty was encountered in assuring a proper placement of backfill around the structure to fill the gap between the structure and the in-situ soil. There was also uncertainty in the level of the ground water table in this test. Both of these variables could drastically affect the response of the structure. Improper backfill would allow unrestrained motion of the structure, and the presence of water could greatly increase the dynamic load. Gage failure may be a better explanation of the apparent underprediction. If gage ASH11 is correct, the TM5 855-1 gave a conservative estimate of horizontal in-structure shock.

The semi-empirical calculational procedure in TM5 855-1 has now been demonstrated to be capable of giving a reasonable estimate of the in-structure shock response of the first three CONWEB tests. Inconsistences in the CONWEB 4 test results made it difficult to evaluate the analysis results for this test. The test was underpredicted when compared to one gage, while the analysis gave reasonable results when compared to another gage at almost the same location. This test may have been overloaded and/or underrestrained due to testing problems or to have had gage problems.

The greatest weakness of this procedure is that it is an empirical method developed for simple box-like structures. The assumptions that must be made to apply this procedure to more complicated structures have not been thoroughly evaluated. Great caution should be used in the application of such an empirically derived method to situations outside of those actually tested.

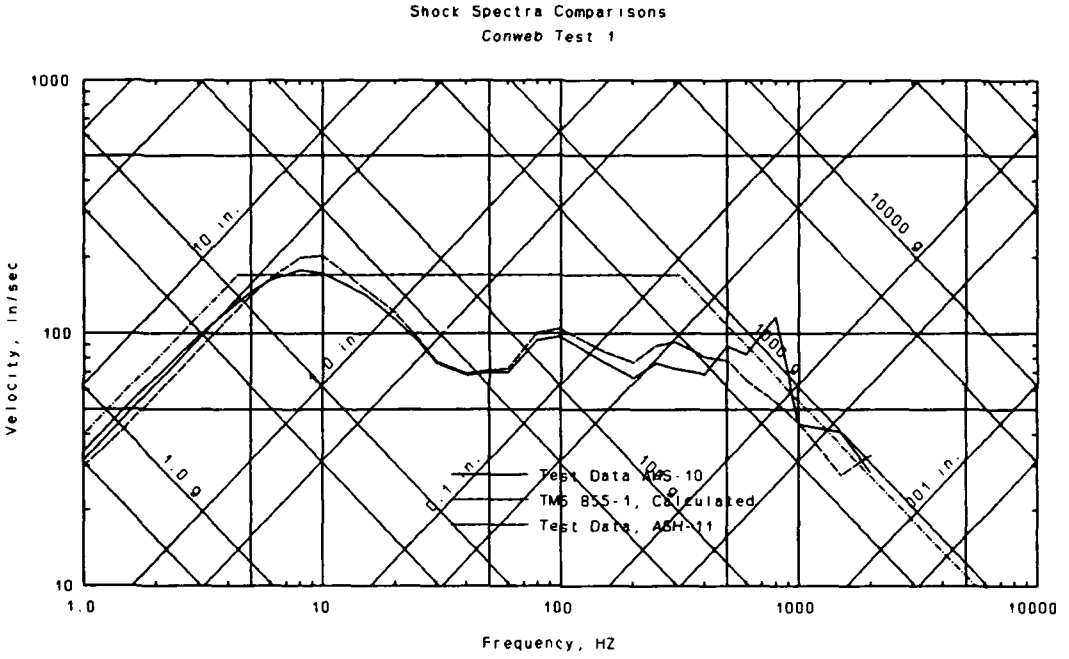

Figure 11. CONWEB 1, TM5 855-1 generated shock spectrum vs. test data.

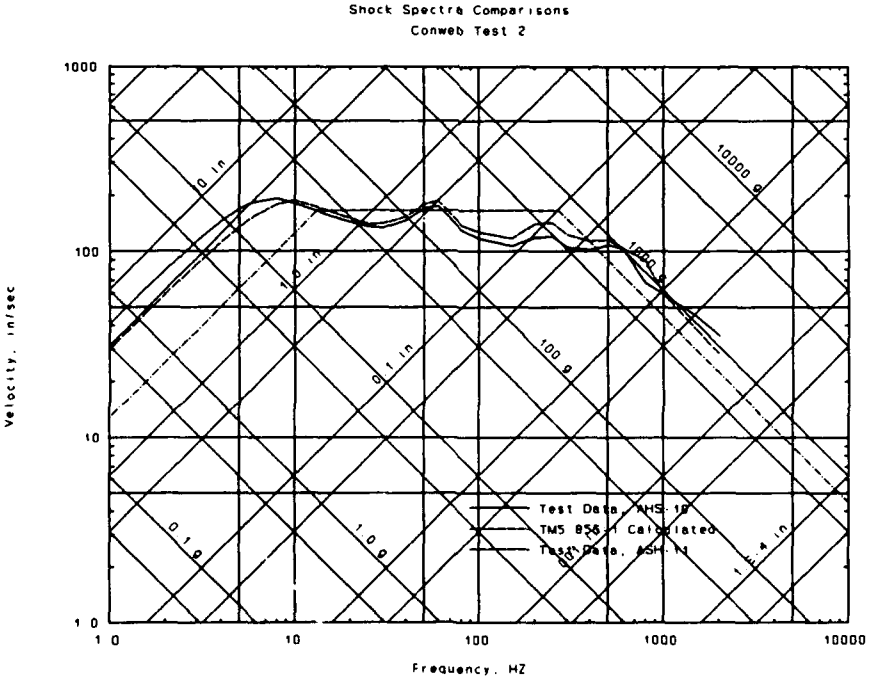

Figure 12. CONWEB 2, TM5 855-1 generated shock spectrum vs. test data.

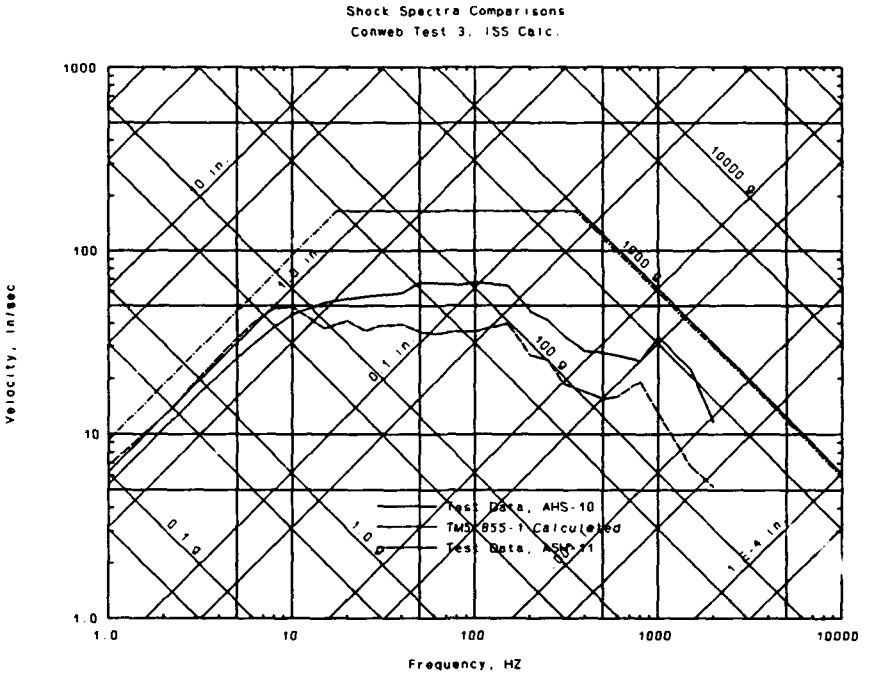

Figure 13. CONWEB 3, TM5 855-1 generated shock spectrum vs. test data.

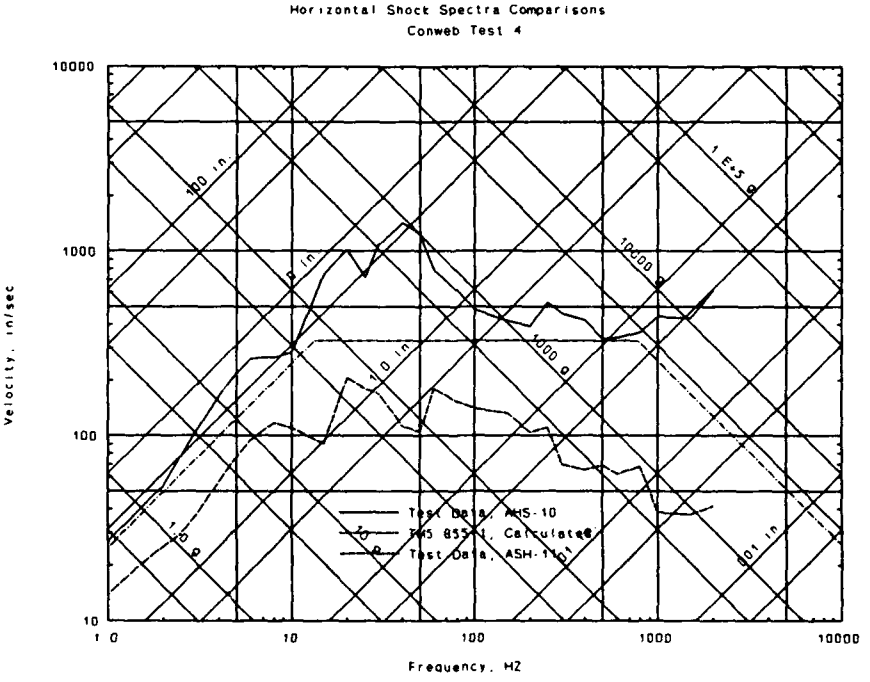

Figure 14. CONWEB 4, TM5 855-1 generated shock spectrum vs. test data.

3.3 SDOF ANALYSES.

The single-degree-of-freedom (SDOF) analysis is the second simplified method examined for in-structure shock calculations. This method consists of the reduction of the problem to a simple spring, mass, and damper system. Application of this type of analysis is widely covered in the literature [1], [7]. In an SDOF model, the spring is a resistance element which models the static resistance of the structural element of interest. The mass and damper are selected so that the resulting system will have the same frequency and damping characteristics as the prototype structure.

The SDOF analysis procedure was used to model the CONWEB tests in two ways, the wall facing the bomb was analyzed as one SDOF system, and the horizontal rigid-body motion of the entire structure was modeled in a second decoupled SDOF analysis. Output from the wall analysis was compared to data from gages on the wall, while the rigid-body analysis results were compared to data from internal gages on the floor. This ignores the contribution of the rigid-body motion to the response of the wall. Since the peak wall response occurs well before the peak rigid-body response, neglecting of the rigid-body contribution is thought to be a reasonable assumption.

3.3.1 FRONT WALL SDOF ANALYSIS.

The front wall SDOF analysis was carried out using the Corps of Engineers PC-based Wall Analysis Code (WAC) [3]. WAC uses the procedures in TM5 855-1 to develop the load mass factors for a given wall. Multilinear resistance functions are computed based on yield-line theory. The resistance functions for the test walls in the CONWEB tests are shown in Figure 15. Note that the calculated resistance functions were the same for CONWEB 1, 3, and 4, as the wall designs were the same for these tests, and the same material properties were used.

The wall loading used, was a modification of the free-field stresses calculated by the procedures in TM5 855-1 [2]. The soil properties used are shown in Table 1 (in chapter II of this report). Free-field stresses were modified by applying a reflected pressure factor of 1.5 to the beginning of the pressure-time history. This models the buildup of reflected pressure on the structure before a tensile relief wave can arrive from the edge of the structure, or before wall movement can relieve the stress. According to TM5

855-1 the duration of this reflected pressure for these tests should be taken as six wave transit times through the thickness of the wall, 0.2 msec in CONWEB 1, and 0.4 msec in CONWEB 2, 3, and 4. Applying this reflected pressure-time history over the entire surface of the test wall is overly conservative, due to the nonuniform nature of conventional explosive loadings. The entire pressure-time history was reduced by applying a uniform load factor of 0.71 as per TM5 855-1, calculated based on the aspect ratio of the wall and the weapon range. The final pressure-time histories used in the analysis are shown in Figure 16 through Figure 19.

Peak deflections, velocities, and accelerations resulting from the wall

Table 5. Peak response output from SDOF wall analysis.

Test	Deflection (in.)	Velocity (in./sec)	Acceleration (g)
CONWEB 1	60	3050	2095
CONWEB 2	7.1	828	874.0
CONWEB 3	0.68	187	443.2
CONWEB 4	25	2310	3391

SDOF analysis are shown in Table 5. As in the TM5 855-1 analysis above, a factor of 1.2, 1.5, and 1.6 was applied to the peak deflection, velocity, and acceleration respectively to create shock spectrum values. The shock spectra generated are shown in Figure 20 through Figure 23. The SDOF procedure overpredicted the peak deflection and velocity portions of the shock spectra and correctly predicted the acceleration portion for CONWEB 1. CONWEB 2 results show a very reasonable comparison to test data, while the CONWEB 3 analysis shows an underprediction of the spectral values. CONWEB 4 was reasonably well predicted for all three parts of the spectrum.

The results of the wall SDOF analysis are relatively inconsistent and reflect a problem often encountered in this type of work; that is, the difficulty of developing reasonable loads to apply to the SDOF model. In work by Hayes [1], in which a similar SDOF structural analysis of the CONWEB test

walls gave similar anomalous results, a major conclusion was that seismic velocity alone is not sufficient to characterize a given backfill material. The loads generated by the TM5 855-1 procedures, which were used here, are very dependent on seismic velocity. Also, it is thought that the TM5 855-1 procedures do not adequately model structure-media interaction; that is, the reflection of the load at the soil-structure interface and the relative movement of the soil and the structure. There is current research at WES to address these deficiencies.

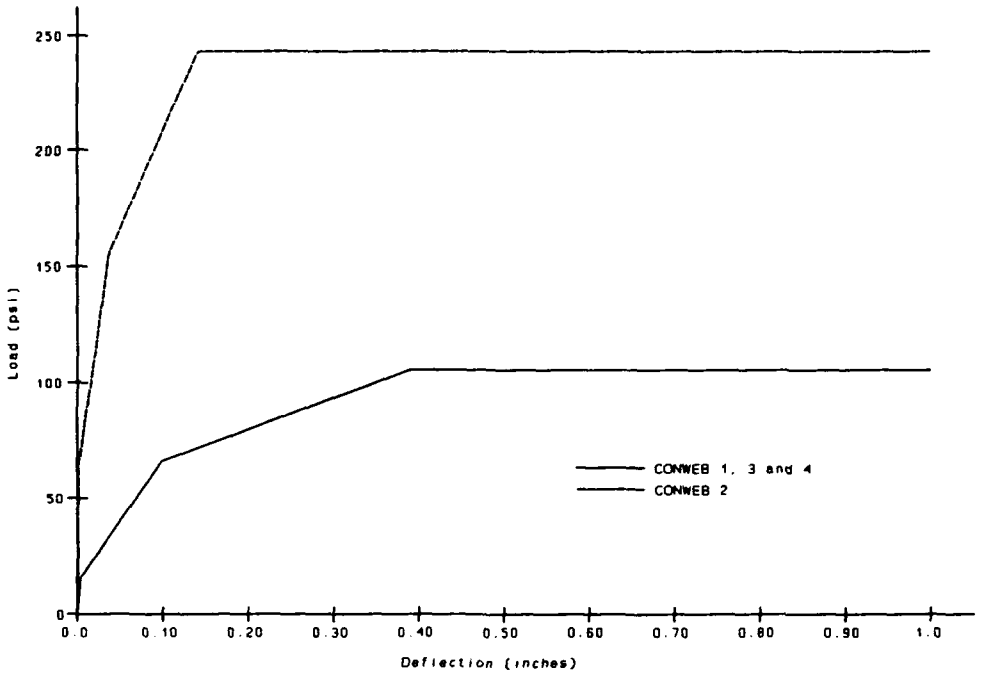

Figure 15. CONWEB, SDOF Wall Analysis resistance functions.

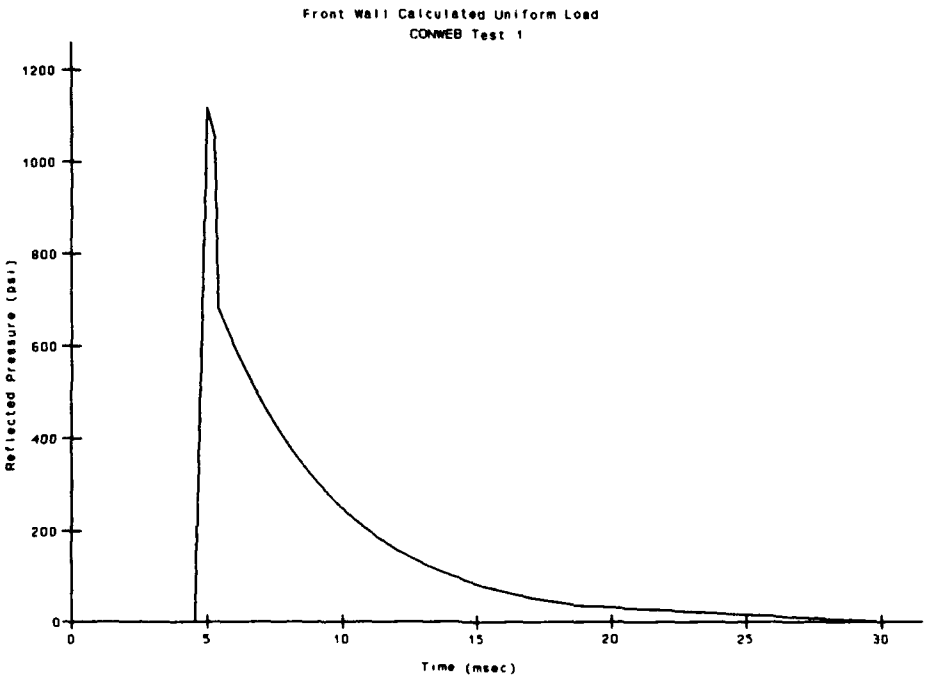

Figure 16. CONWEB 1, SDOF Wall Analysis, calculated interface load.

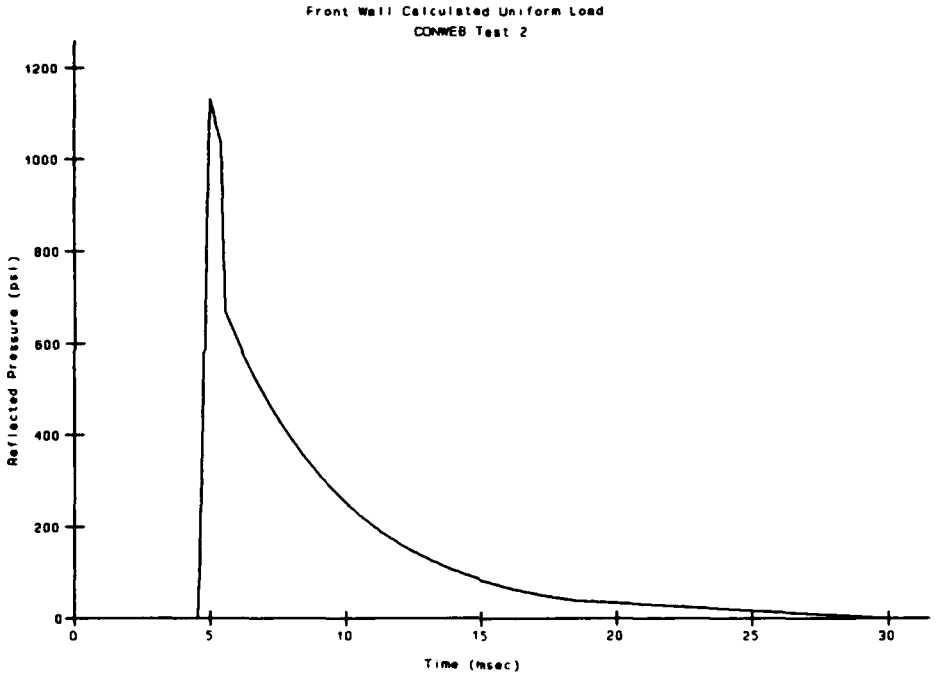

Figure 17. CONWEB 2, SDOF Wall Analysis, calculated interface load.

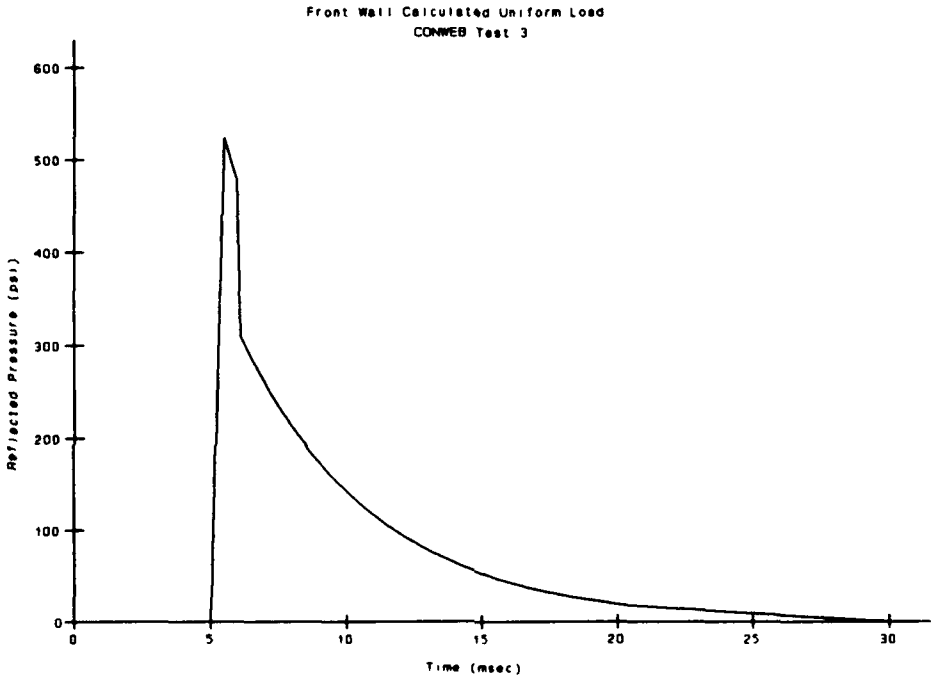

Figure 18. CONWEB 3, SDOF Wall Analysis, calculated interface load.

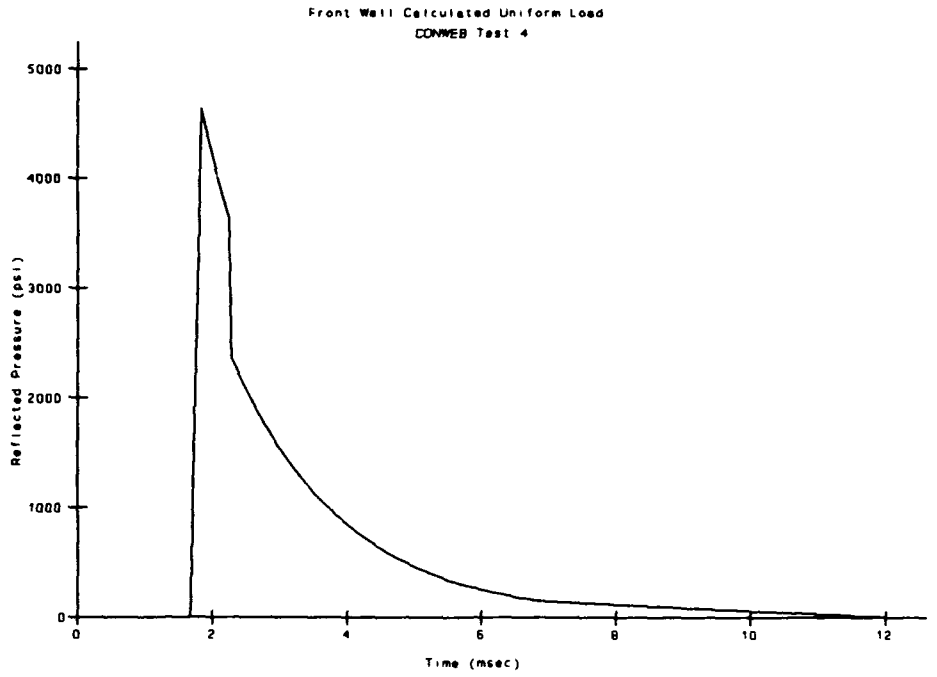

Figure 19. CONWEB 4, SDOF Wall Analysis, calculated interface load.

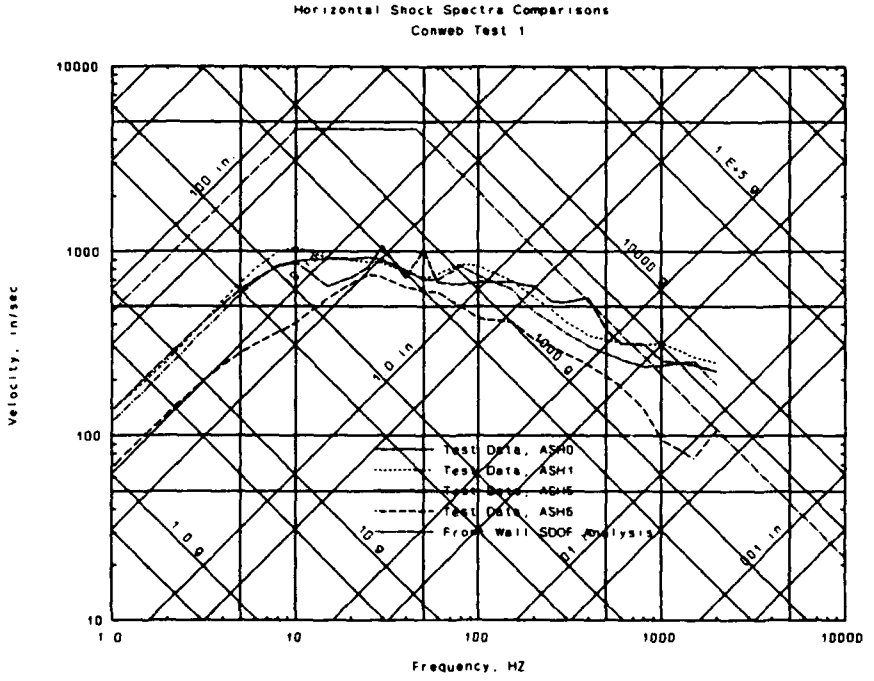

Figure 20. CONWEB 1, SDOF Wall Analysis, shock spectrum vs. test data.

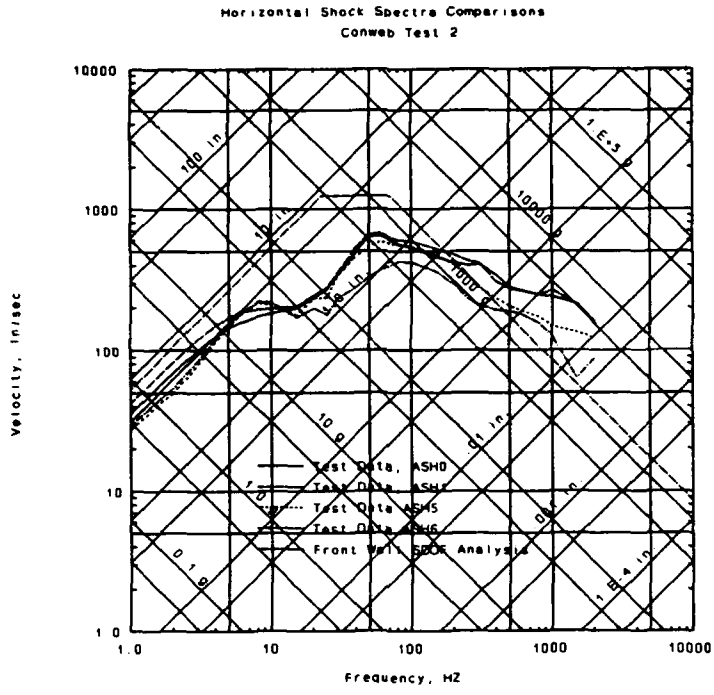

Figure 21. CONWEB 2, SDOF Wall Analysis, shock spectrum vs. test data.

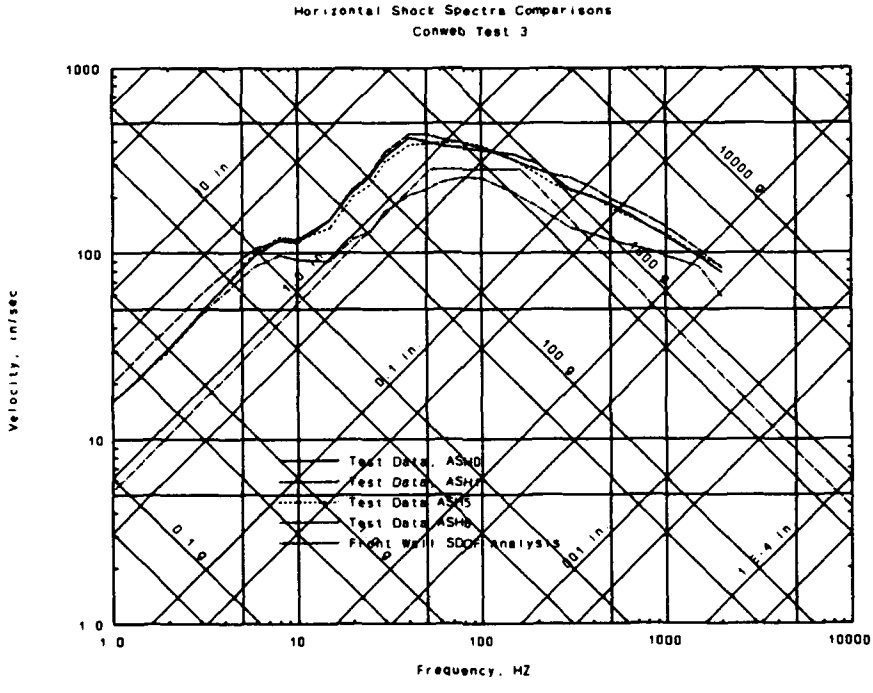

Figure 22. CONWEB 3, SDOF Wall Analysis, shock spectrum vs. test data.

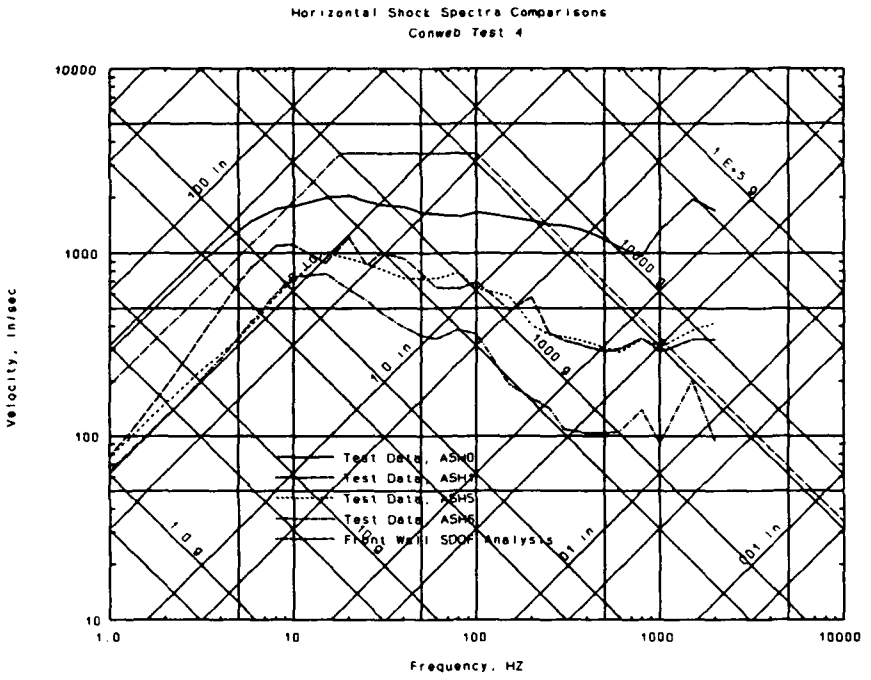

Figure 23. CONWEB 4, SDOF Wall Analysis, shock spectrum vs. test data.

3.3.2 RIGID-BODY SDOF ANALYSIS.

A simple approximation of the horizontal shock environment on the floor of a structure is the overall rigid-body motion of the entire structure. Rigid-body motion was analyzed by reducing the problem to an SDOF system, with the total mass of the structure concentrated to a single point, and with the soil behind the structure acting as a simple linear spring. The load used was the same as that calculated for the wall SDOF above. Shock spectra were generated from the resulting motion histories and compared to those from internal acceleration gages located on the structure's floor. It should be noted that this SDOF model only gives meaningful results up to the initial peak positive deflection. The procedure does not model the complex interactions which take place at later times as the structure rebounds. However, the highest deflections, velocities, and accelerations almost always take place before this happens and this limitation does not hamper the generation of shock spectra.

The soil-spring constant was calculated using a procedure presented by Whitman and Richart [11] for dynamically loaded foundations. Equation (9) was used to compute the soil-spring constant for elastic response of the soil at the back of the structure, where G is the soil's shear modulus (psi); B_z a

$$k=\frac{G}{1-\mu}B_z\sqrt{BL} \tag{9}$$

dimensionless aspect ratio coefficient; μ the Poisson's ratio for the soil; and B and L the height and width of the structure respectively (inches). The shear modulus G, was calculated from the soil density (ρ) and shear wave velocity, V_s, using Equation (10). The shear wave velocity was calculated using Equation (11) from the compressive seismic velocity. Table 6 shows the values used for this calculation and the resulting soil-spring constant; the total mass of the structure is also shown. The Poisson's Ratios used were

$$G = \rho V_s^2 \tag{10}$$

$$V_s^2 = V_c^2\frac{(1-2\mu)}{2(1-\mu)} \tag{11}$$

chosen based on soil tests conducted in conjunction with the CONWEB test

series [1]. These values are relatively high but are within the range of those suggested by Bowels [12]. Frictional forces that exist at the top and bottom of the structure are neglected in this analysis. A relatively low damping value of one percent of critical was included for stability and does not affect the first peak response.

Given the above mass, soil-spring constant, damping coefficient, and the load calculated earlier, the rigid-body SDOF analysis was completed using a computerized version of the procedures developed by Biggs [7]. Velocity-time histories up to the time of maximum positive deflection were input into the same shock-spectra generation program used for the test data. Comparisons of these SDOF spectra with spectra generated from test data are shown in Figure 24 through Figure 27. As can be seen in these figures, the rigid-body SDOF analysis gave reasonable predictions of peak deflections and accelerations for CONWEB 1, 2, and 3. Peak velocities were overpredicted for these same tests. The same trends can be detected in the CONWEB 4 predictions in comparison with gage ASH11. In comparison to ASH10 the CONWEB 4 predictions were low for deflection and acceleration and reasonable for velocity, indicating that the overall response in this test was underpredicted. Underprediction of CONWEB 4 in comparison with gage ASH10 has occurred in each of the analysis procedures used so far, perhaps lending more credence to the possibility of testing or gage problems as discussed above.

Table 6. Rigid-body SDOF, soil-spring parameters.

Test	μ	V_s ft/sec	G psi	B_z	k lb/in.	M lb-sec^2/in.
CONWEB 1	.45	332	2906	2.22	1.269×10^6	73.21
CONWEB 2	.45	332	2935	2.22	1.281×10^6	84.48
CONWEB 3	.33	504	6370	2.22	2.283×10^6	73.21
CONWEB 4	.45	904	21176	2.22	9.245×10^6	73.21

The consistent overprediction of peak spectral velocity in the rigid-body SDOF analysis is more difficult to explain. Possible overloading of the

structure due to problems in modeling structure media interaction, as discussed above, has more effect on the total impulse imparted into structure than it does on the peak pressure experienced at the front wall. The peak acceleration of an SDOF model is very dependent on peak pressure, while the peak velocity is more dependent on the impulse. Thus, overloading the structure with impulse leads to overprediction of velocity. This should also lead to an overprediction of deflection. The fact that deflection predictions are reasonable, indicates a compensating overrestraint of the model, perhaps because the Poisson's Ratios assumed in the analysis were on the high end of expected values. Taken together, all this illustrates the difficulty of analyzing the complex response of a buried structure using a simple SDOF model It should be noted, however, that the velocity predictions were conservative.

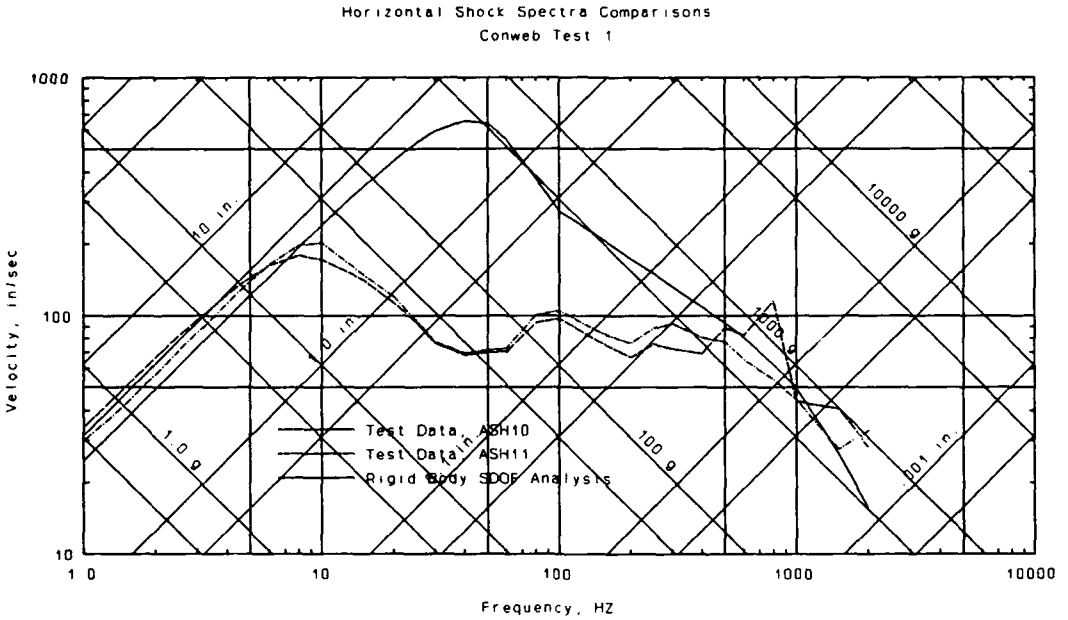

Figure 24. CONWEB 1, Rigid-Body SDOF Analysis, shock spectrum vs. test data.

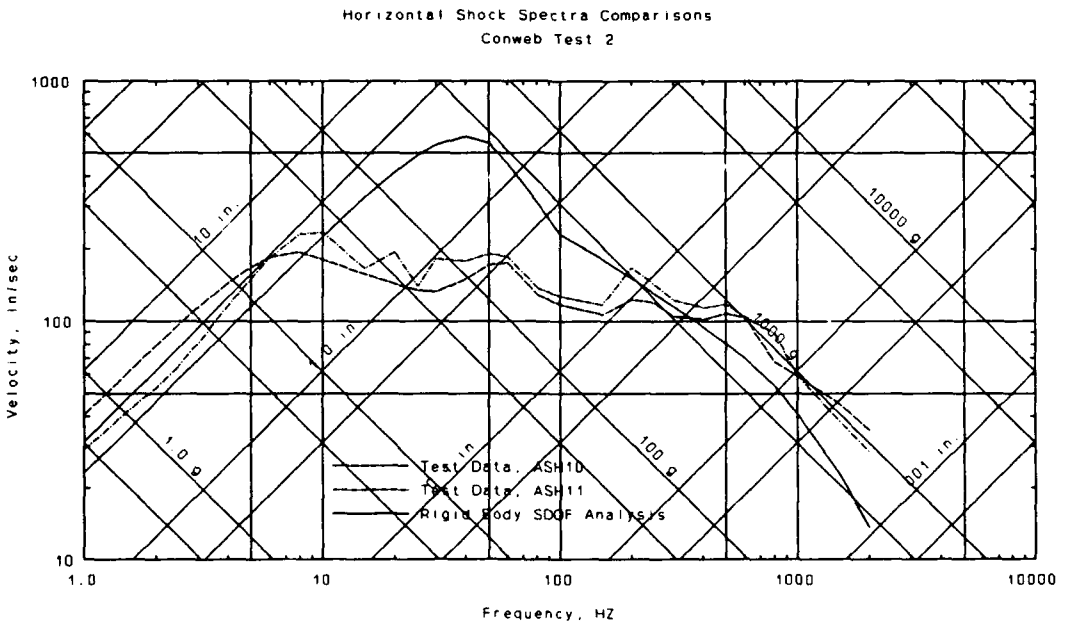

Figure 25. CONWEB 2, Rigid-Body SDOF Analysis, shock spectrum vs. test data.

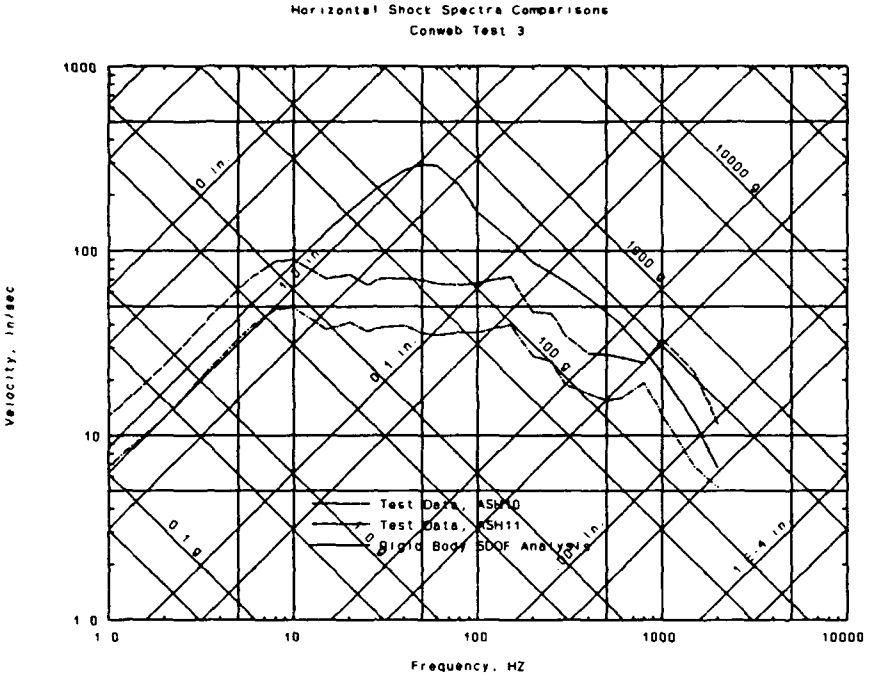

Figure 26. CONWEB 3, Rigid-Body SDOF Analysis, shock spectrum vs. test data.

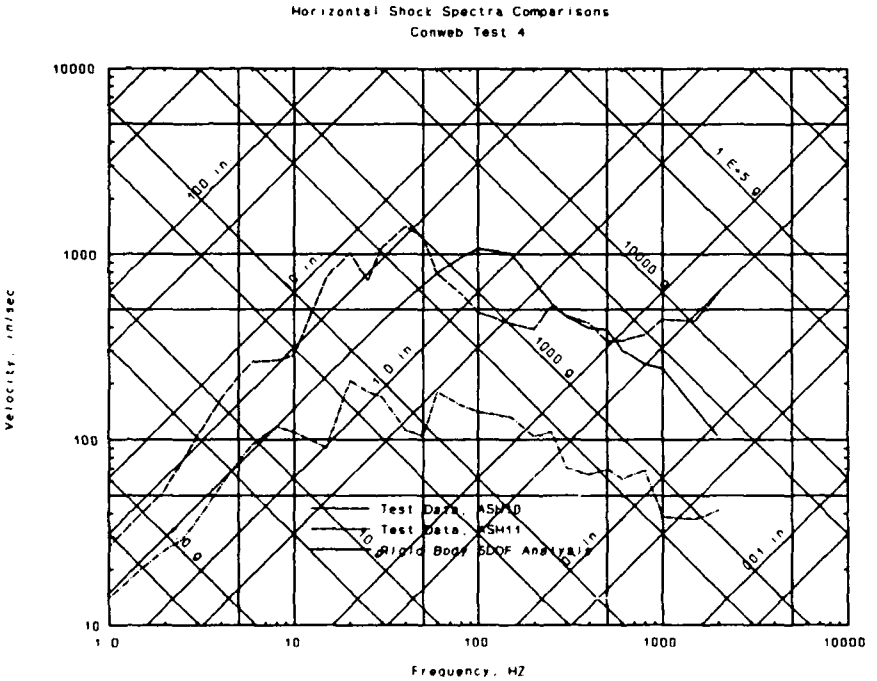

Figure 27. CONWEB 4, Rigid-Body SDOF Analysis, shock spectrum vs. test data.

SECTION 4
IMPLICIT FINITE-ELEMENT ANALYSIS TECHNIQUE

4.1 STABLE PROGRAM.

STABLE is an implicit finite-element program for the dynamic analysis of frames subjected to blast and ground shock loadings. This program is in the public domain and was written by JAYCOR, Vicksburg, MS, for the US Army Engineer District, Omaha. STABLE was in existence at the beginning of this project and, as a validated program, was selected as a candidate for incorporation into an in-structure shock design tool. This program was not specifically designed for in-structure shock calculations, and the following is an evaluation of the application of STABLE to this class of problems.

4.2 STABLE PROGRAM FORMULATION.

Extensive documentation of the formulation and validation of the computer code, STABLE, has been provided by Bryant, Campbell, Smith, and Flathau [4], [13], and [14]. The following is a brief overview of the formulation of STABLE as it applies to the evaluation of the program as an in-structure shock tool.

The general formulation of STABLE is an implicit finite-element analysis program. Implicit formulation refers to the solution method used to solve the equations of motion as the problem proceeds through time. In this case the Newmark integration scheme which is widely covered in the literature [16] was used. As such, the implicit solution of the structural equations is unconditionally stable; that is, the choice of a large time step will not cause the solution to go unstable. This large time step is the main advantage of such a formulation. However, with each time step the solution of the equations of motion requires a relatively large amount of calculational effort and, hence, computer time. An alternative formulation of a finite-element analysis program is an explicit type, in which the time step must be small to assure stability but the computational effort is smaller at each step. The program, ISSV3, which will be examined later, is of an explicit formulation.

The elements available in STABLE are one-dimensional, prismatic, beam elements of constant cross section, moment of inertia, and plastic moment capacity. The material model available in STABLE is a general bilinear,

elasto-plastic material. A steel shape table allows direct input of standard steel shape properties. Reinforced concrete is modeled by use of an equivalent steel section, inputting equivalent areas, moment of inertia, and plastic moment capacity. A reinforced concrete material model, which appears in the STABLE manual, has implementation problems that did not allow its use.

Dynamic loading models used in this analysis included direct input pressure-time histories and loads developed through structure media interaction (SMI). Pressure-time histories that were input were simplified waveforms taken from the interface pressure gage data at the front wall of the structure. Restraint of the horizontal motion of the structure was provided by; frictional forces modeled by Coulomb dampers at the top and bottom of the structure, and SMI loads at the back of the structure. SMI was also modeled at the top and bottom of the structure for vertical reactions. STABLE calculates SMI loads using a simplified approach as shown in Equations (12) and (13).

$$\sigma_n = \rho c_1 V_{ffn} \pm \rho c_1 (V_{ffn} - V_{sn}) \qquad \sigma_n > 0$$

$\sigma_n \equiv$ *SMI normal stress.*
$\rho \equiv$ *Soil mass density.*
$c_1 \equiv$ *Free-field compression wave speed.*
$V_{ffn} \equiv$ *Normal free-field soil velocity.*
$V_{sn} \equiv$ *Normal structure velocity.*

(12)

$$\tau = \rho c_s V_{fft} \pm \rho c_s (V_{fft} - V_{st})$$

$$|\tau| \leq c + \sigma_n \tan\phi$$

$\tau \equiv$ *SMI shear stress.*
$\rho \equiv$ *Soil mass density.*
$c_s \equiv$ *Free-field shear wave speed.*
$V_{fft} \equiv$ *Tangential free-field soil velocity.*
$V_{st} \equiv$ *Tangential structure velocity.*
$\phi \equiv$ *Soil friction angle.*

(13)

Normal and shear stresses resulting from the SMI model are a combination of the free-field stresses and the stresses due to the relative movement of the free-field and the structure. In this analysis, no free-field stresses were applied at the nodes where SMI was being calculated. Thus, only the relative motion stresses were in existence at these points. The application of actual interface loads at the front face already includes all SMI effects in the data.

4.3 STABLE CONWEB ANALYSIS.

The evaluation of STABLE as an in-structure shock analysis technique focused on the analysis of the CONWEB 2 test. It was planned that if this evaluation was favorable, the other CONWEB tests would be analyzed. As will be discussed below, the results of CONWEB 2 analysis led to the rejection of this program as an in-structure shock analysis tool, and no further analyses were conducted. The analyses, which were conducted on the CONWEB 2 test, included a coarse grid analysis, a fine grid analysis, and a fine grid analysis with soil springs replacing the SMI at the back of the structure. The following is a discussion of the results of each of these analyses:

4.3.1 CONWEB 2 COARSE GRID ANALYSIS.

For this analysis, a relatively coarse two-dimensional finite-element grid was generated to model CONWEB 2 (Figure 28). The model consists of a 1-foot-thick slice taken through the centerline of the structure. All major reinforcement in the structure are in this plane, and the effects of all out-of-plane reinforcement was neglected.

Equivalent steel sections were used to model the concrete cross sections. Equation (14) was used to find the equivalent area and is taken from TM5-1300 [16].

$$A = A_g + (E_s/E_c - 1)A_s$$

$A \equiv$ *Equivalent Area (inches²)*
$E_s \equiv$ *Steel Youngs Modulus (psi)*
$E_c \equiv$ *Concrete Youngs Modulus (psi)*
$A_s \equiv$ *Steel Area (inches²)*
$A_g \equiv$ *Gross Concrete Area (inches²)*

(14)

Equation (15) was used to find the thrust capacity and came from the same source [16].

$$P_o = 0.85 fd'_c (A_g - A_s) + A_s fd_s$$

$P_o \equiv$ *Compressive Capacity (psi)*
$fd'_c \equiv$ *Dynamic Concrete Strength (psi)*
$fd_s \equiv$ *Dynamic Steel Yield Strength (psi)*
$A_g \equiv$ *Gross Area (inches²)*
$A_s \equiv$ *Steel Area (inches²)*

(15)

Equivalent moment capacity is given by Equation (16) also from TM5 1300 [16].

$$M_o = (A_s - A'_s) fd_s (d - a/2) + A'_s fd_s (d - d')$$
$$a = (A_s - A_s) fd_s / (0.85 b fd_c)$$

M_o ≡ *Moment Capacity (in.-lb)*
fd_s ≡ *Dynamic Steel Yield Strength (psi)* (16)
fd_c ≡ *Dynamic Concrete Strength (psi)*
b ≡ *Section Width (inches)*
A'_s ≡ *Tensile Steel Area (inches²)*
A_s ≡ *Compressive Steel Area (inches²)*

Equation (17), Biggs [7], gives the equivalent moment of inertia.

$$I = \frac{bd^3}{2}(5.5\rho + 0.083)$$

I ≡ *Moment of Inertia (inches⁴)* (17)
b ≡ *Section Width (inches)*
d ≡ *Depth to Tension Steel (inches)*
ρ ≡ *Reinforcement Ratio*

The resulting equivalent section properties are shown in Table 7.

Table 7. Section properties, CONWEB 2 STABLE analysis.

Section	Compressive Capacity lb	Moment Capacity in.-lb	Moment of Inertia inches^4	Equivalent Area inches^2
Front Wall	677358	224515	303	109.2
Reaction Structure	844401	603711	870	144

The results of the coarse grid analysis are presented in Figure 29 through Figure 36. Figure 29 shows a comparison of the horizontal acceleration record produced by STABLE at node 10, compared to the test data at that same location. The initial peak values of acceleration compare reasonably well. However, a late-time, high-frequency oscillation occurs in the STABLE output, which is not seen in the test data. This oscillation or noise in the acceleration output is disturbing, but not fatal, in an in-structure shock analysis. The integration of the acceleration record to yield the velocity record (Figure 30) smooths out much of this noise, giving a velocity record which compares favorably with the test data. It should be noted that the test

data velocity record does not return to zero as is physically required. Thus, only the initial velocity records can be compared. In the integration of the velocity data to give the deflection record (Figure 31), all evidence of high-frequency oscillation has been smoothed out. However, it can also be seen in this figure that the test data deflection does not reach a constant value before the end of the data record. Thus, any comparisons between calculated total deflection and measured total deflection are suspect.

This problem in late-time deflection measurement is unfortunate, but it illustrates a very common problem in the measurement of in-structure shock with accelerometers. The range of an accelerometer must be set high enough to capture the high initial accelerations and as a result lacks the sensitivity to record late-time accelerations. These late-time accelerations are what account for the overall rigid-body motion of the structure, and hence total deflection.

Given the problem of high-frequency noise in the calculated acceleration record and lack of sensitivity to measure late time accelerations and hence total deflections in the test data, it is difficult to make meaningful comparisons between the calculated and measured motion-time histories. However, the generation of a shock spectrum (Figure 32) is driven by the velocity time history, which has the fewest problems in both cases. Calculated spectral acceleration and velocity compare quite well, while deflection comparisons must be made with care due to the above-mentioned problems in the test data.

Calculated vertical acceleration (Figure 33) at the mid-floor does not show much high frequency noise and compares favorably with the test data. Vertical velocity (Figure 34) and initial deflection (Figure 35) show fair comparisons. The vertical shock spectra (Figure 36) show favorable comparisons for peak accelerations and velocities and a reasonable value for deflection.

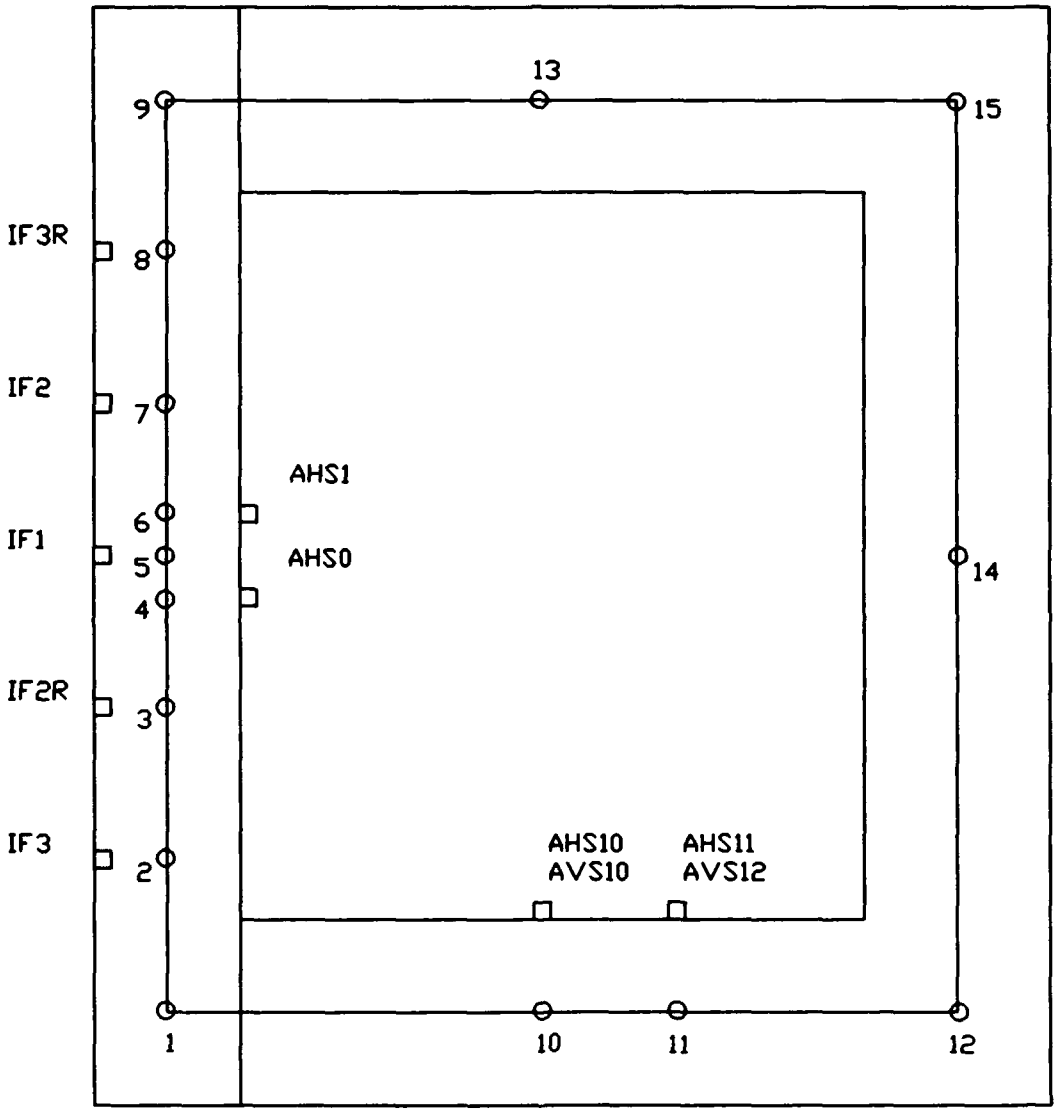

Figure 28. CONWEB 2, STABLE coarse finite-element grid.

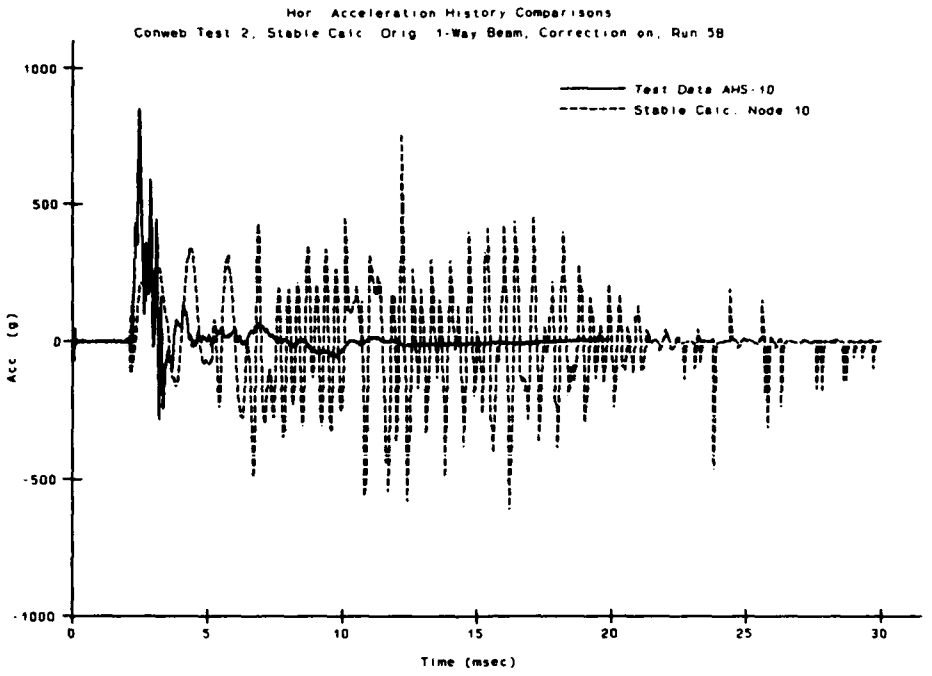

Figure 29. CONWEB 2, midfloor horizontal acceleration, coarse grid STABLE analysis vs. test data.

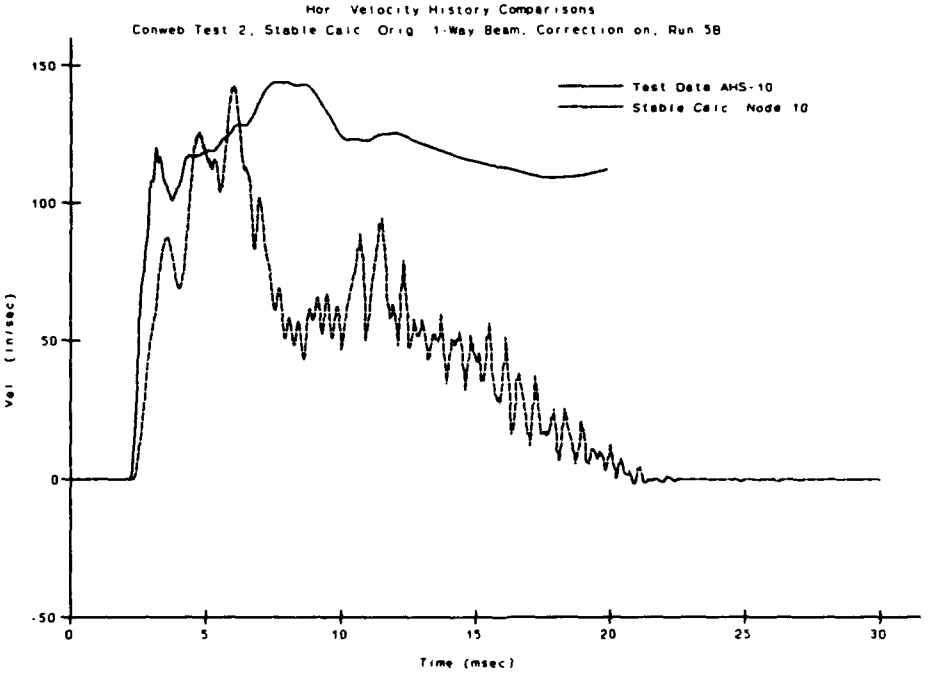

Figure 30. CONWEB 2, midfloor horizontal velocity, coarse grid STABLE analysis vs. test data.

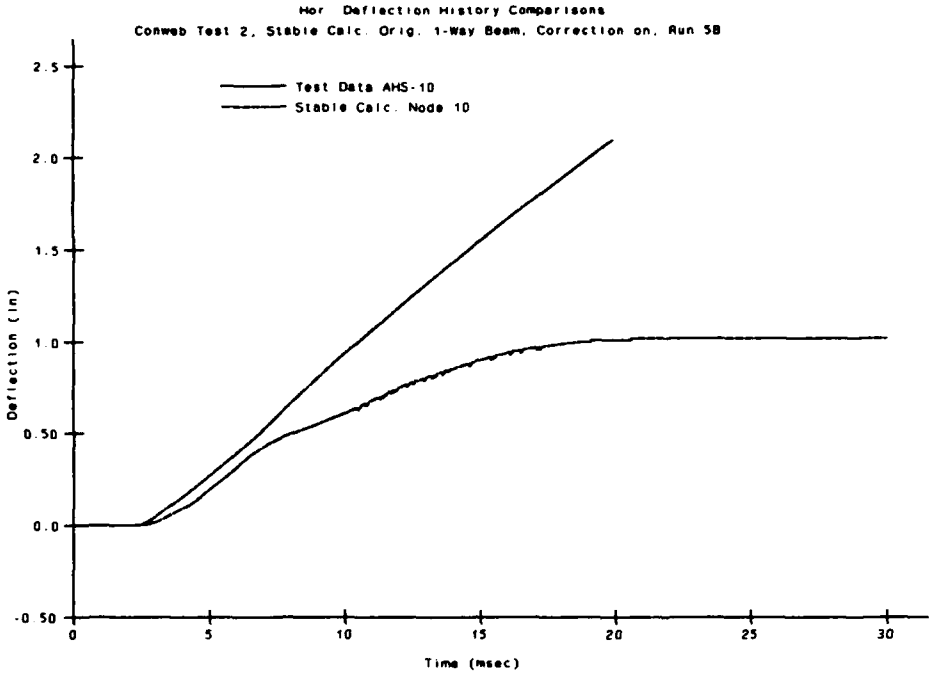

Figure 31. CONWEB 2, midfloor horizontal deflection, coarse grid STABLE analysis vs. test data.

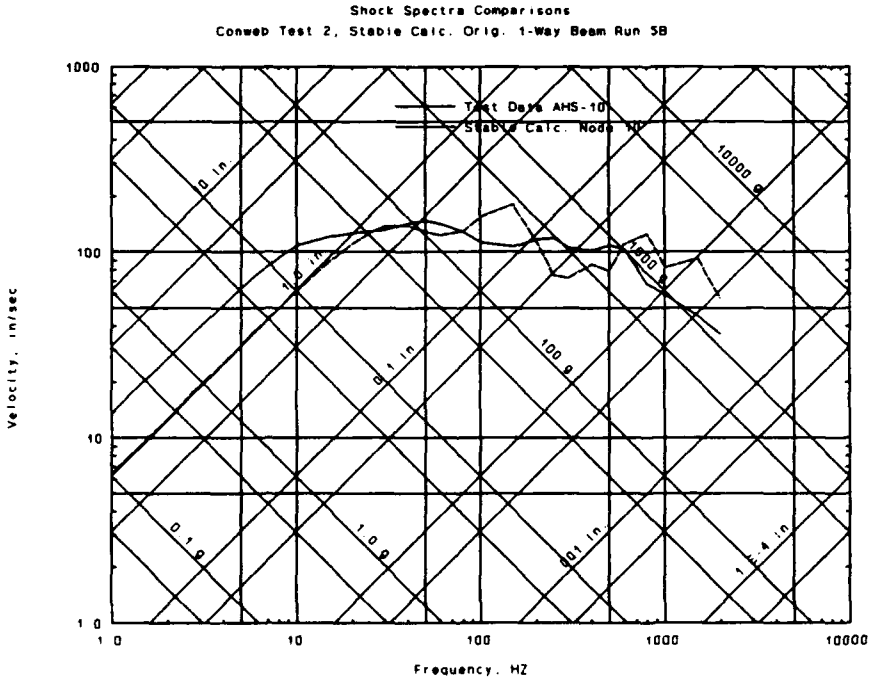

Figure 32. CONWEB 2, midfloor horizontal shock spectra, coarse grid STABLE analysis vs. test data.

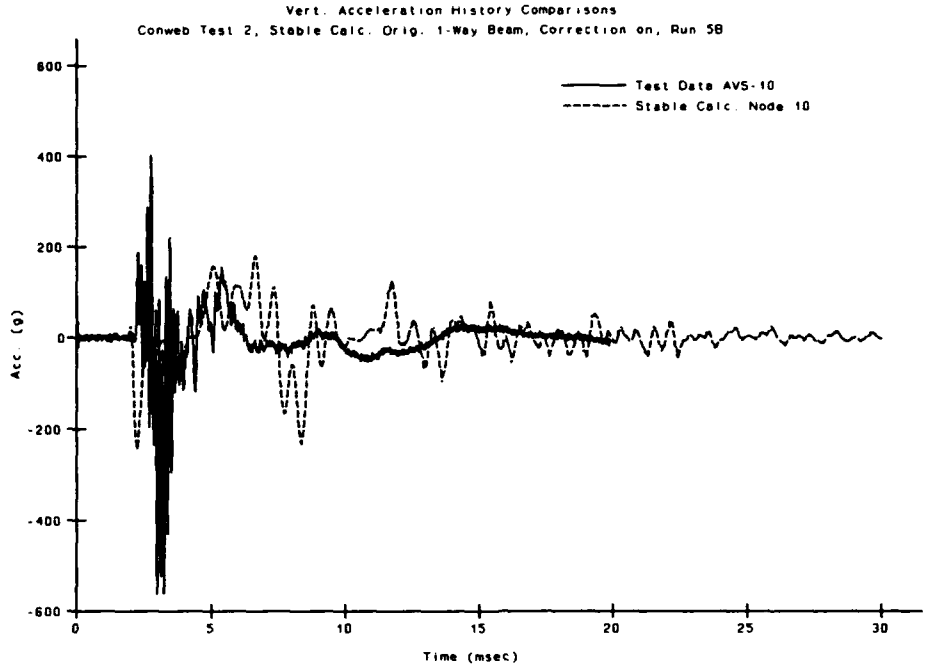

Figure 33. CONWEB 2, midfloor vertical acceleration, coarse grid STABLE analysis vs. test data.

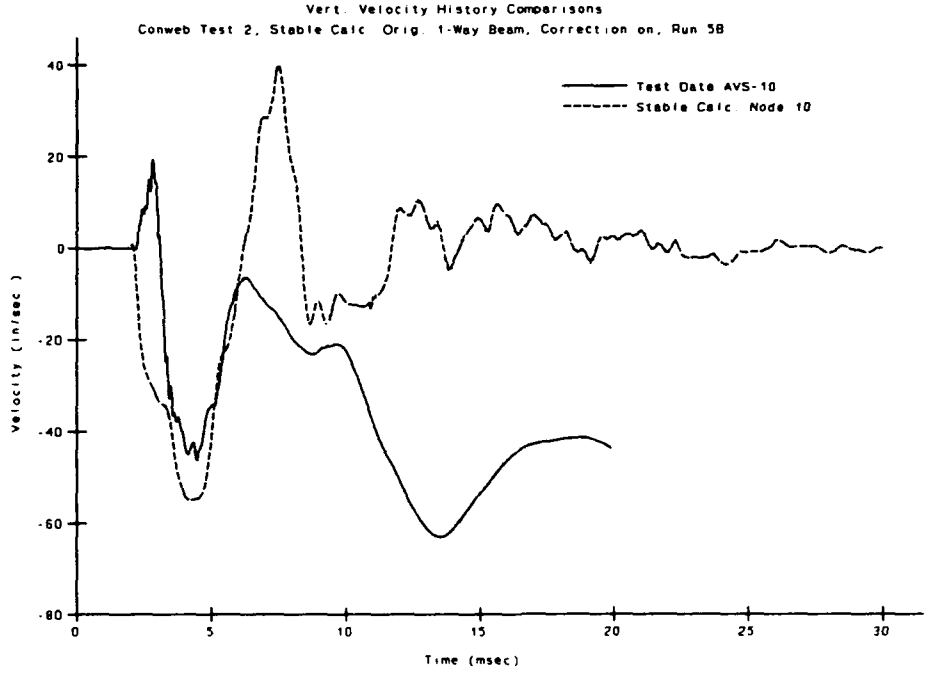

Figure 34. CONWEB 2, midfloor vertical velocity, coarse grid STABLE analysis vs. test data.

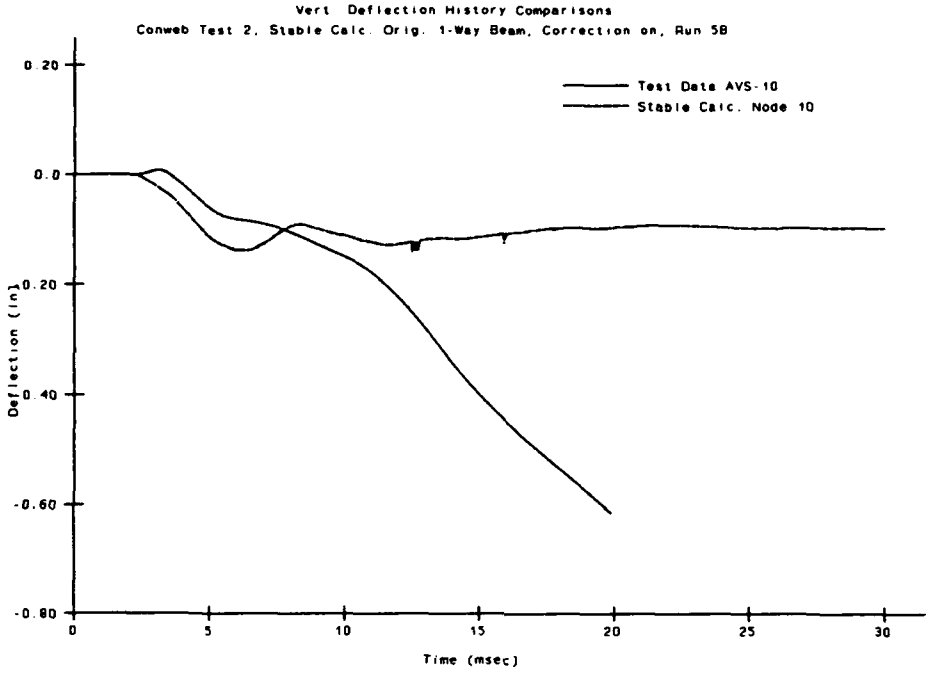

Figure 35. CONWEB 2, midfloor vertical deflection, coarse grid STABLE analysis vs. test data.

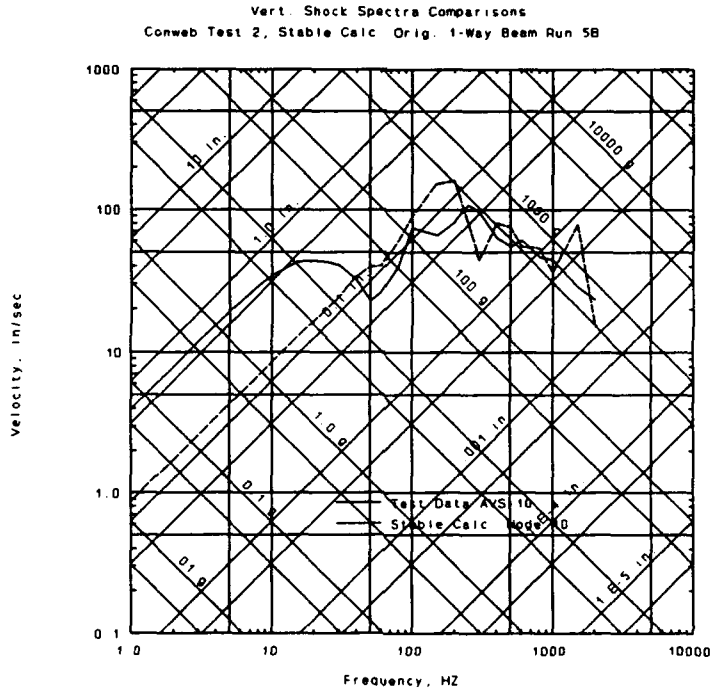

Figure 36. CONWEB 2, midfloor vertical shock spectra, coarse grid STABLE analysis vs. test data.

4.3.2 CONWEB 2 FINE GRID ANALYSIS.

The problem of high frequency noise in the calculated acceleration record was thought to indicate a problem in the modeling of this structure using a coarse grid. A finer grid analysis was therefore conducted. Figure 37 shows the finer grid used in this analysis. All other parameters remained the same as the coarse grid analysis.

Results of a 10-msec calculation of the response of the CONWEB 2 structure using the fine grid are shown in Figure 38 to Figure 43. More, not less, high frequency noise is evident in both the horizontal and vertical acceleration records. Making the grid finer did not correct this problem, and another explanation must be found for this phenomenon. Again, the velocity and deflection records showed less noise, and in fact, showed a good correlation to the test data.

In the calculation of this fine grid analysis, another problem with STABLE was observed. This relatively simple problem required 16 hours of run time on a 20-MHz, 386 personal computer. The ultimate aim of this research project is the qualification of an in-structure shock analysis tool, which will operate on just such a machine. Run times such as this are orders of magnitude too large for this application.

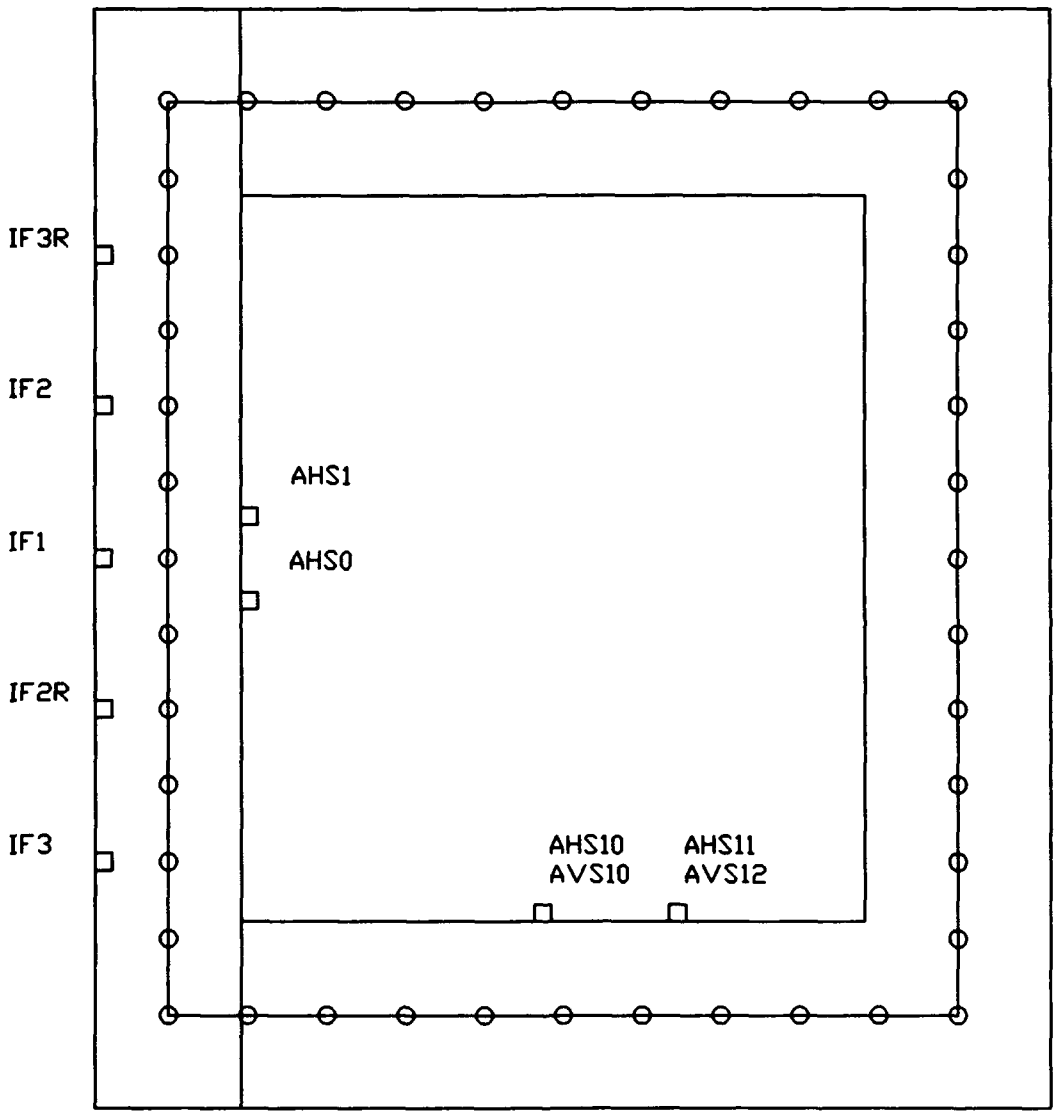

Figure 37. CONWEB 2, STABLE fine finite-element grid.

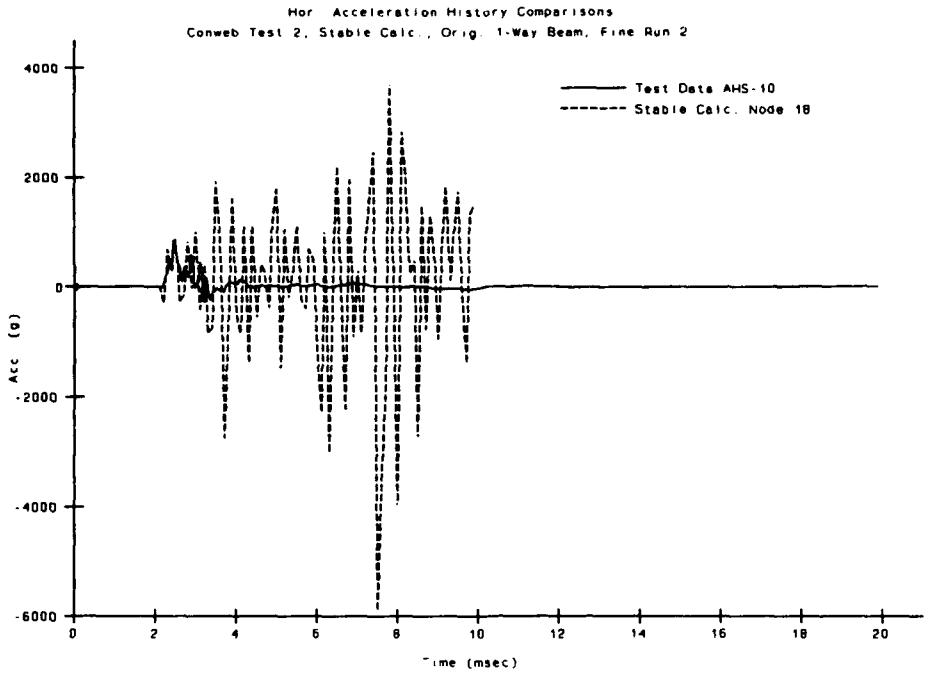

Figure 38. CONWEB 2, midfloor horizontal acceleration, fine grid STABLE analysis vs. test data.

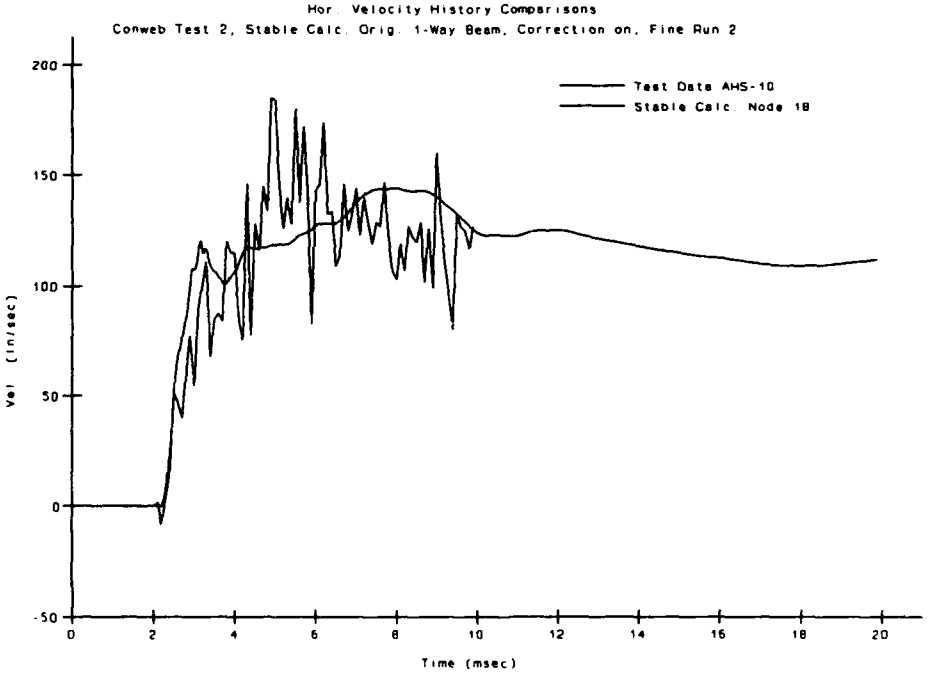

Figure 39. CONWEB 2, midfloor horizontal velocity, fine grid STABLE analysis vs. test data.

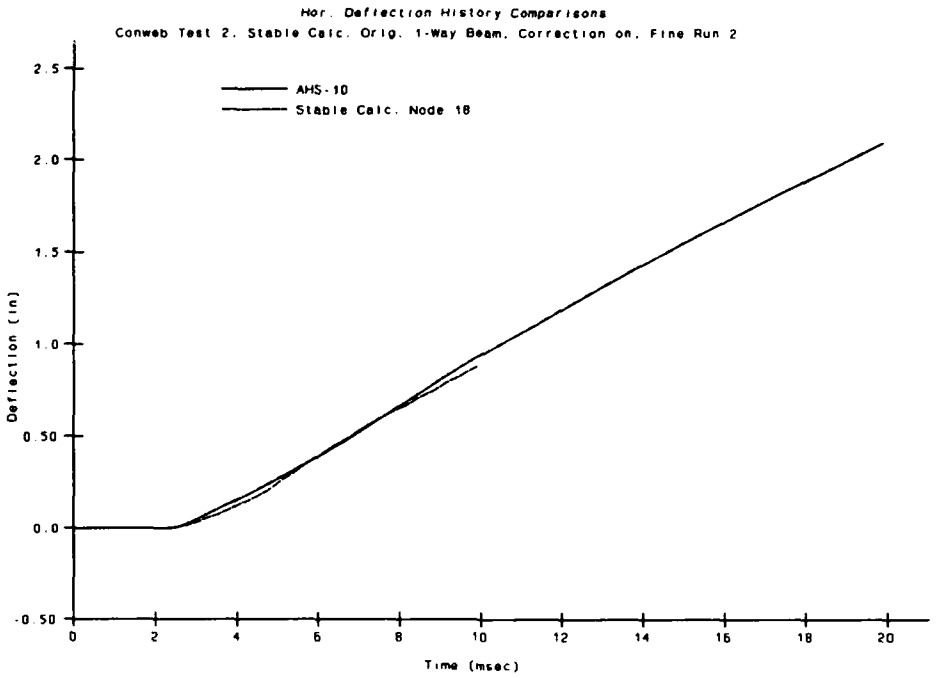

Figure 40. CONWEB 2, midfloor horizontal deflection, fine grid STABLE analysis vs. test data.

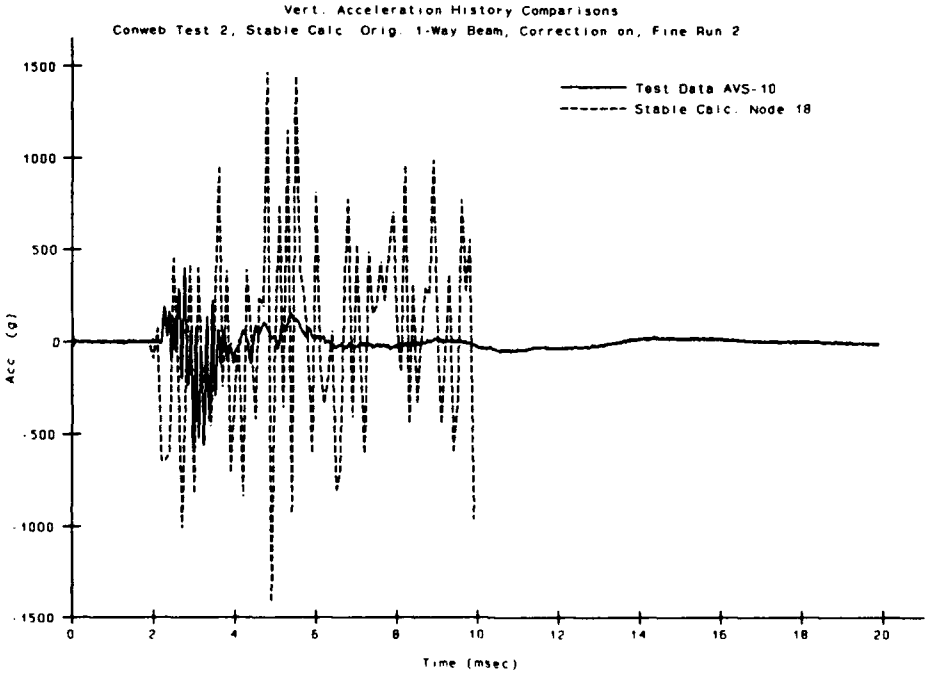

Figure 41. CONWEB 2, midfloor vertical acceleration, fine grid STABLE analysis vs. test data.

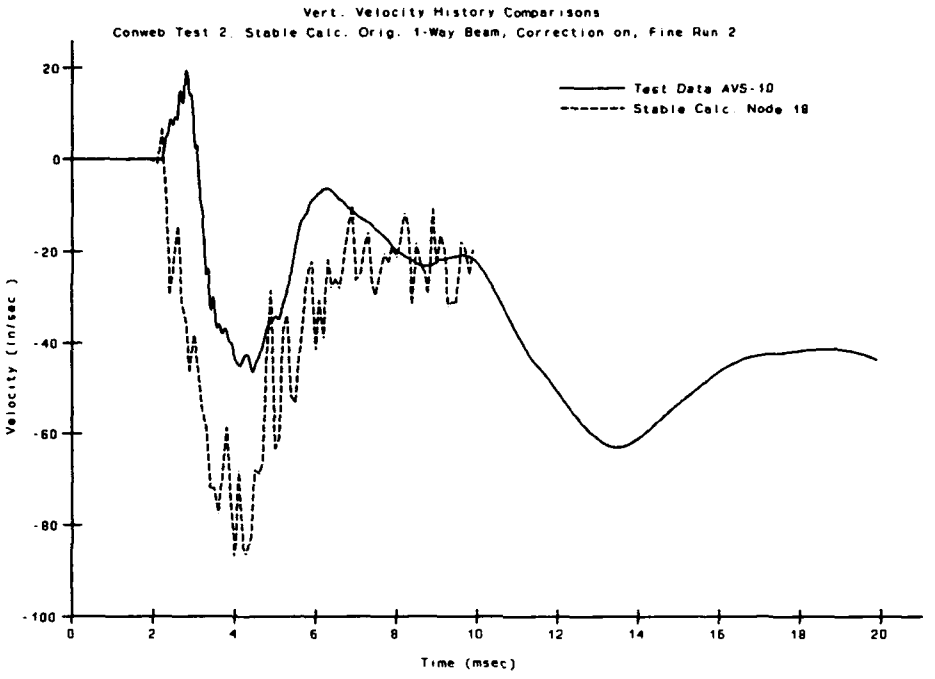

Figure 42. CONWEB 2, midfloor vertical velocity, fine grid STABLE analysis vs. test data.

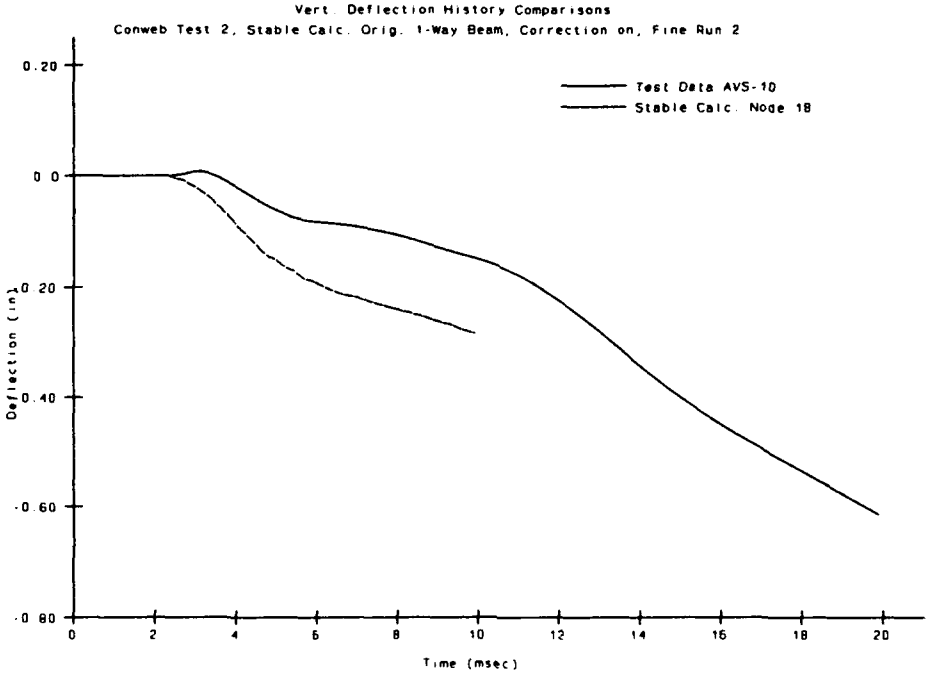

Figure 43. CONWEB 2, midfloor vertical deflection, fine grid STABLE analysis vs. test data.

4.3.3 SOIL-SPRING FINE GRID ANALYSIS.

In a final attempt to determine the cause of excessive noise in the calculated acceleration records, the fine grid STABLE calculation of CONWEB 2 was repeated. In this analysis, the SMI at the back face of the structure was replaced by equivalent soil springs. It was hypothesized that problems in the calculation of the relative motion of the structure and the soil on a non-loaded interface could cause fictitious loads to be generated. These false loads could account for high frequency noise in the acceleration record.

The soil-spring properties included in this calculation were generated by assuming an elastic soil response. A typical soil modulus of elasticity of 1,000 psi was assumed based on recommendations by Bowles [12]. Soil-spring stiffness was calculated based on an effective depth of elastic response of 18 inches at the back of the structure. This is a very crude model of the complex SMI at the back of the structure, but should be sufficient to examine the problem of SMI-induced instability.

Results of a 20-msec calculation of the response of the CONWEB 2 structure using the fine grid are shown in Figure 44 through Figure 49. High frequency noise is evident in both the horizontal and vertical acceleration records. There was less noise than in the fine grid analysis, but more noise than in the coarse grid analysis. Removing the SMI from the model did not correct this problem. This implies that the phenomenon is related to some other problem in the analysis. Again, the velocity and deflection records showed less noise and, in fact, showed a very good correlation to the test data.

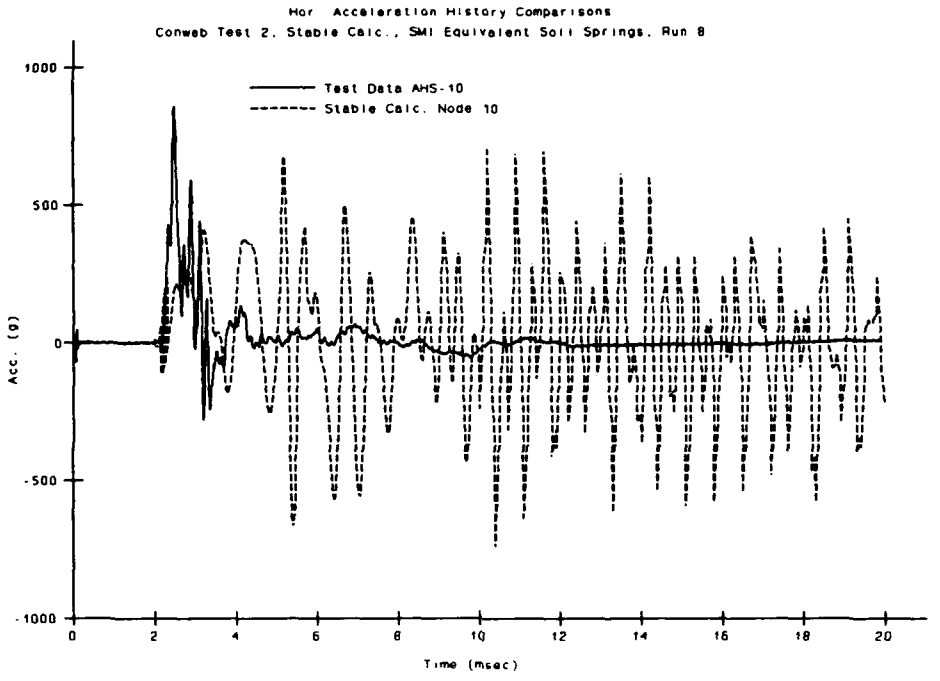

Figure 44. CONWEB 2, midfloor horizontal acceleration, soil-spring fine grid STABLE analysis vs. test data.

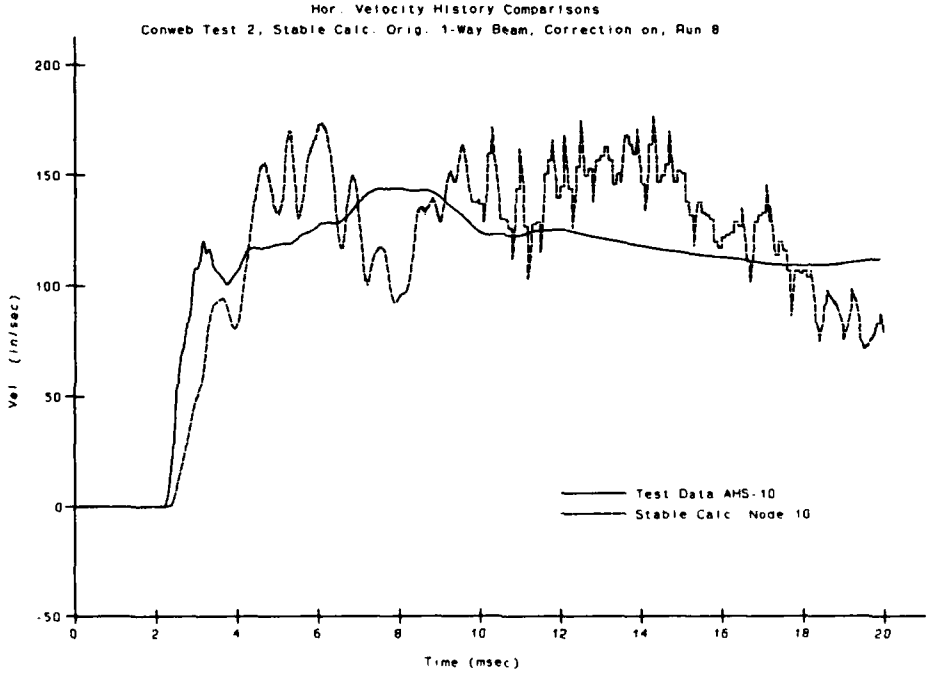

Figure 45. CONWEB 2, midfloor horizontal velocity, soil-spring fine grid STABLE analysis vs. test data.

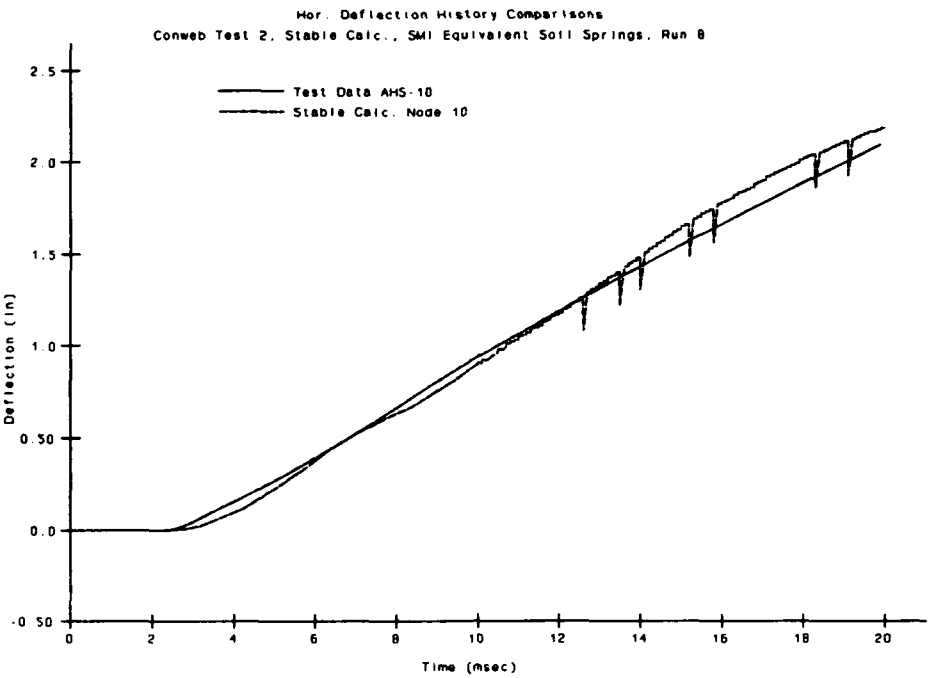

Figure 46. CONWEB 2, midfloor horizontal deflection, soil-spring fine grid STABLE analysis vs. test data.

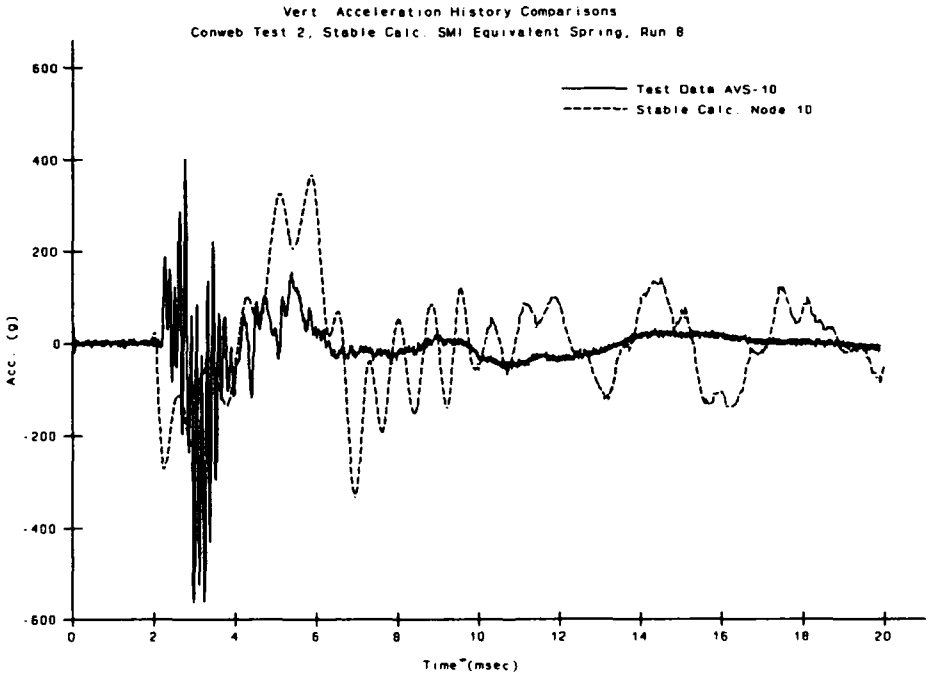

Figure 47. CONWEB 2, midfloor vertical acceleration, soil-spring fine grid STABLE analysis vs. test data.

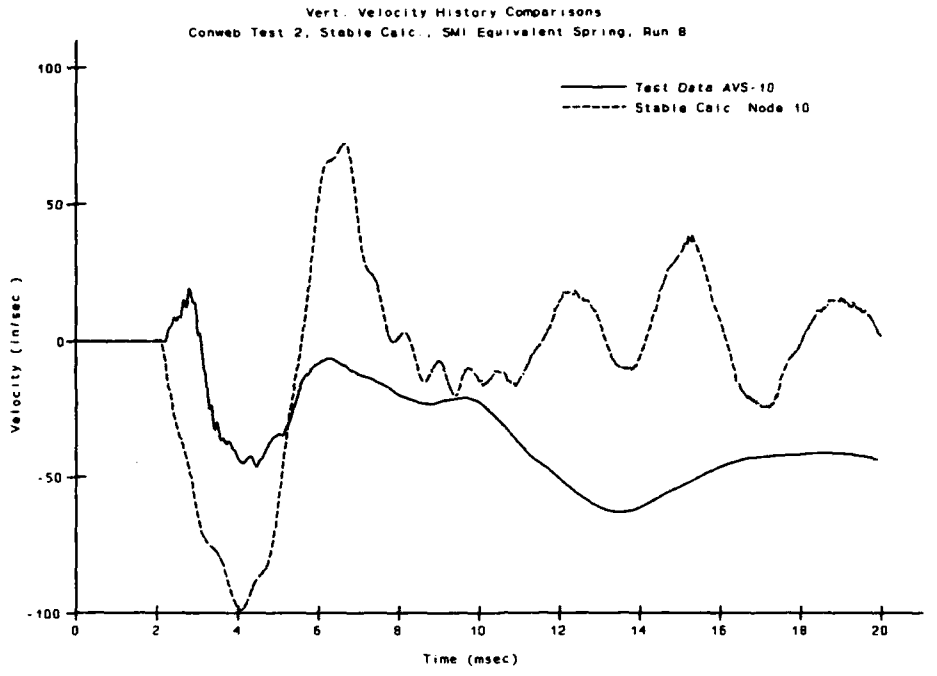

Figure 48. CONWEB 2, midfloor vertical velocity, soil-spring fine grid STABLE analysis vs. test data.

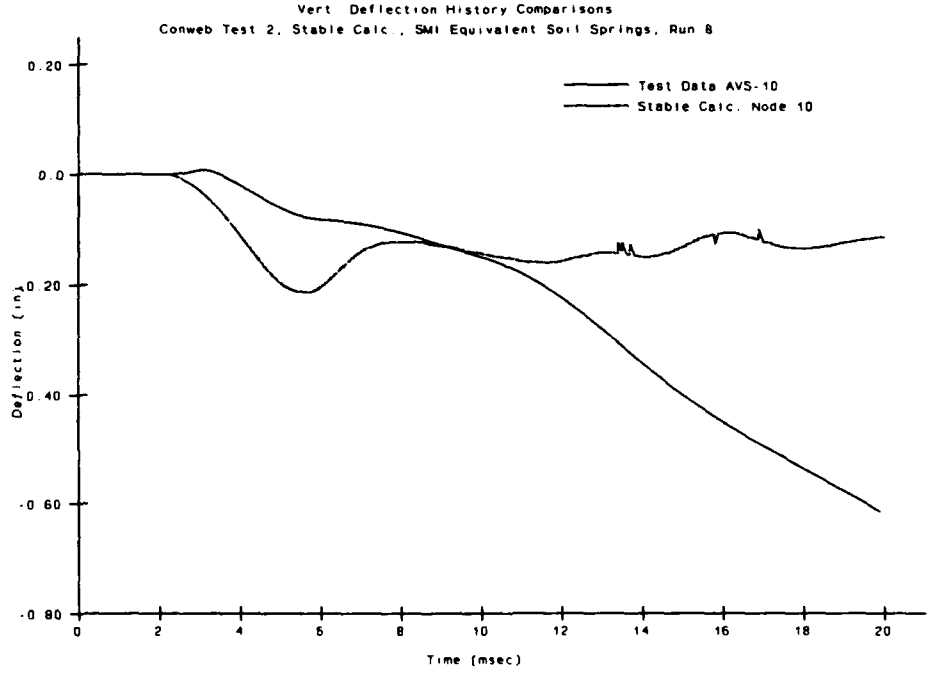

Figure 49. CONWEB 2, midfloor vertical deflection, soil-spring fine grid STABLE analysis vs. test data.

4.4 STABLE ANALYSIS SUMMARY.

The evaluation of STABLE as an in-structure shock analysis technique leads to the rejection of this program from further consideration. This rejection is not based on the problem of high frequency noise in the acceleration records that plagued this analysis. Favorable comparisons of the calculations results to CONWEB 2 test data indicate that the program is capable of handling this type of application. Modification of the program to eliminate the problem of high frequency noise in the acceleration records is quite possible. The basis for the rejection of the application of STABLE to in-structure analysis is excessive run times on the target computer. The fine grid analysis required approximately 16 hours to complete on a 20 MHz, 386 personal computer.

Excessive run times for STABLE are directly related to its formulation as an implicit finite-element analysis program. As discussed, above the implicit formulation refers to the solution method used to solve the equations of motion as the problem proceeds through time. Using a large time step is the main advantage of such a formulation; however, with each time step, the solution of the equations of motion requires a relatively large amount of calculational effort and, hence, computer time. Unfortunately, the application of STABLE to in-structure shock analysis requires a small time step and a large number of iterations to capture the high frequency response of the structure and to keep the SMI calculation from going unstable. As a result, you have a combination of the worst of both worlds; that is, the requirement for many short time steps that require a large amount of computer time for each calculation. Modifications are possible that could increase the computational efficiency of STABLE, but it is felt that such modifications could not overcome such a fundamental limitation.

SECTION 5
EXPLICIT FINITE-ELEMENT TECHNIQUE

5.1 ISSV3 PROGRAM.

With the rejection of STABLE, a new candidate program was selected for development as an in-structure shock analysis tool. This program, ISSV3, is an explicit type finite-element analysis program in which the time step must be small to assure stability, but the computational effort is smaller at each step or iteration. As will be seen below, the result is a program with orders-of-magnitude shorter run times.

ISSV3 was developed by Robert E. Walker, James L. Drake, William L. Boyt, and Thomas R. Slawson of Applied Research Associates, Inc., Southern Division. The work was conducted under WES contract DACA39-90-0041 for Dr. J. P. Balsara and under supervision of the author of this report, Mr. Richard Dove. Included in this work was a report written by Walker, Drake, Boyt, and Slawson [5]. The following brief discussion of the formulation of ISSV3 draws extensively from information in this report but will focus on the application of the program to in-structure shock analysis of underground structures. After this discussion, ISSV3 will be applied to in-structure shock analysis of the CONWEB test series, and the results will be evaluated against test data and compared to other calculation techniques.

5.2 ISSV3 PROGRAM FORMULATION.

ISSV3 is a two-dimensional, lumped-parameter beam model, explicit finite-element analysis program. It includes nonlinear structural behavior, SMI, and the calculation of the ground shock or airblast loads. Given the distance of a bomb from a structure and backfill properties, the program calculates the free-field environment. These free-field loads are converted to structural nodal loads by an SMI model.

The central finite-difference direct integration method is used to solve the equations of motion as the solution progresses through time. As such, the displacements and rotations at a given time step are calculated from the displacements and rotations from the prior time step. From these calculations the nodal displacements and rotations are used to calculate element end moments, shears, and thrusts. These forces are used to update the equations

of motion for the next calculational step. Damping is included as an internal force for each element not as a global term. One of the main advantages of this solution scheme is that the stiffness and mass matrices do not need to be reassembled for each time step, greatly decreasing calculational effort. This solution method is widely covered in the literature and those interested should refer to [16] by Bathe and Wilson.

Program output includes nodal displacements, velocities, and accelerations. This motion is the in-structure shock response for each node in the structure. A graphical representation of the rigid-body motion and the shape of the deformed grid is available. In addition to the in-structure shock information generated, structural response data such as element thrusts, shears, moments, and strains are also output.

5.2.1 FREE-FIELD LOAD GENERATION.

The equations used in ISSV3 to characterize the free-field environment are essentially those found in the TM5 855-1 [2]. As such, the stress and particle velocities at a given point in the free field are described by an exponential decay time history.

Equations (18) and (19) are used in ISSV3 for the pressure-time and velocity-time histories at a given point. As the range from

$$P(t) = P_0 e^{-\alpha t/t_a} \qquad t \geq 0$$

$P(t) \equiv$ *Free-field stress.*
$P_0 \equiv$ *Peak free-field stress.*
$t_a \equiv$ *Time of arrival.*
$\alpha \equiv$ *Time constant* (1.0). (18)

the bomb increases, the amplitude of each history decreases and its duration increases.

$$V(t) = V_0(1-\beta t/t_a)\, e^{-\beta t/t_a} \qquad t \geq 0$$

$V(t) \equiv$ *Free-field velocity.*
$V_0 \equiv$ *Peak radial partical velocity.*
$t_a \equiv$ *Time of arrival.*
$\beta \equiv$ *Time constant,* (α/8.5). (19)

It can be seen in these equations that the amplitude and duration of both pressure-time and velocity-time histories are dependent on the time of arrival

(t_a). In the default mode ISSV3 calculates a t_a is dependent only on range and average seismic velocity. It has been found, Hayes [1], that this may be an oversimplification. Equation (20) shows that ISSV3 can also use a non-linear arrival time which is a function of peak stress, peak free-field velocity and backfill properties.

$$t_a = \int_0^R \frac{dr}{c_1} \qquad c_1 = c + SV_0$$

$t_a \equiv$ *Time of arrival* (sec).
$R \equiv$ *Range* (ft).
$c_1 \equiv$ *Loading Wave Velocity* (ft/sec).
$c \equiv$ *Seismic velocity* (ft/sec).
$S \equiv$ *Backfill Variable* $\approx 1/$(*Air Filled Voids*)
$V_0 \equiv$ *Peak Free Field Velocity* (ft/sec). (20)

Time constants α and β are generally taken to be 1.0 and 1/8.5, respectively. P_0 and V_0 are the peak pressure and particle velocity at the point of interest and are calculated using (21) and (22). P_0 is dependent on the backfill properties of mass density, seismic velocity, and attenuation coefficient, as well as the range, bomb weight, and coupling factor.

$$P_0 = 160 f \rho c \left(\frac{R}{W^{1/3}}\right)^{-n}$$

$P_0 \equiv$ *Peak free-field stress* (psi).
$f \equiv$ *Coupling factor.*
$n \equiv$ *Attenuation coefficient.*
$\rho \equiv$ *Mass density* (lb-sec^2/ft^4).
$c \equiv$ *Seismic velocity* (ft/sec)
$R \equiv$ *Range* (ft).
$W \equiv$ *Charge weight* (lb). (21)

V_0 is dependent only on the attenuation coefficient and the range, bomb weight, and coupling factor.

$$V_0 = 160 f \left(\frac{R}{W^{1/3}}\right)^{-n}$$

$V_0 \equiv$ *Peak particle velocity* (ft/sec).
$f \equiv$ *Coupling factor.*
$n \equiv$ *Attenuation coefficient.*
$R \equiv$ *Range* (ft).
$W \equiv$ *Charge weight* (lb). (22)

These parameters were discussed in some detail in the TM5 855-1 in-structure shock analysis section of this report. As mentioned above, the characterization of the free-field environment using these equations is thought to be an

oversimplification. There is research underway to address this problem, and when better models are available, they will be incorporated into ISSV3.

5.2.2 STRUCTURE MEDIA INTERACTION.

Free-field loads must be applied to the structure through SMI. The SMI models used in ISSV3 are similar to the ones used in the STABLE program discussed above. Interface pressures are dependent on the relative motion of the backfill and the structure as well as the backfill properties. Equations (23) and (24) are used to calculate the interface normal and shear stresses at each node on the outside of the structure.

$$\sigma_i = \sigma_n + \rho c_p (V_n - \dot{X}_n) \geq 0 \qquad (23)$$

$\sigma_i \equiv$ *SMI interface stress.*
$\sigma_n \equiv$ *Normal ground shock stress.*
$\rho \equiv$ *Soil mass density.*
$c_p \equiv$ *Free-field compression wave speed.*
$V_n \equiv$ *Normal free-field soil velocity vector.*
$\dot{X}_n \equiv$ *Normal structure velocity vector.*

$$\tau_i = \rho c_s (V_t - \dot{X}_t) \qquad |\tau_i| \leq \mu(\sigma_n + W) \text{ or } Y \qquad (24)$$

$\tau_i \equiv$ *SMI interface shear stress.*
$\sigma_n \equiv$ *Normal ground shock stress.*
$\rho \equiv$ *Soil mass density.*
$c_s \equiv$ *Free-field shear wavespeed.*
$V_t \equiv$ *Tangential free-field soil velocity vector.*
$\dot{X}_t \equiv$ *Tangential structure velocity vector.*
$W \equiv$ *Gravity stress.*
$Y \equiv$ *Ultimate shear stress.*
$\mu \equiv$ *Coefficent of Friction.*

It should be noted that the free-field and SMI models used in ISSV3 do not take into account the fact that the structure perturbs the free-field stress. In other words, the free-field stress is calculated as if the structure does not exist, and is then applied to the structure through SMI. This is thought to be a conservative assumption, and might best be considered on a case-by-case basis.

5.2.3 INTERNAL FORCES.

A standard beam element is the element type used in ISSV3. The internal element forces are calculated using Equations (25), (26), and (27). The new

thrusts at each time step are calculated from the old thrusts plus the difference due to relative displacement of the end nodes during the time step.

$$T_{new} = T_{old} + EA\frac{\Delta L}{L} \qquad |T_{new}| \leq T_{ult} \tag{25}$$

$T \equiv$ *Element Thrust.*
$E \equiv$ *Element Youngs Modulus.*
$A \equiv$ *Element Area.*
$L \equiv$ *Element Length.*

The new moments are calculated from the old moments plus the moments due to the end rotations.

$$M_{new_i} = M_{old_i} + \frac{2EI}{L}(2\theta_i + \theta_j) \qquad |M_{new}| \leq M_{ult} \tag{26}$$

$M \equiv$ *Element End Moments.*
$E \equiv$ *Youngs Modulus.*
$I \equiv$ *Moment of Inertia.*
$L \equiv$ *Element Length.*
$\theta_i, \theta_j \equiv$ *Near and Far End Element End Rotation.*

The new shears are developed from the unbalanced new moments.

$$V_{new_1} = \frac{1}{L}(M_{new_1} + M_{new_2}) \qquad V_2 = -V_1 \tag{27}$$

$V \equiv$ *Element End Shears.*
$M \equiv$ *Element Moments.*
$L \equiv$ *Element Length.*

When the ultimate values of the thrusts and moments are reached plastic deformation occurs. These ultimate values are calculated prior to the analysis based on the section properties. A moment thrust diagram is constructed, and a balanced pair of ultimate values are selected.

Internal damping is included as an internal force to reduce high frequency oscillations. The interaction of the structure and the surrounding soil lead to situations were the structure moves away from the soil or cavitation takes place. In such a situation the damping usually provided by the soil ceases to exist. Internal damping forces are calculated via Equations (28) and (29) to damp out numerical oscillations associated with the axial and double curvature flexural mode of each element. These forces are transformed from the local to global coordinates and summed into the internal force vector.

$$CX = D\,C_R\,\frac{\Delta L}{\Delta t} \qquad C_R = 2A\sqrt{E\,\rho}$$

$CX \equiv$ *Axial Damping Force.*
$D \equiv$ *Input Damping Ratio.*
$C_R \equiv$ *Critical Damping Ratio.*
$\Delta L \equiv$ *Change in Length.*
$\Delta t \equiv$ *Time Step.*
$A \equiv$ *Element Area.*
$E \equiv$ *Youngs Modulas.*
$\rho \equiv$ *Density.*

(28)

$$CM = D\,C_R\left(\frac{\Theta_1+\Theta_2}{\Delta t}\right) \qquad C_R = 4\sqrt{\frac{3EI}{L}\left(\frac{\rho AL^3}{24}+\frac{1}{2}\,\rho LI\right)}$$

$CM \equiv$ *Damping Force.*
$D \equiv$ *Input Damping Ratio.*
$C_R \equiv$ *Critical Damping Ratio.*
$\Theta \equiv$ *Element End Rotation.*
$\Delta t \equiv$ *Time Step.*
$E \equiv$ *Youngs Modulus.*
$I \equiv$ *Moment of Inertia.*
$L \equiv$ *Element Length.*
$A \equiv$ *Element Area.*
$\rho \equiv$ *Density.*

(29)

5.2.4 EQUILIBRIUM EQUATIONS.

The equilibrium equations solved at each time step are constructed from the internal and external forces transformed into the global coordinate system as shown in Equation (30). As discussed before, the central difference integration method is used to solve this equation for motions as the solution progresses through time.

$$\ddot{X} = (F_E - F_I)/M$$

$\ddot{X} \equiv$ *Nodal Acceleration.*
$F_E \equiv$ *External Forces.*
$F_I \equiv$ *Internal Forces.*
$M \equiv$ *Nodal mass.*

(30)

5.3 ISSV3 CONWEB ANALYSES.

Development of section properties for inputting into the ISSV3 program requires some preanalysis. The ultimate moment and thrust capacities must be selected from a calculated moment-thrust diagram for each section. A load path is selected, giving a moment-thrust value just below the balanced condition. Using the material properties for the CONWEB test series, section

properties were generated for each component. These section properties are shown in Table 8.

Table 8. ISSV3, CONWEB section properties.

Test Component	E psi	ρ lb/ft^3	I in^4	A in^2	Mult in-lb	Tult lb
CONWEB 1, 3, 4 Test Wall	4E6	150	4.7	4.3	1.42E4	4.58E3
CONWEB 2 Test Wall	4E6	150	32.0	8.6	5.90E4	1.30E4
Reaction Structure	4E6	150	83	11	1.8E5	2.4E4

5.3.1 CONWEB 1 ANALYSIS.

The finite-element grid for the ISSV3 in-structure analysis of CONWEB 1 is shown in Figure 50. This same grid was used for the calculation of CONWEB 3 and 4, with modifications to the backfill properties. Section properties used were shown above in Table 8, and backfill properties were shown in Table 1.

Results from the CONWEB 1 analysis are shown in Figure 51 to Figure 72. It is immediately obvious on examination of the interface pressure comparison that the calculated time of arrival (t_a) of the load at the face of the structure lags the actual value by about 4 msec. This phenomenon was observed throughout the CONWEB calculations. Interestingly enough, the shape and magnitude of the calculated interface stress compare very favorably with the test data, in spite of the strong relationship between t_a and free-field stress.

As a result of the time lag in the loading, all the data comparisons for structural response also lag. Comparisons to test data of calculated acceleration, velocity, deflection histories, and shock spectra are shown in Figure 53 to Figure 72. Horizontal acceleration, velocity, and deflection histories were reproduced reasonably well by the ISSV3 analysis. Examination

of the late-time horizontal velocity records shows that ISSV3 underpredicts the late-time velocity. This is thought to stem from the inability of the current free-field model to capture the late-time flow of a clay-type material, a problem which should be solved in later versions of the program. Also, as discussed in the STABLE analysis section, there is great difficulty measuring rigid-body displacements with accelerometers, due to the low level of acceleration for these late-time motions.

Vertical acceleration, velocity, and deflection histories were also reproduced reasonably well by the ISSV3 analysis. Due to the much smaller magnitudes of the vertical velocities and deflections, uncertainties in measurement of late-time motions have a larger relative effect than in the horizontal measurements. Given the uncertainties of these measurements, the magnitudes calculated for vertical velocity and deflection by ISSV3 are reasonable.

Shock spectra were generated from the velocity histories for each position in the structure. These spectra show a good correlation between the calculated values and spectra generated for test data. The only consistent underprediction was for the rigid-body deflection as seen on the low frequency portion of the spectra. This underprediction is thought to be due to a combination of the problem with the modeling of clay backfill in the analysis and the problem of measuring late-time motions with accelerometers .

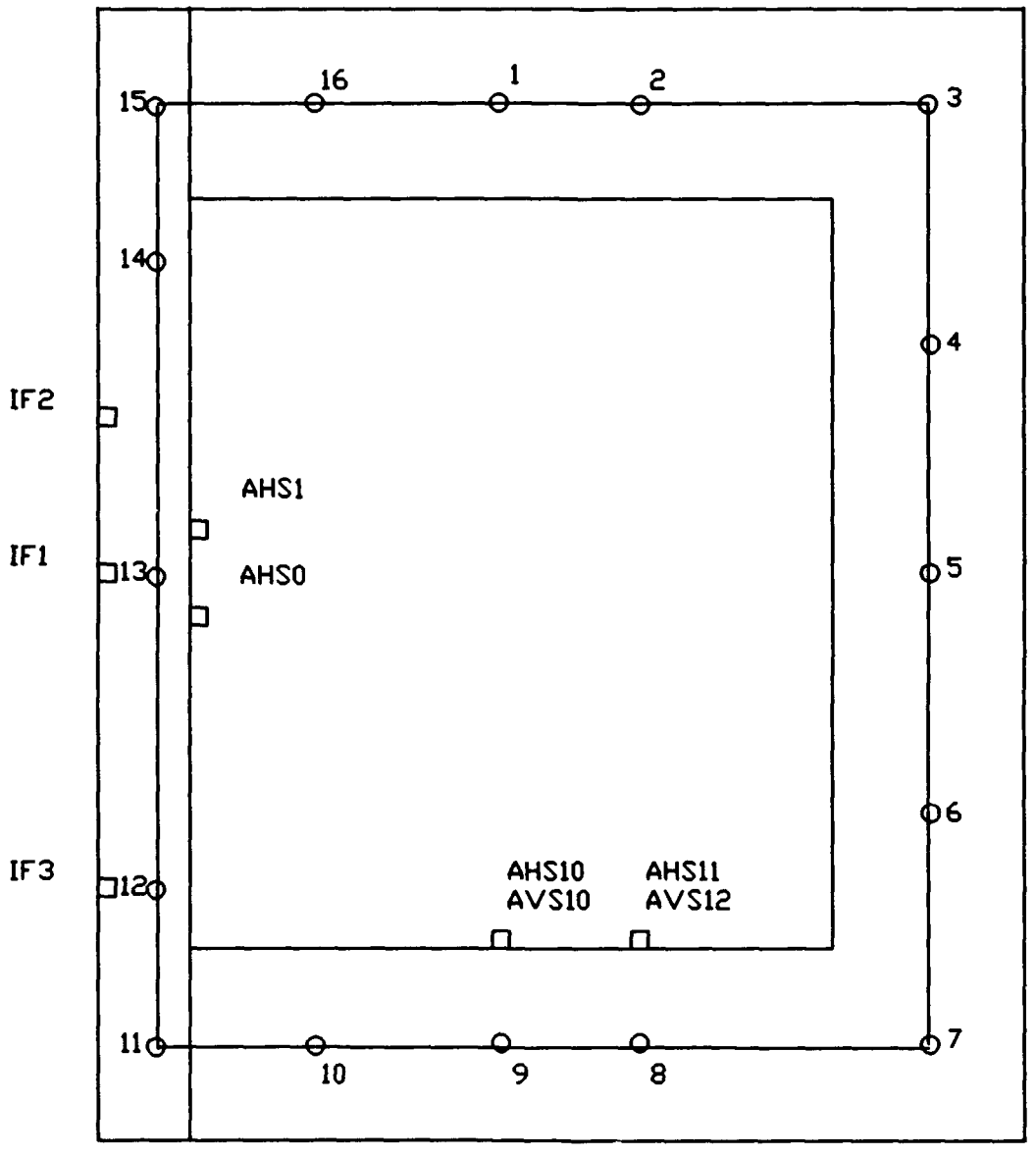

Figure 50. CONWEB 1, 3, and 4, ISSV3 finite-element grid superimposed on structure cross section.

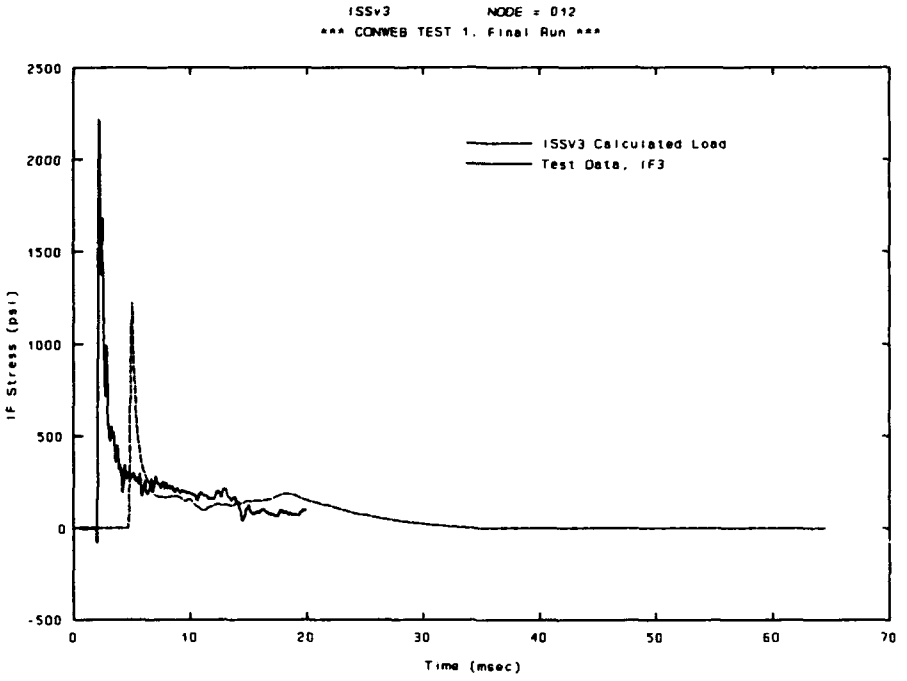

Figure 51. CONWEB 1, lower wall interface pressure load, ISSV3 Node 12, analysis vs. test data.

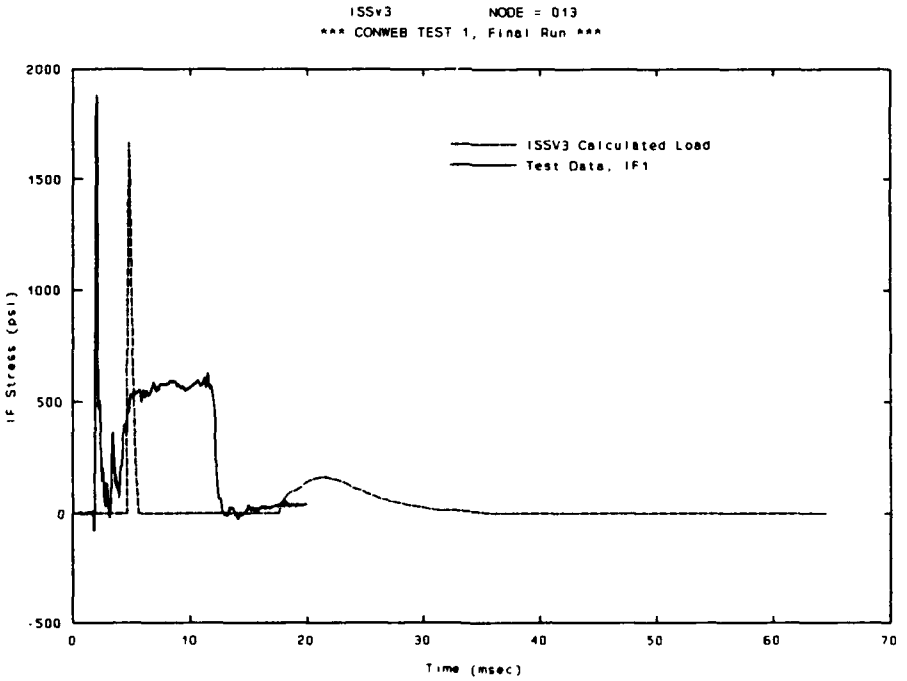

Figure 52. CONWEB 1, midwall interface pressure load, ISSV3 Node 13, analysis vs. test data.

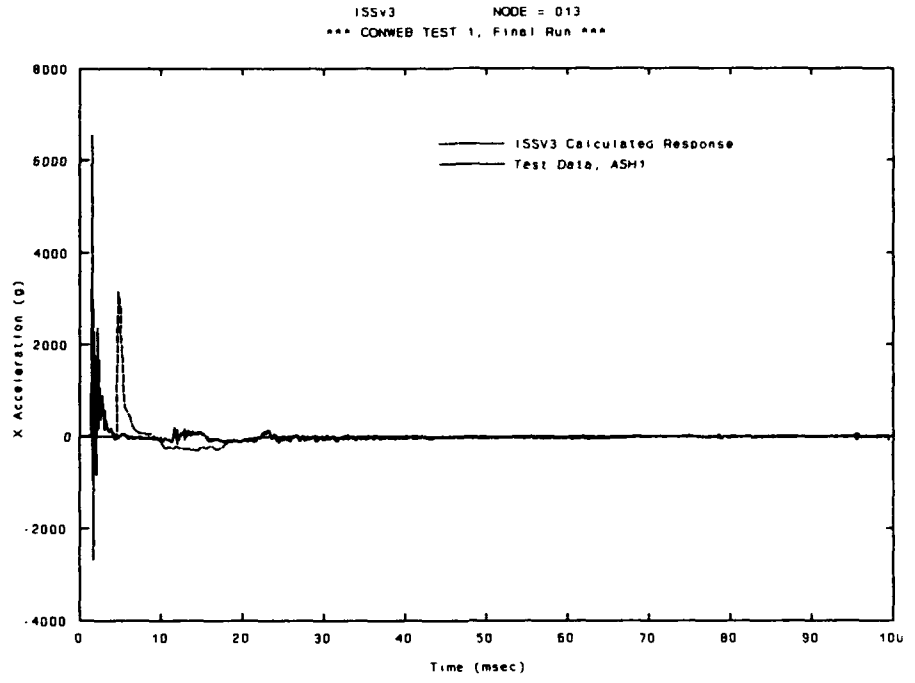

Figure 53. CONWEB 1, midwall horizontal acceleration, ISSV3 Node 13, analysis vs. test data.

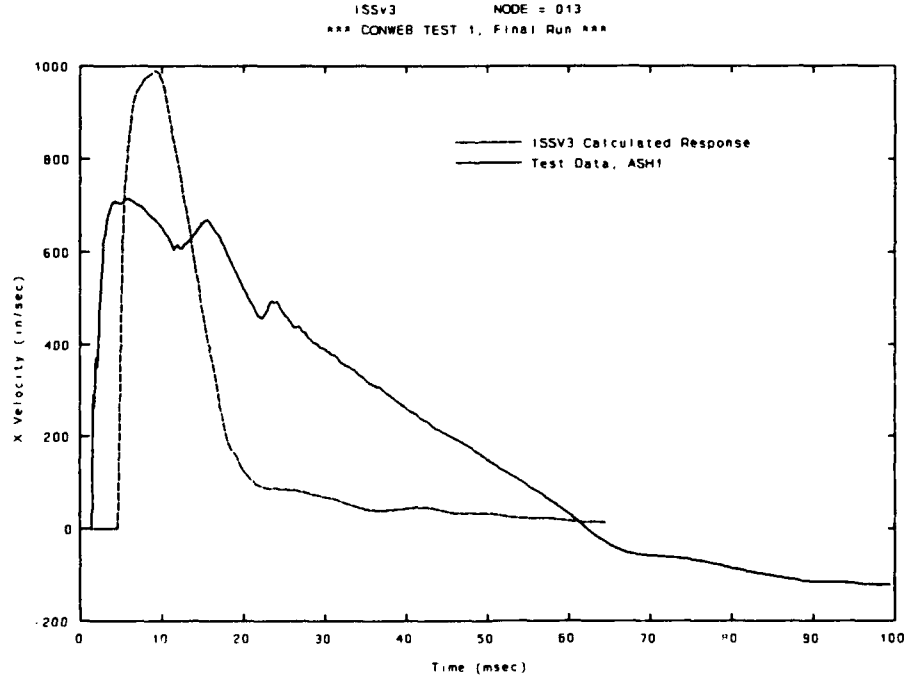

Figure 54. CONWEB 1, midwall horizontal velocity, ISSV3 Node 13, analysis vs. test data.

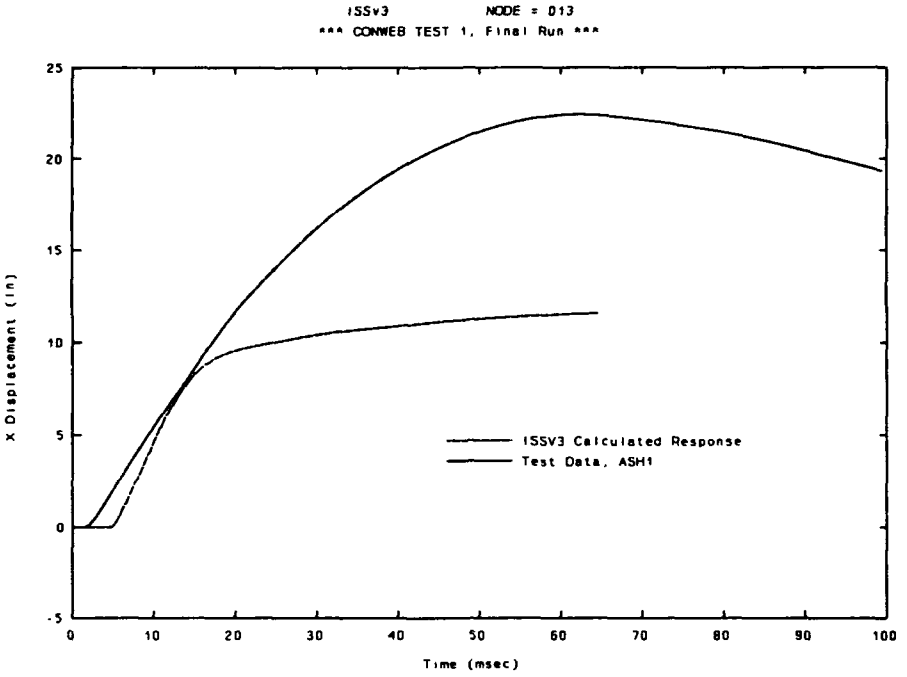

Figure 55. CONWEB 1, midwall horizontal deflection, ISSV3 Node 13, analysis vs. test data.

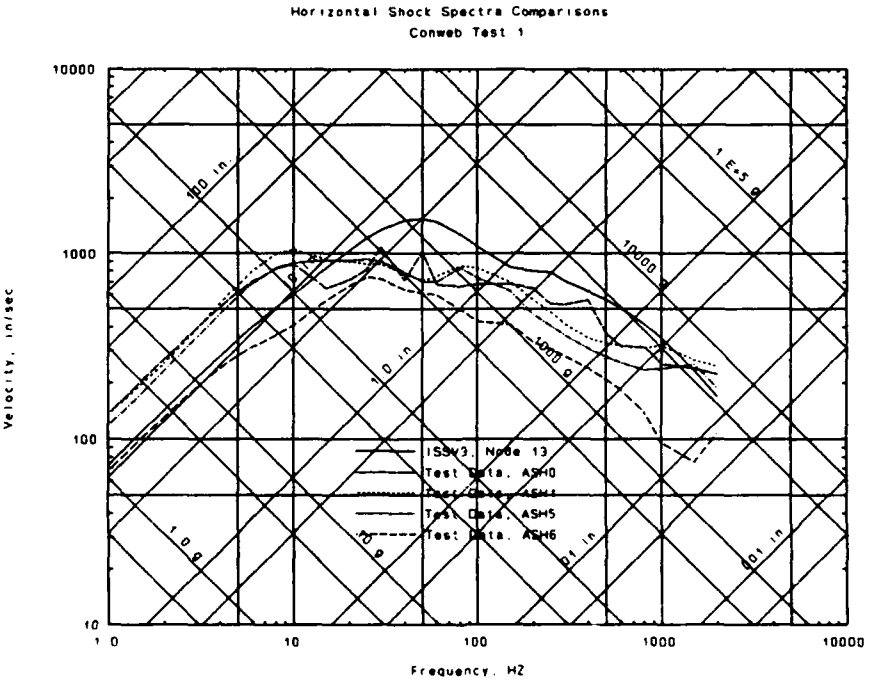

Figure 56. CONWEB 1, midwall horizontal shock spectra, ISSV3 Node 13, analysis vs. test data.

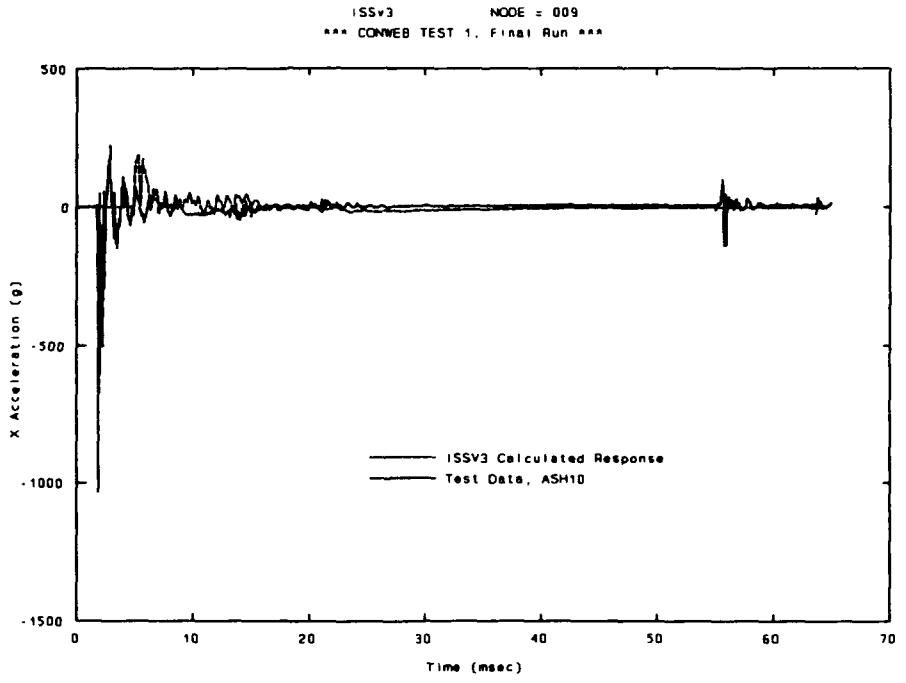

Figure 57. CONWEB 1, midfloor horizontal acceleration, ISSV3 Node 9, analysis vs. test data.

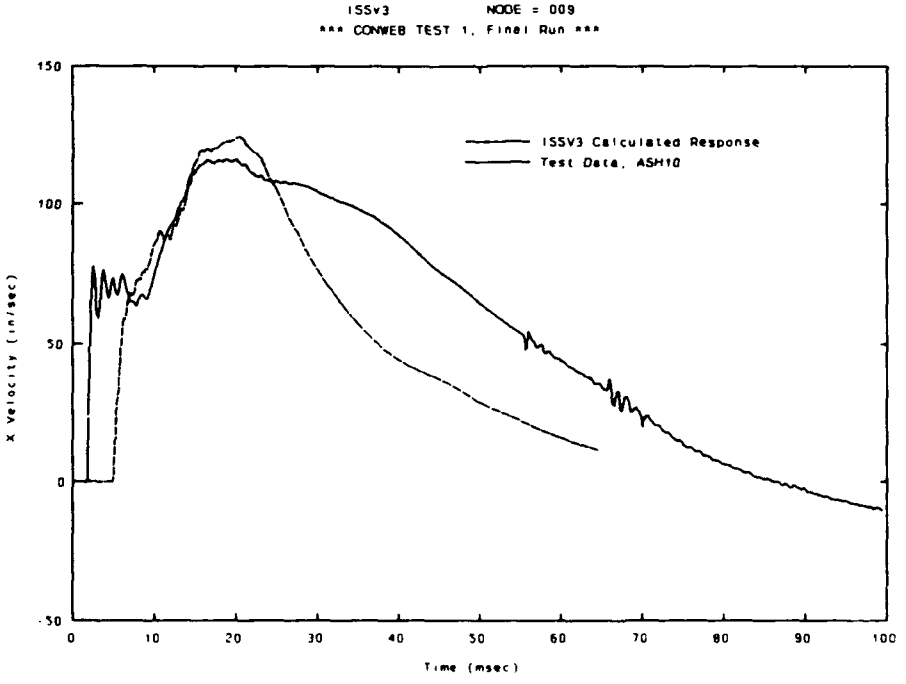

Figure 58. CONWEB 1, midfloor horizontal velocity, ISSV3 Node 9, analysis vs. test data.

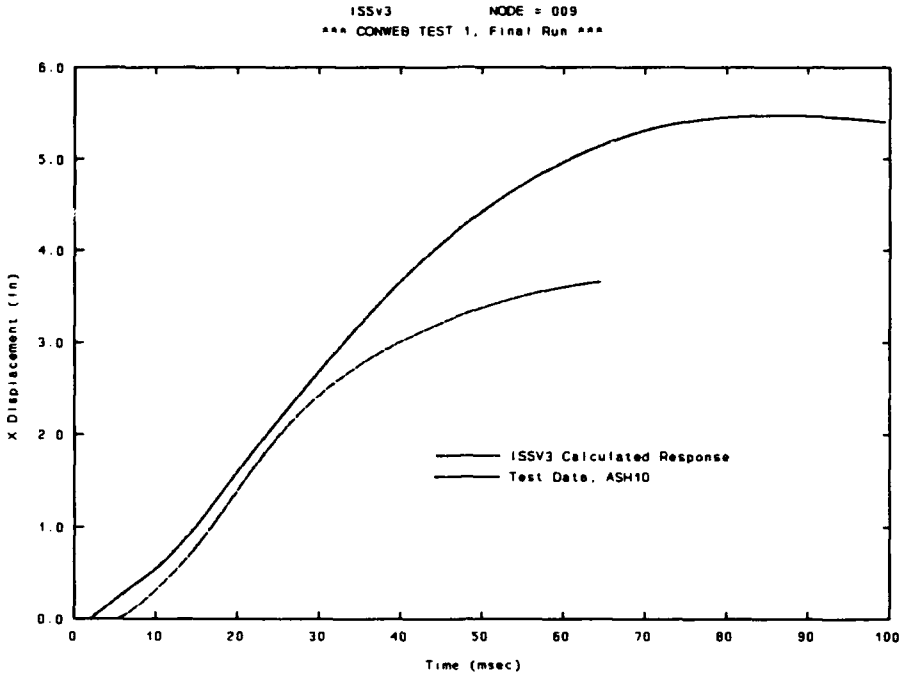

Figure 59. CONWEB 1, midfloor horizontal deflection, ISSV3 Node 9, analysis vs. test data.

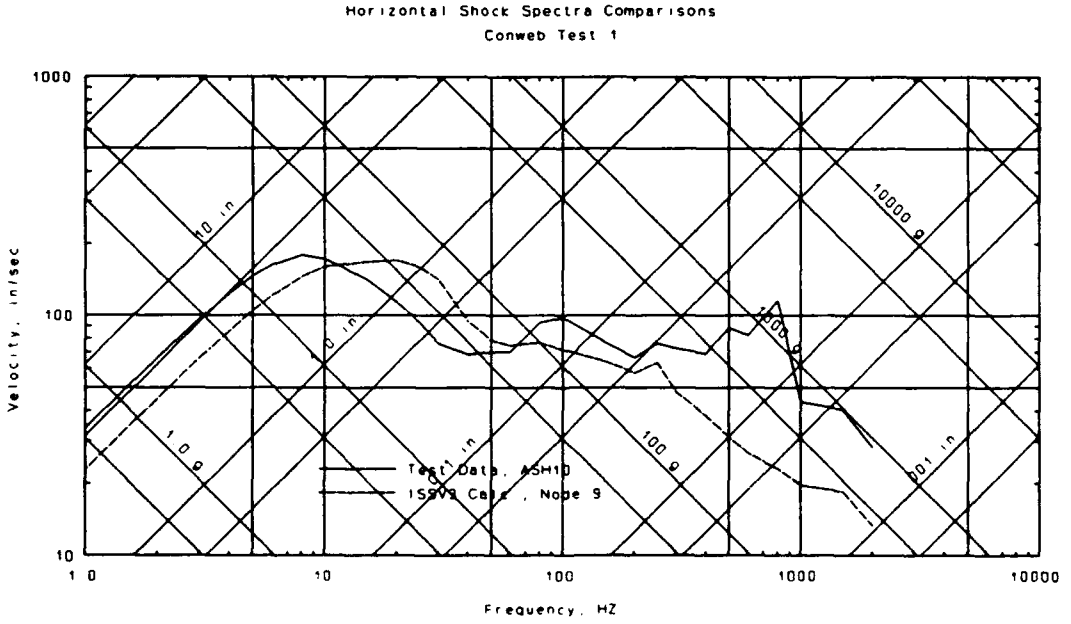

Figure 60. CONWEB 1, midfloor horizontal shock spectra, ISSV3 Node 9, analysis vs. test data.

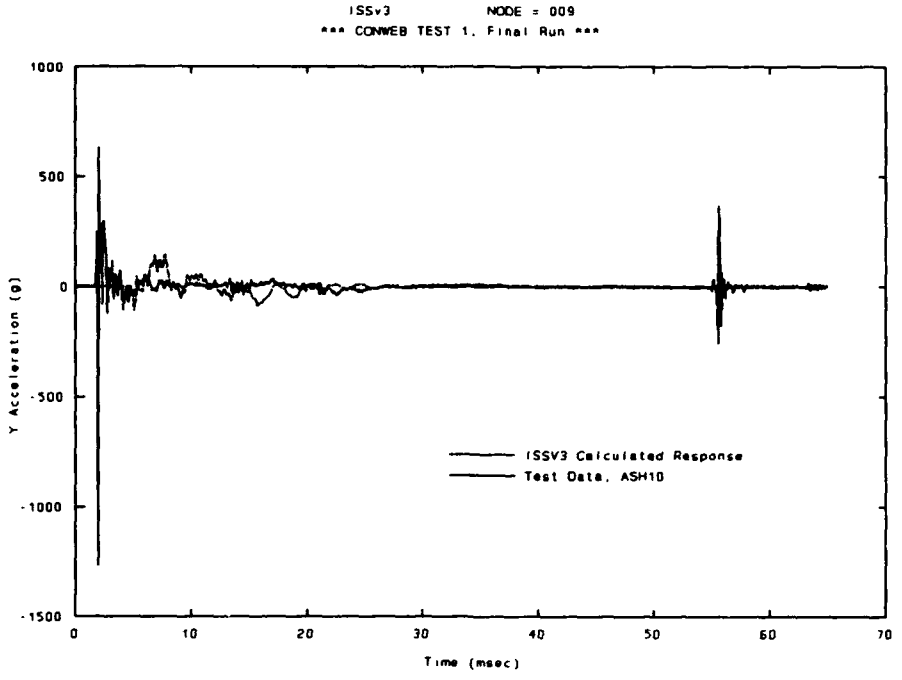

Figure 61. CONWEB 1, midfloor vertical acceleration, ISSV3 Node 9, analysis vs. test data.

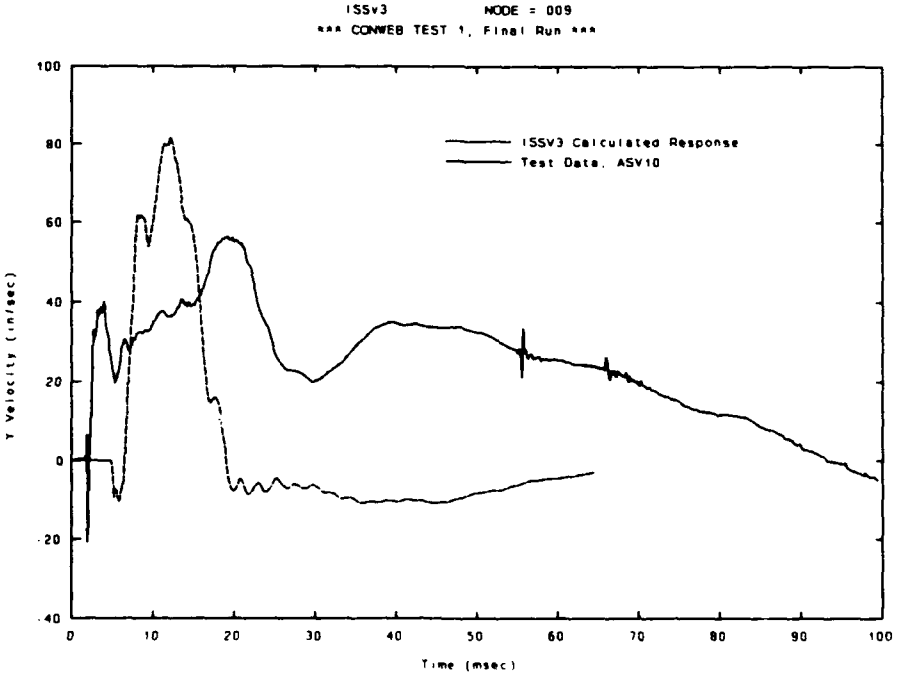

Figure 62. CONWEB 1, midfloor vertical velocity, ISSV3 Node 9, analysis vs. test data.

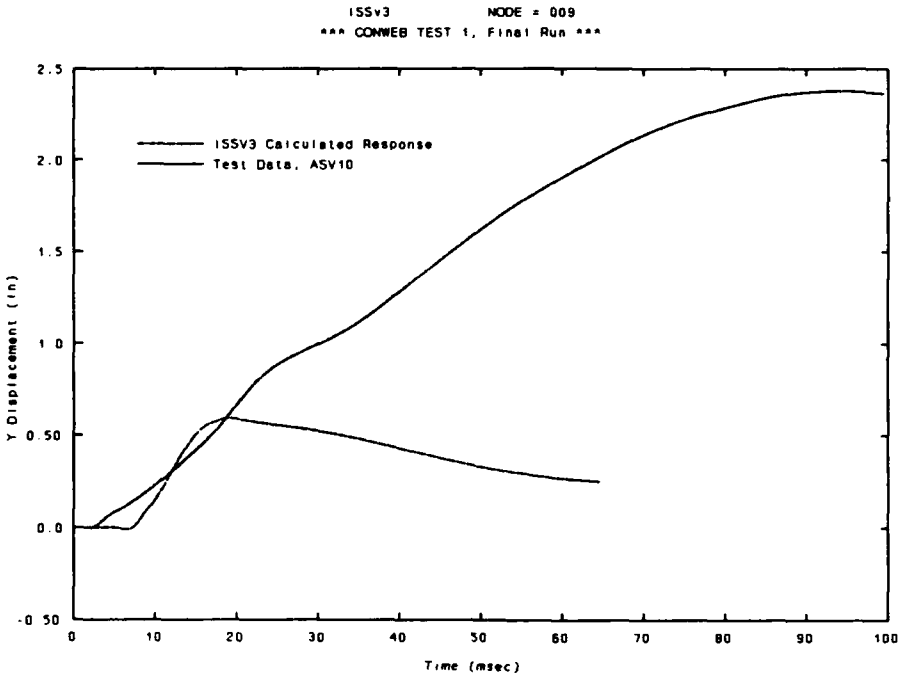

Figure 63. CONWEB 1, midfloor vertical deflection, ISSV3 Node 9, analysis vs. test data.

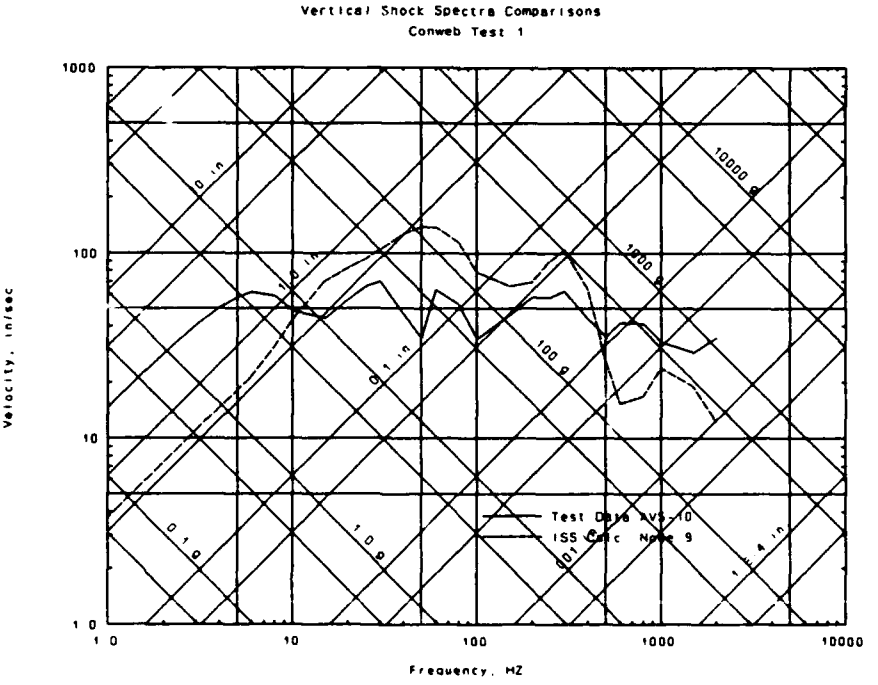

Figure 64. CONWEB 1, midfloor vertical shock spectra, ISSV3 Node 9, analysis vs. test data.

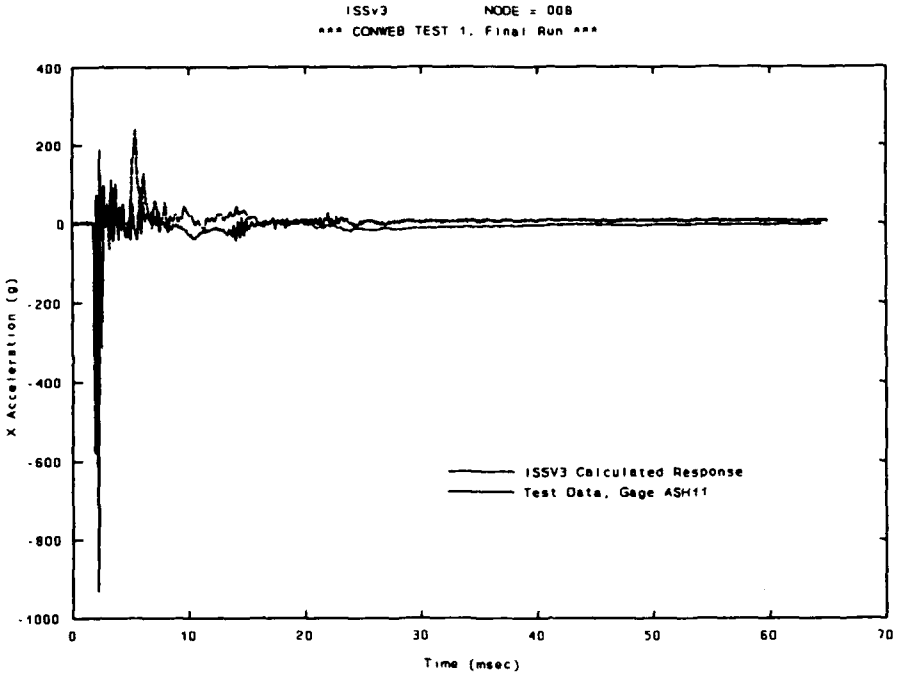

Figure 65. CONWEB 1, floor horizontal acceleration, ISSV3 Node 8, analysis vs. test data.

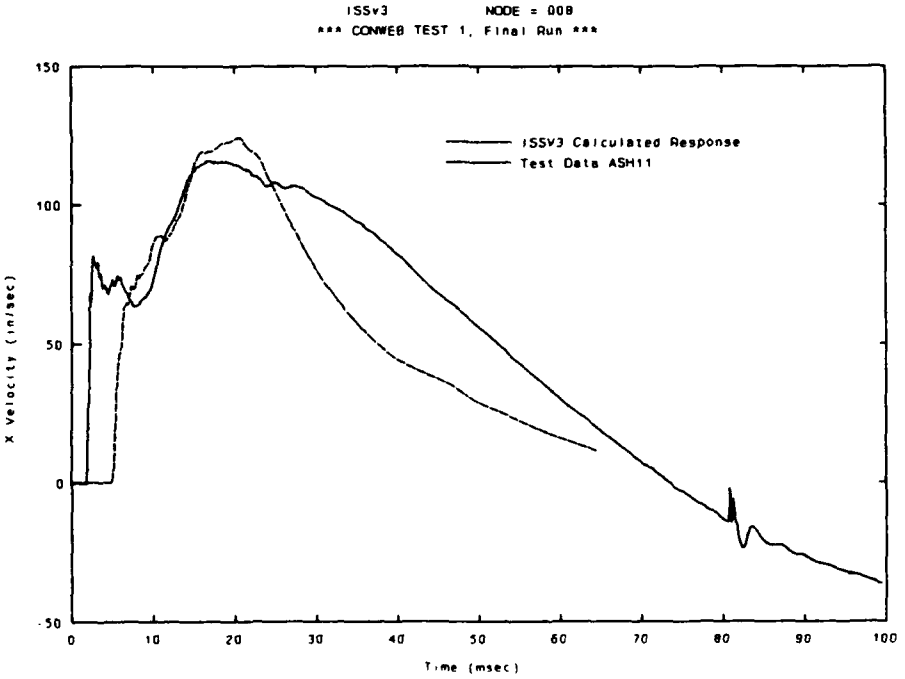

Figure 66. CONWEB 1, floor horizontal velocity, ISSV3 Node 8, analysis vs. test data.

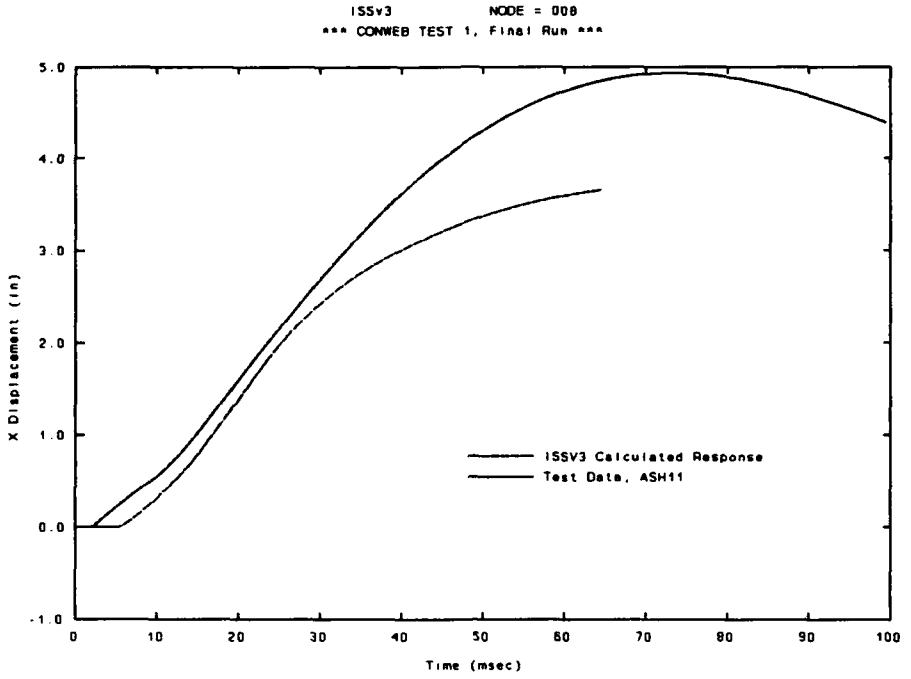

Figure 67. CONWEB 1, floor horizontal deflection, ISSV3 Node 8, analysis vs. test data.

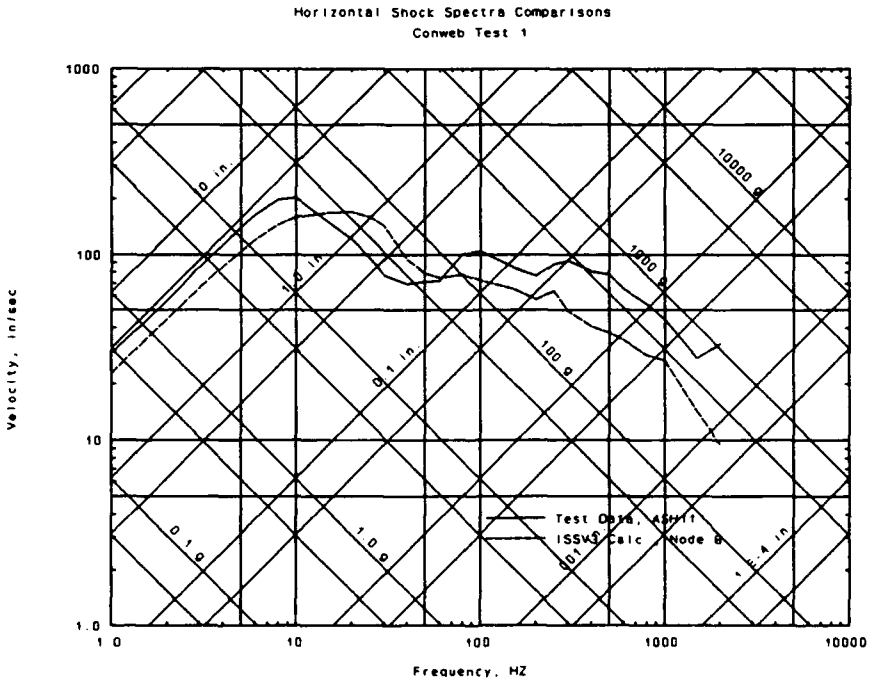

Figure 68. CONWEB 1, floor horizontal shock spectra, ISSV3 Node 8, analysis vs. test data.

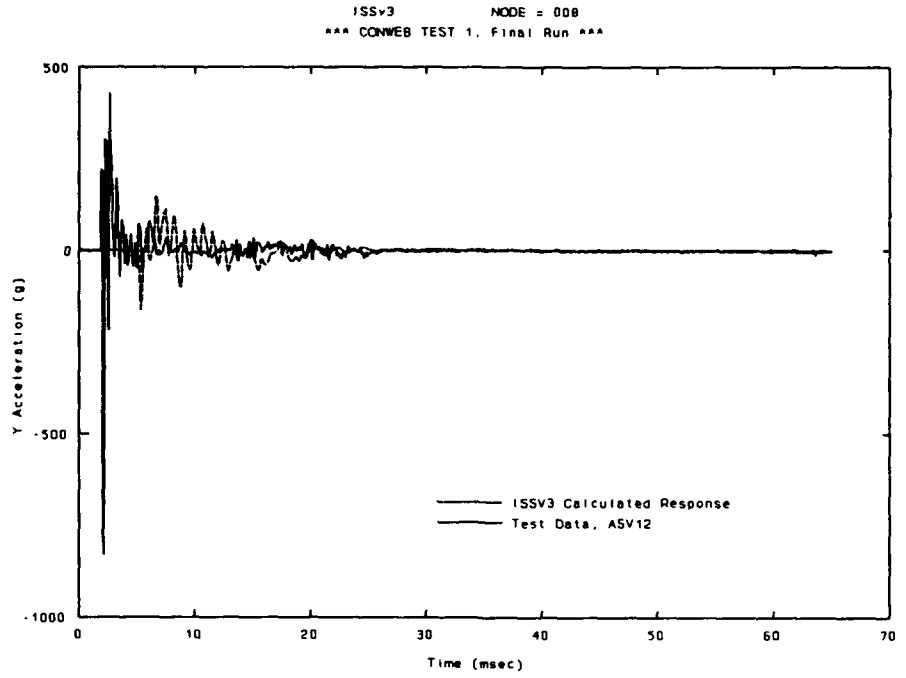

Figure 69. CONWEB 1, floor vertical acceleration, ISSV3 Node 8, analysis vs. test data.

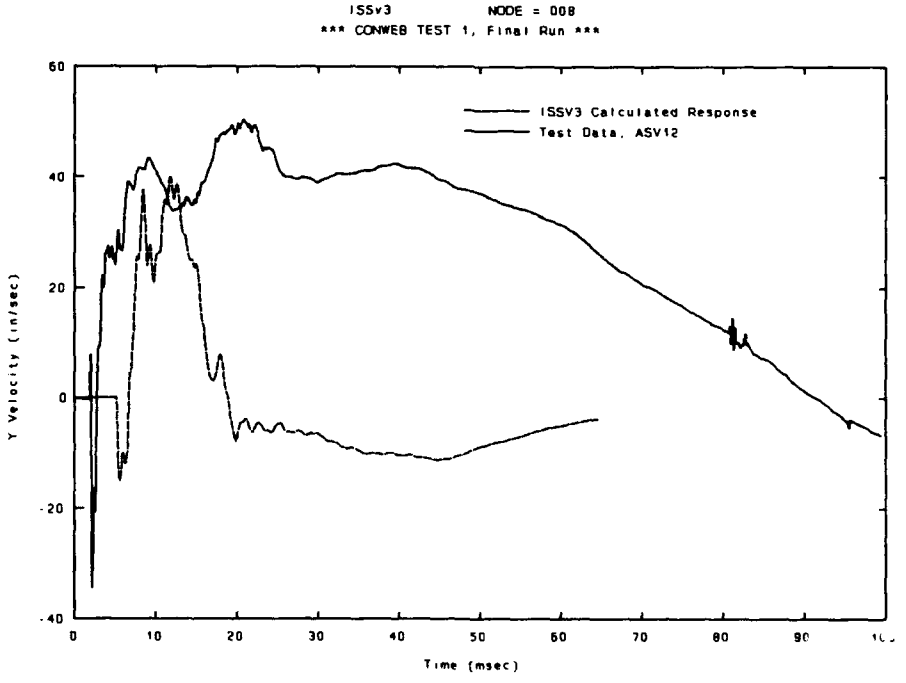

Figure 70. CONWEB 1, floor vertical velocity, ISSV3 Node 8, analysis vs. test data.

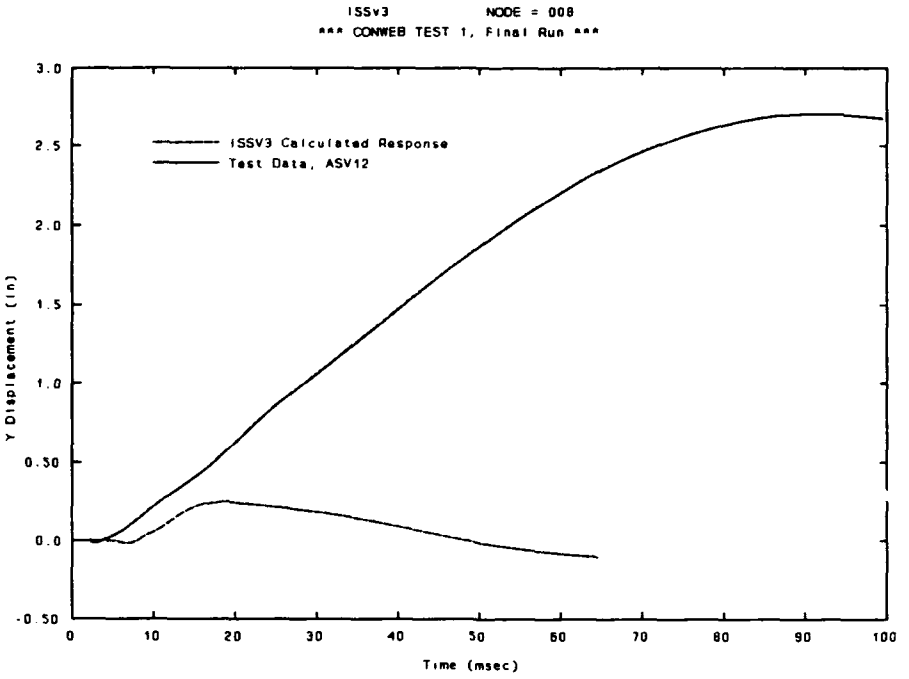

Figure 71. CONWEB 1, floor vertical deflection, ISSV3 Node 8, analysis vs. test data.

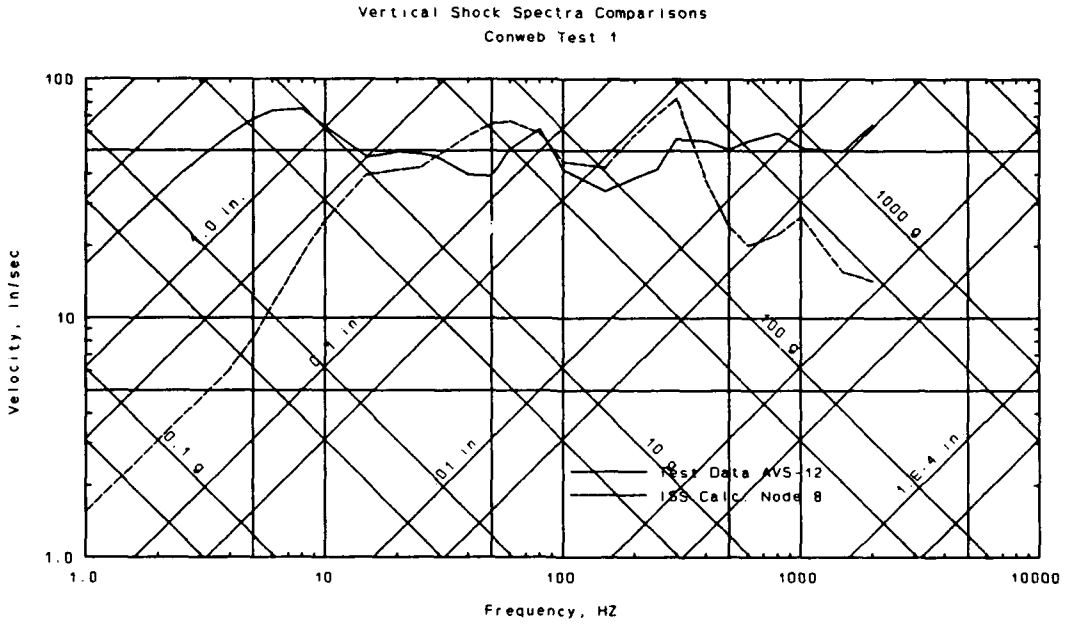

Figure 72. CONWEB 1, floor vertical shock spectra, ISSV3 Node 8, analysis vs. test data.

5.3.2 CONWEB 2 ANALYSIS.

As discussed above, CONWEB 2 was a test with the same clay backfill as in CONWEB 1. The test wall was twice as thick as in the other tests, with an L/d ratio of 5. The finite-element grid for the ISSV3 in-structure shock analysis of CONWEB 2 is shown in Figure 73. This grid is different from the one used for the calculation of CONWEB 1, 3, and 4, due to the different test wall. Section properties used in this analysis were shown in previously Table 8.

Results from the CONWEB 2 analysis are shown in Figure 74 to Figure 95. As in CONWEB 1, examination of the interface pressures show that the calculated time of arrival (t_a) of the load at the face of the structure lags the actual value by about 4 msec. Again, the shape and magnitude of the calculated interface stress compare very favorably with the test data, in spite of the strong relationship between t_a and free-field stress.

As before, all structural response data also lag by about 4 msec. Comparisons to test data of calculated acceleration, velocity, deflection histories, and shock spectra are shown in Figure 76 to Figure 95. Horizontal acceleration, velocity, and deflection histories were reproduced reasonably well by the ISSV3 analysis. The front wall response (Figure 76 to Figure 79) shows an overprediction of velocity and deflection response. Even here, examination of the late time horizontal velocity records show that ISSV3 under predicts the late-time velocity due to late-time clay backfill effects. On the whole, however, the calculated horizontal in-structure shock response compares very favorably with the test data throughout the structure, given the difficulty of measuring rigid-body displacements with accelerometers. CONWEB 2 vertical acceleration, velocity, and deflection histories were also reproduced reasonably well by the ISSV3 analysis. As in CONWEB 1 the small magnitudes of the vertical velocities and deflections cause the uncertainties in measurement of late-time motions to have a large relative effect. Given the uncertainties of these measurements, the magnitudes calculated for vertical velocity and deflection by ISSV3 are reasonable.

Shock spectra were generated from the velocity histories for each position in the structure. These spectra show a very good correlation between the calculated values and spectra generated for test data. As in CONWEB 1 the only consistent underprediction was for the rigid-body deflection as seen on

the low-frequency portion of the spectra. Again, this underprediction is thought to be due to a combination of the problem with the modeling of clay backfill in the analysis, and the problem of measuring late-time motions with accelerometers. The front wall response was slightly over-predicted, which implies that the model of the wall was softer than in the actual test. The modeling of the front wall as a one-way slab, neglecting all two-way effects, could account for this relatively minor effect. Also, the fact that this phenomenon did not occur in the thinner test wall in CONWEB 1 seems to imply that the difference is due to the relative importance of shear response for the thicker CONWEB 2 wall. However, it will be seen later that the response of the thin walls in CONWEB 3 and 4 was overpredicted, which does not support this hypothesis. Shear response is not modeled in the current version of the ISSV3 program.

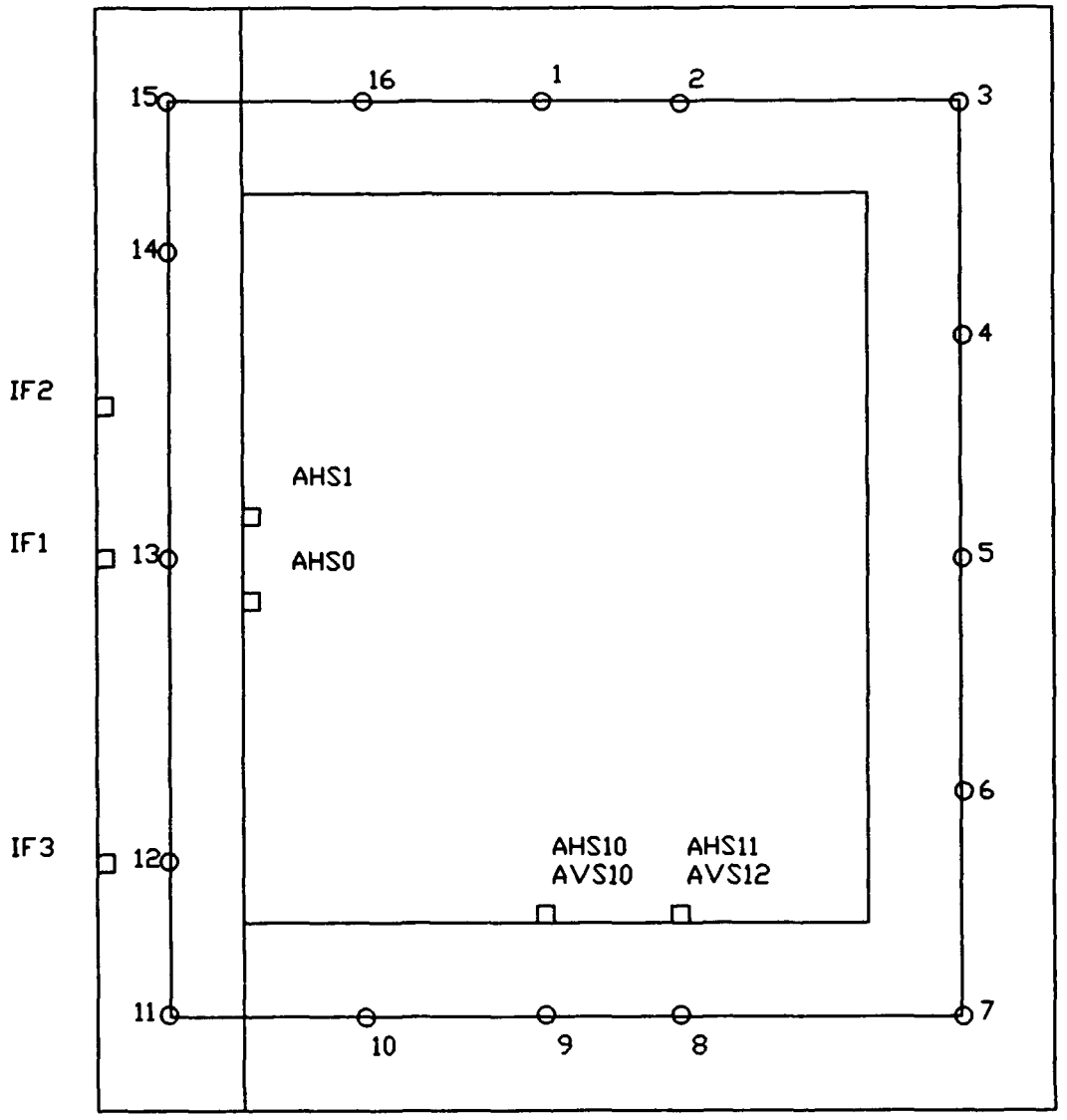

Figure 73. CONWEB 2, ISSV3 finite-element grid superimposed on structure cross section.

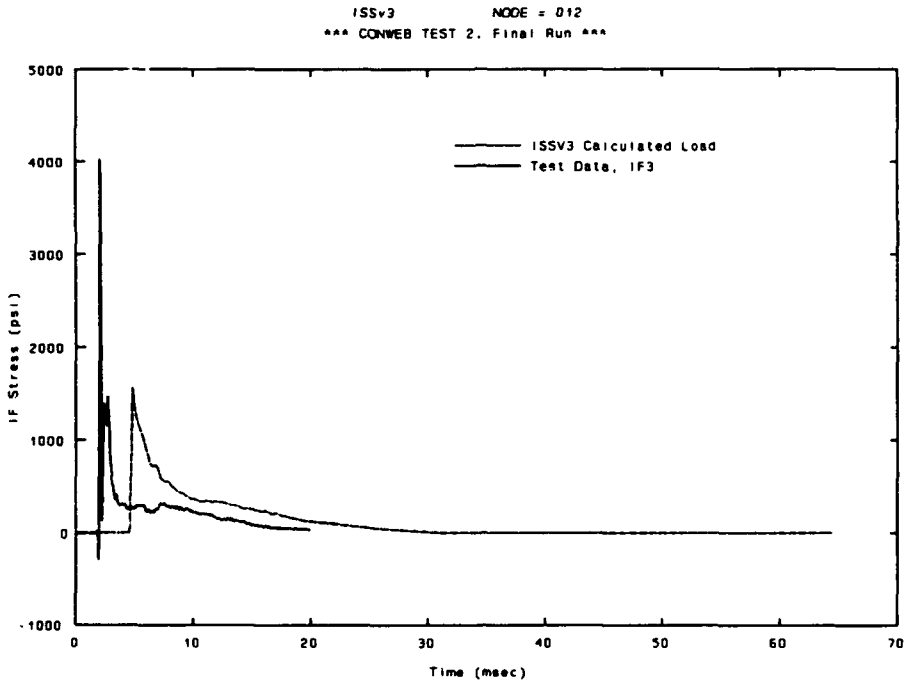

Figure 74. CONWEB 2, lower wall interface pressure load, ISSV3 Node 12, analysis vs. test data.

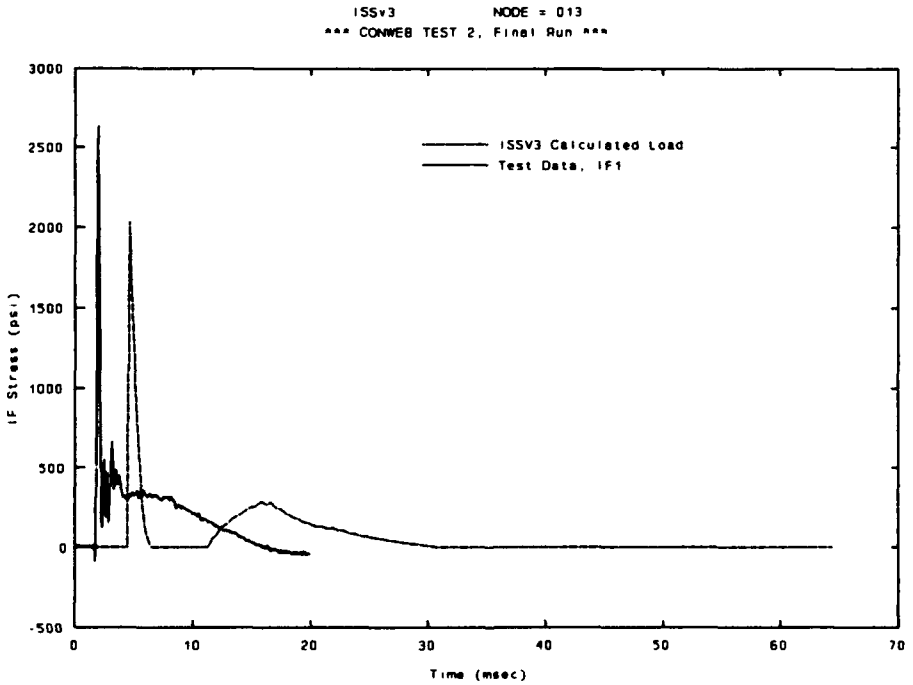

Figure 75. CONWEB 2, midwall interface pressure load, ISSV3 Node 13, analysis vs. test data.

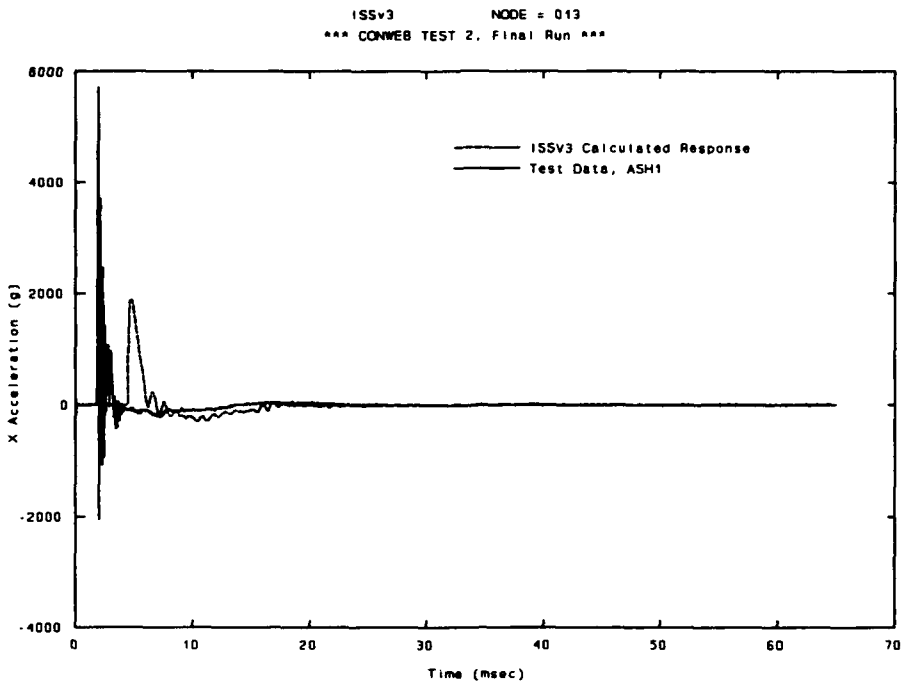

Figure 76. CONWEB 2, midwall horizontal acceleration, ISSV3 Node 13, analysis vs. test data.

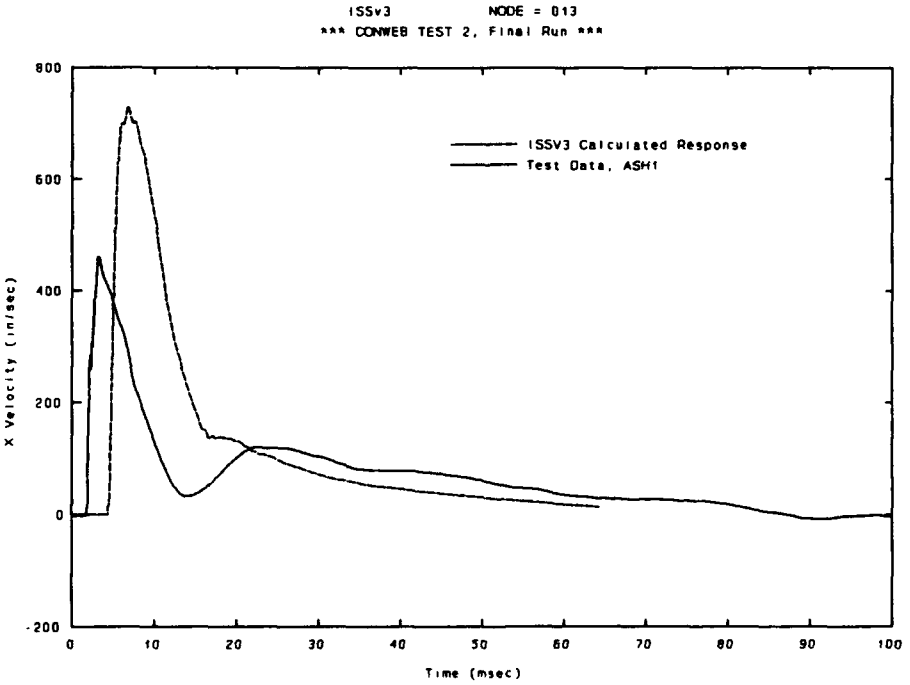

Figure 77. CONWEB 2, midwall horizontal velocity, ISSV3 Node 13, analysis vs. test data.

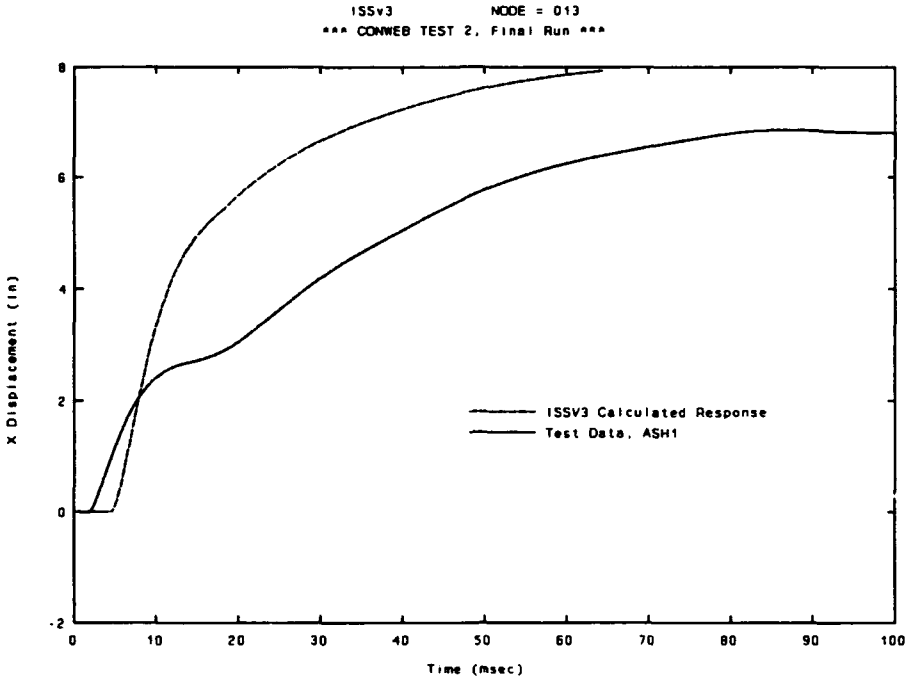

Figure 78. CONWEB 2, midwall horizontal deflection, ISSV3 Node 13, analysis vs. test data.

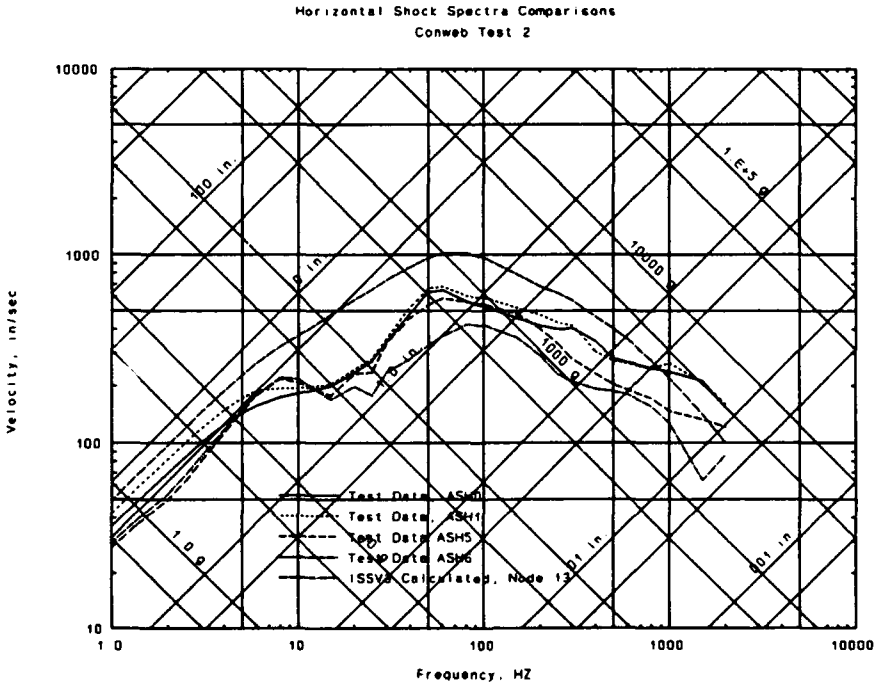

Figure 79. CONWEB 2, midwall horizontal shock spectra, ISSV3 Node 13, analysis vs. test data.

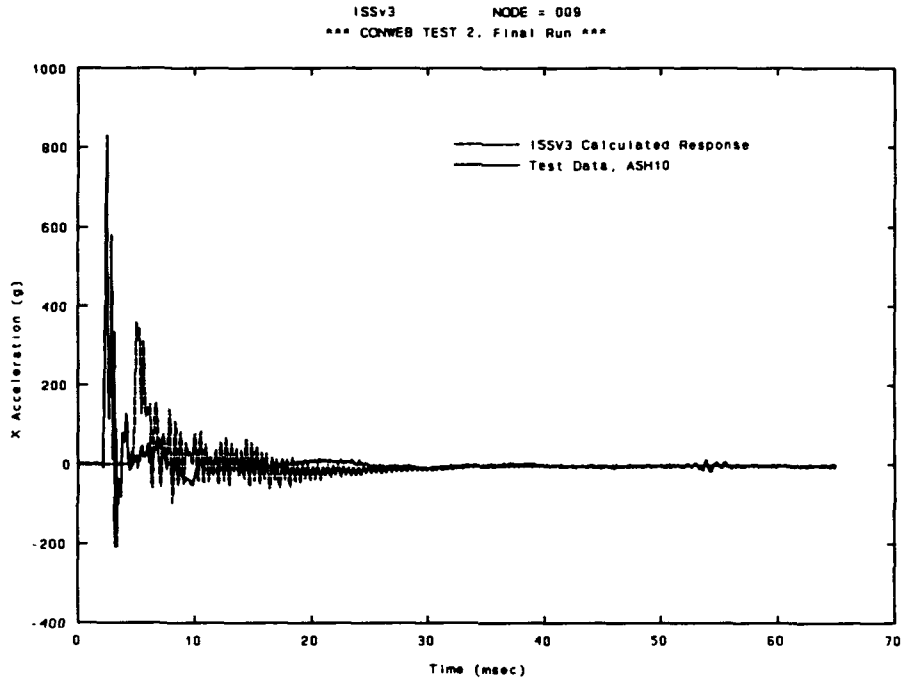

Figure 80. CONWEB 2, midfloor horizontal acceleration, ISSV3 Node 9, analysis vs. test data.

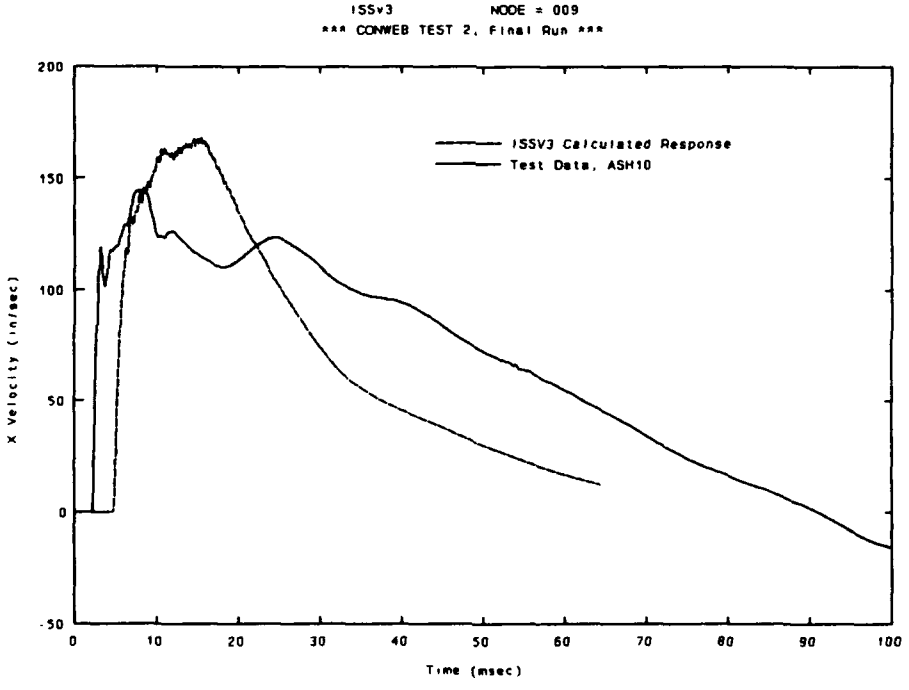

Figure 81. CONWEB 2, midfloor horizontal velocity, ISSV3 Node 9, analysis vs. test data.

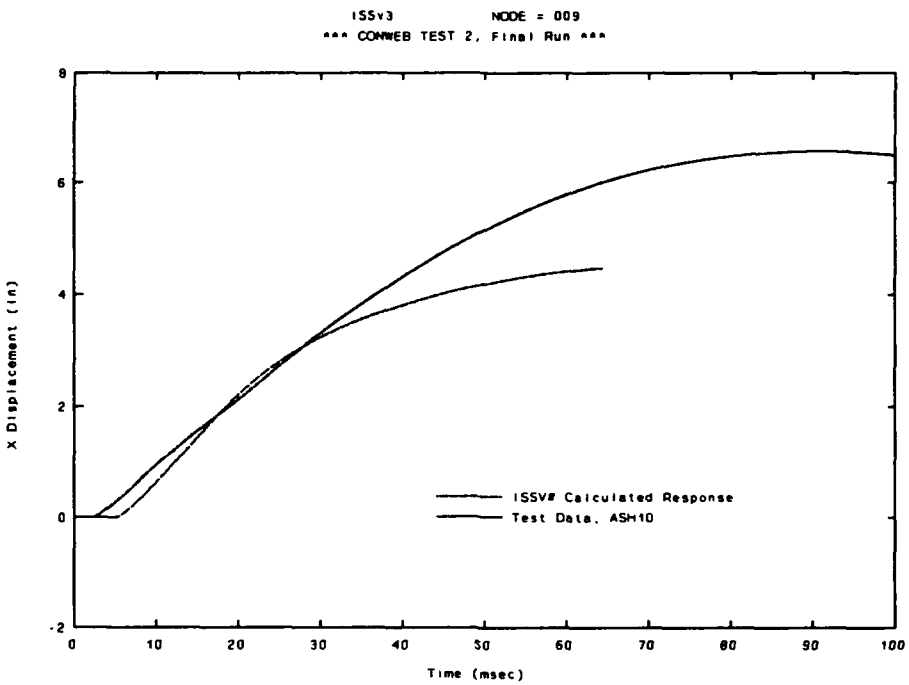

Figure 82. CONWEB 2, midfloor horizontal deflection, ISSV3 Node 9, analysis vs. test data.

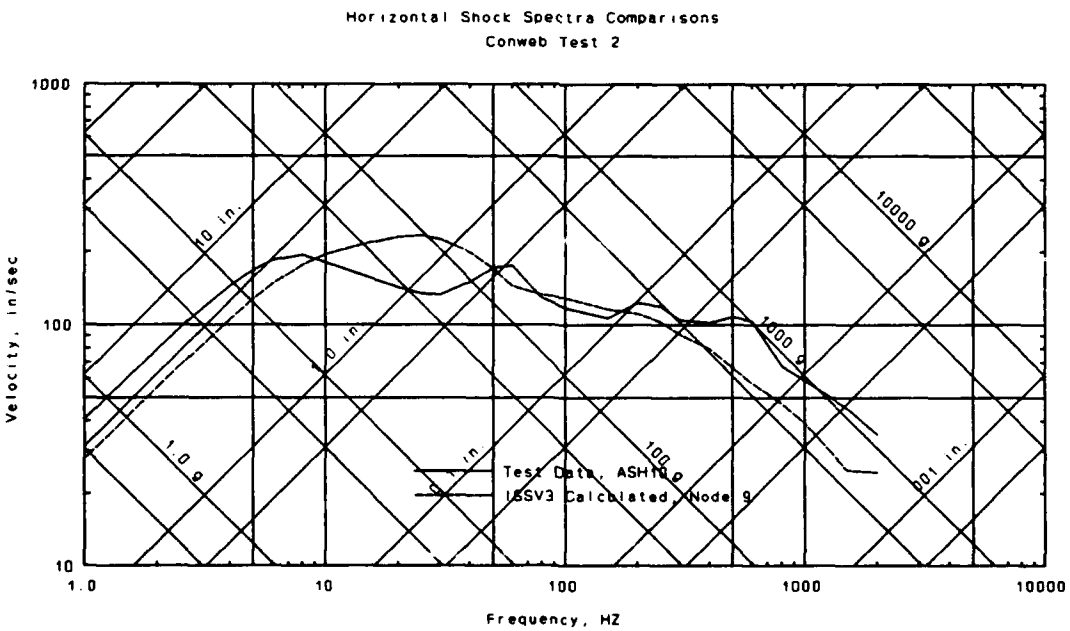

Figure 83. CONWEB 2, midfloor horizontal shock spectra, ISSV3 Node 9, analysis vs. test data.

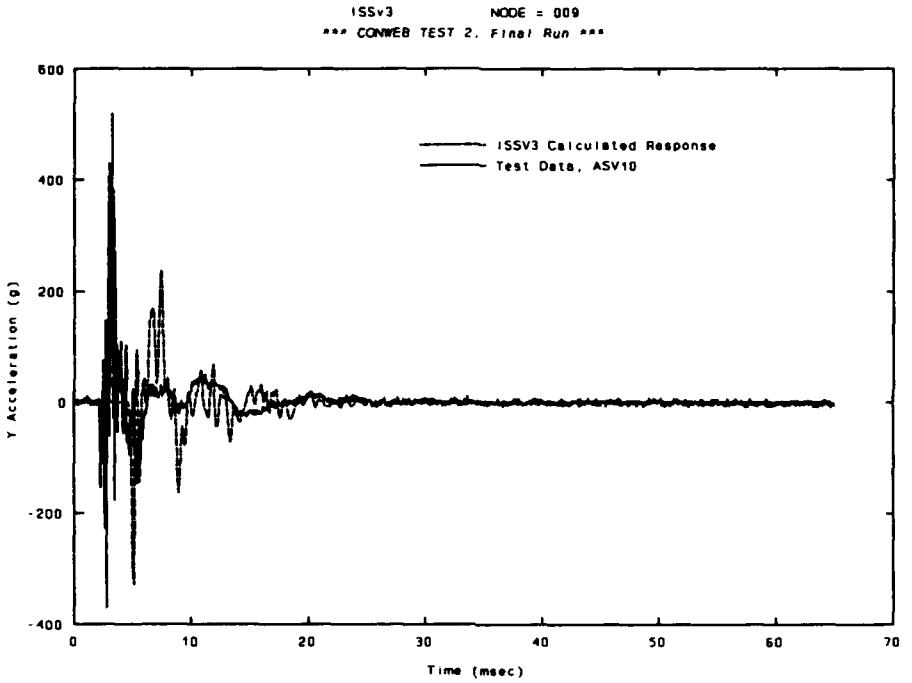

Figure 84. CONWEB 2, midfloor vertical acceleration, ISSV3 Node 9, analysis vs. test data.

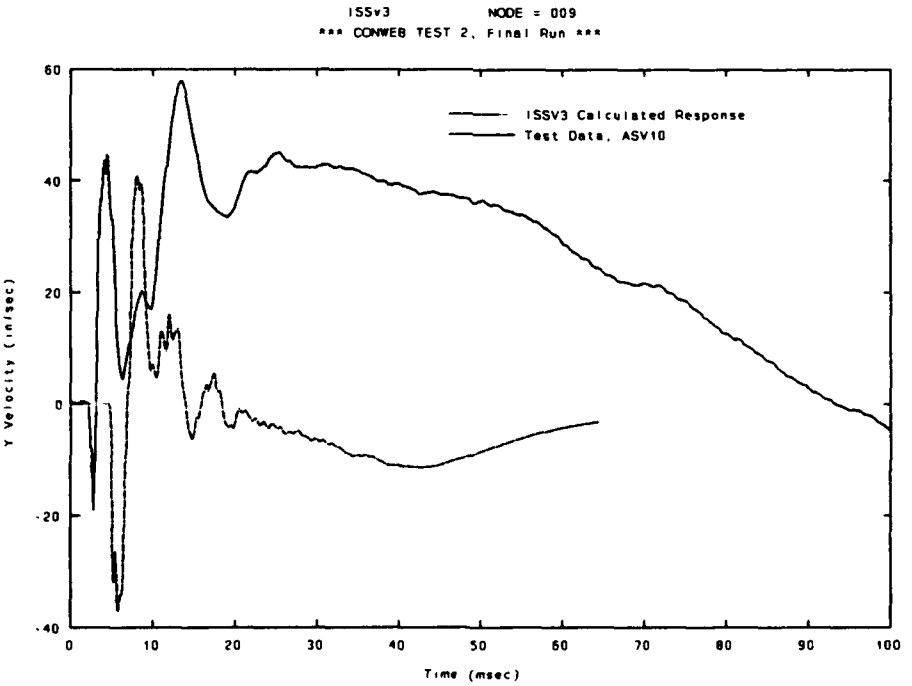

Figure 85. CONWEB 2, midfloor vertical velocity, ISSV3 Node 9, analysis vs. test data.

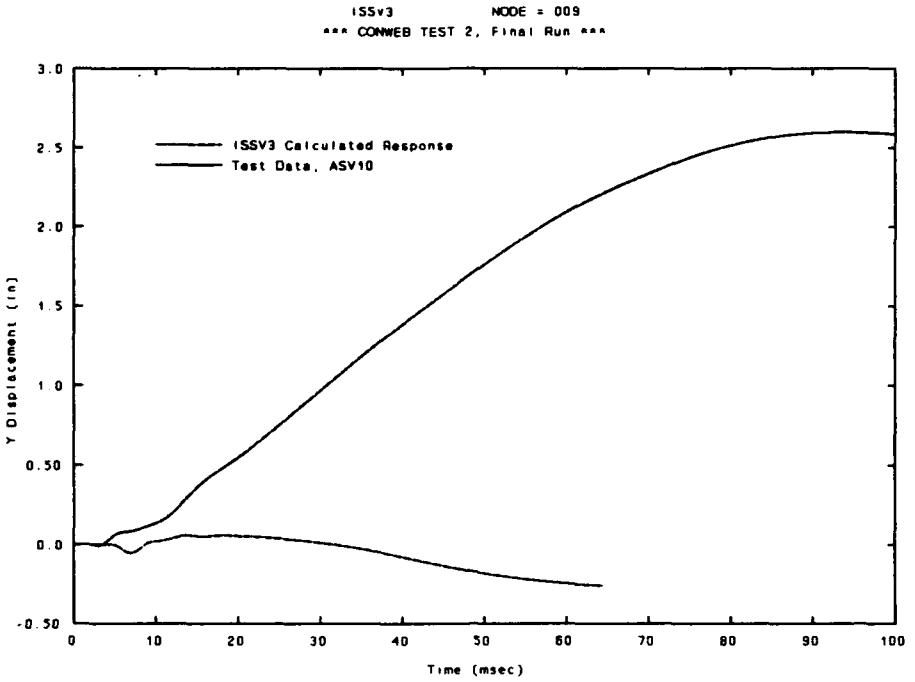

Figure 86. CONWEB 2, midfloor vertical deflection, ISSV3 Node 9, analysis vs. test data.

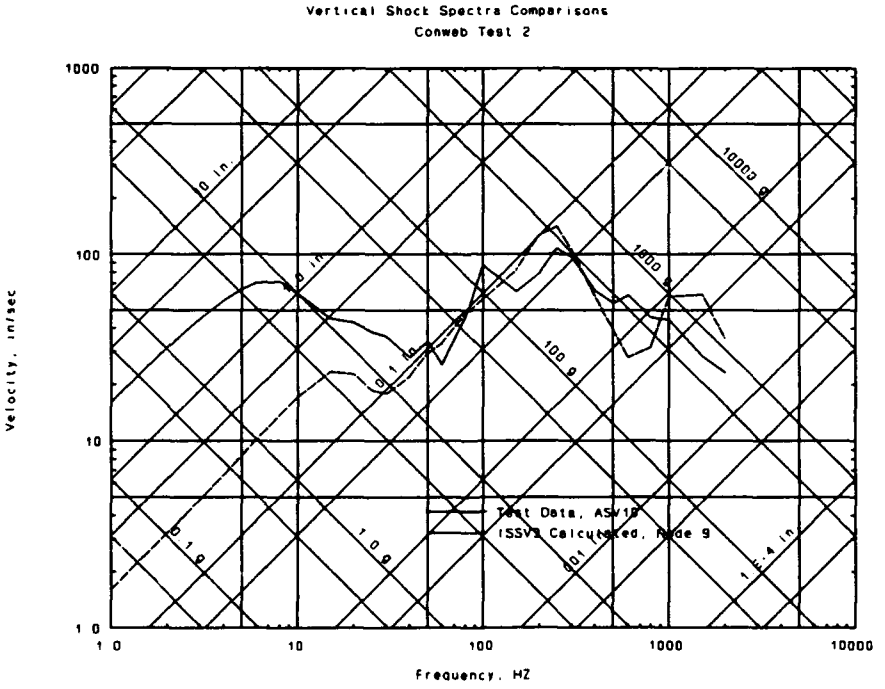

Figure 87. CONWEB 2, midfloor vertical shock spectra, ISSV3 Node 9, analysis vs. test data.

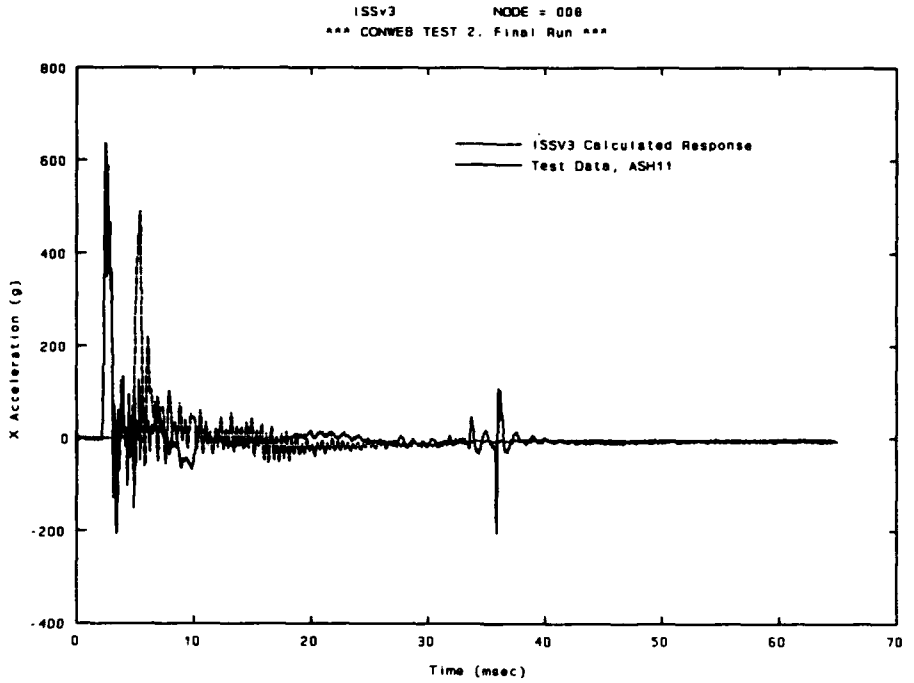

Figure 88. CONWEB 2, floor horizontal acceleration, ISSV3 Node 8, analysis vs. test data.

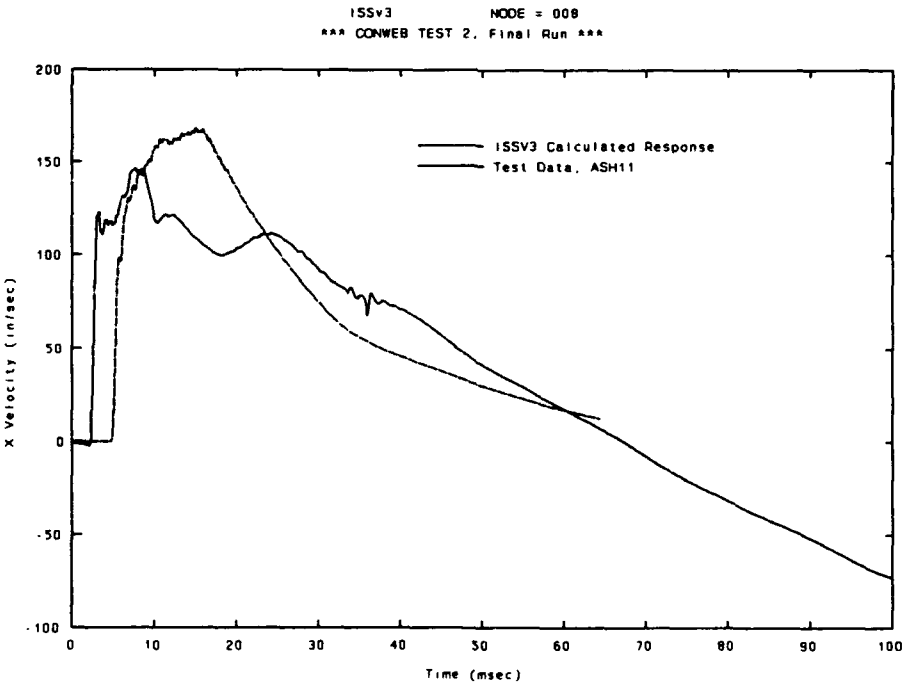

Figure 89. CONWEB 2, floor horizontal velocity, ISSV3 Node 8, analysis vs. test data.

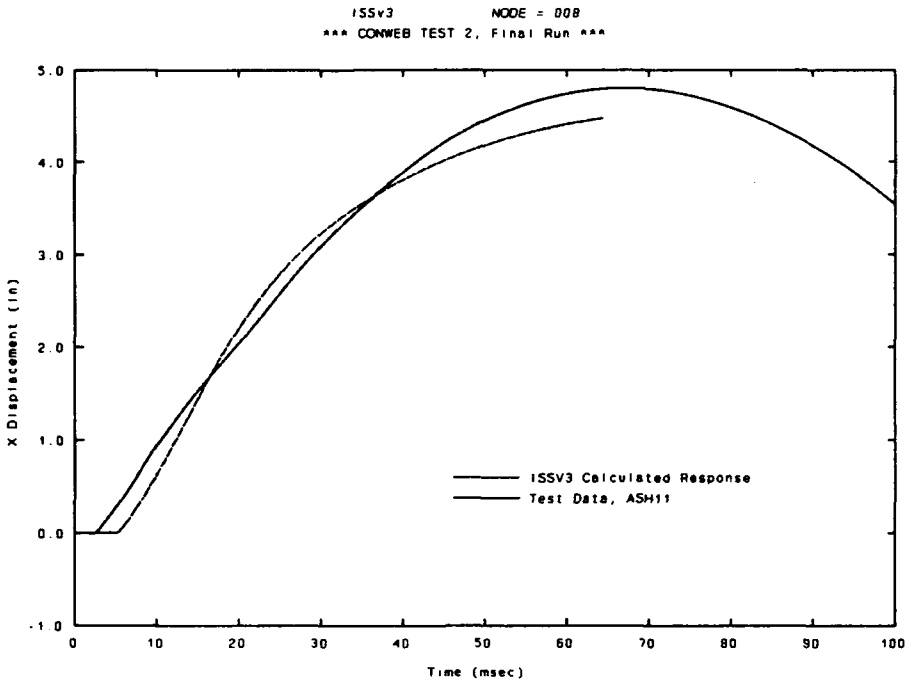

Figure 90. CONWEB 2, floor horizontal deflection, ISSV3 Node 8, analysis vs. test data.

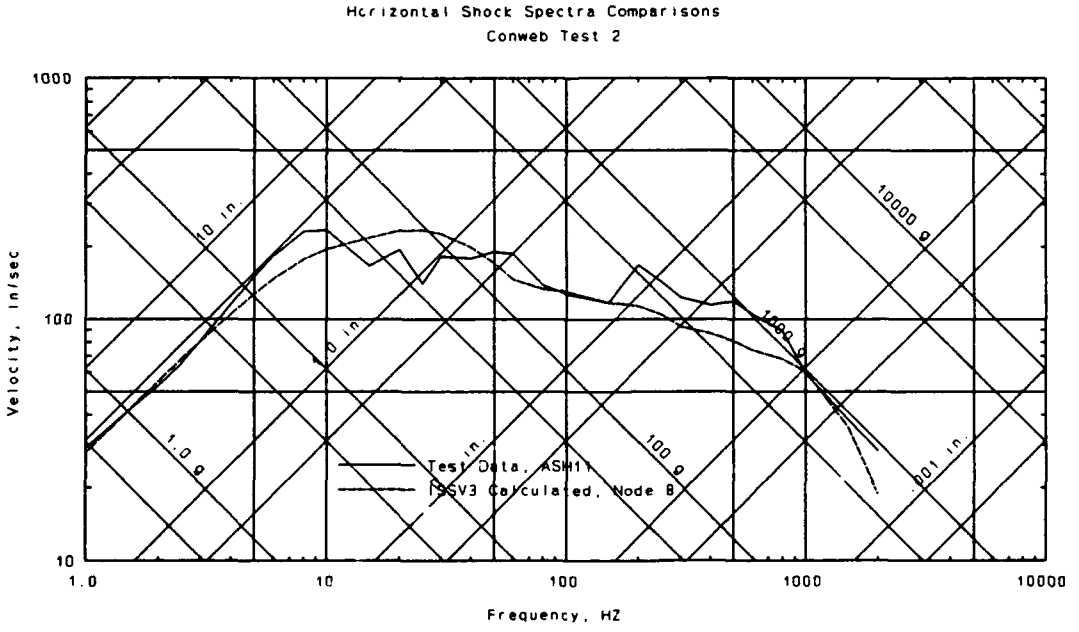

Figure 91. CONWEB 2, floor horizontal shock spectra, ISSV3 Node 8, analysis vs. test data.

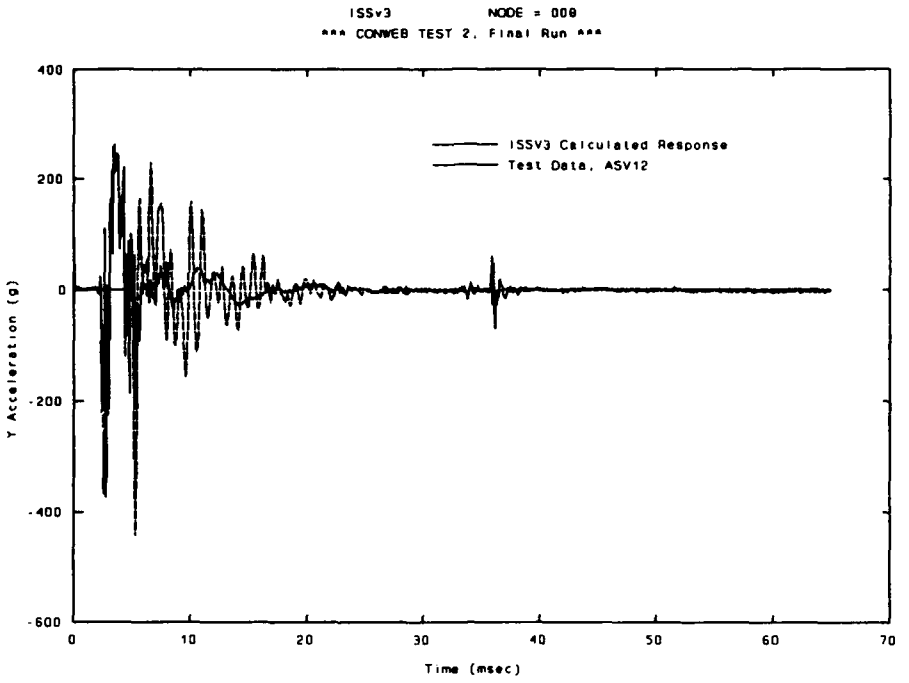

Figure 92. CONWEB 2, floor vertical acceleration, ISSV3 Node 8, analysis vs. test data.

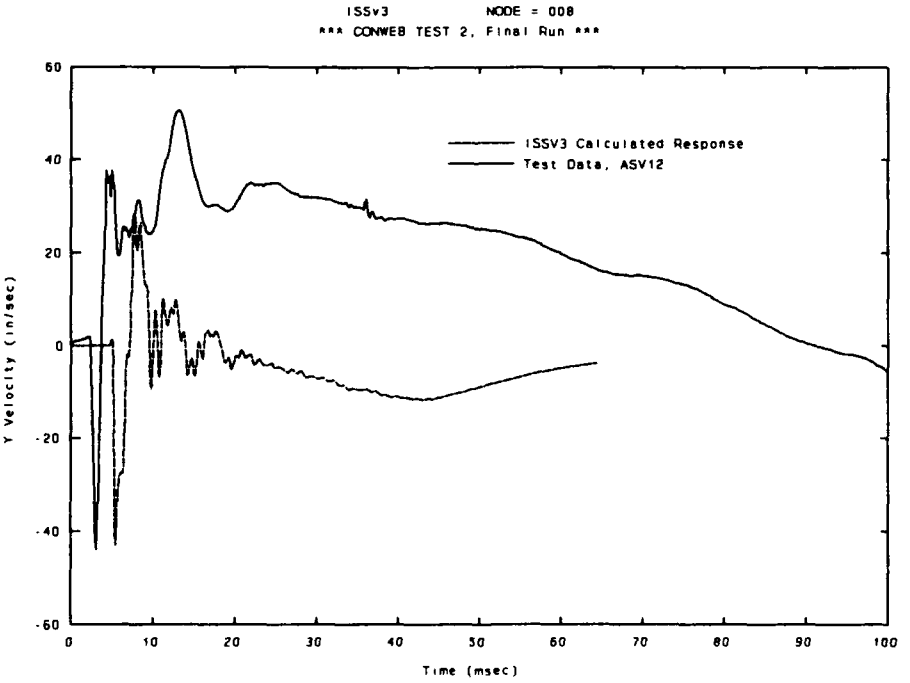

Figure 93. CONWEB 2, floor vertical velocity, ISSV3 Node 8, analysis vs. test data.

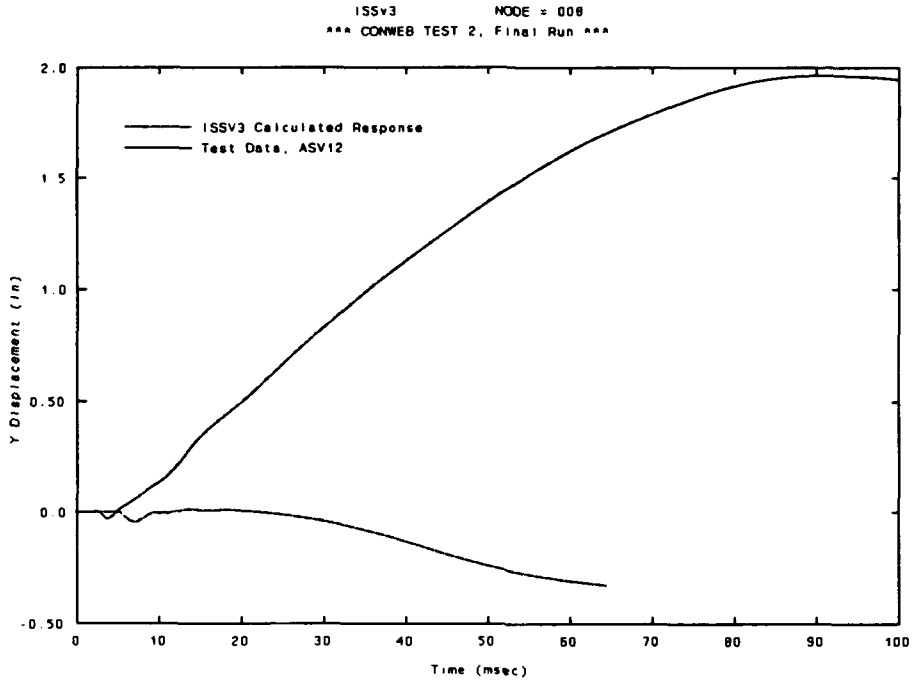

Figure 94. CONWEB 2, floor vertical deflection, ISSV3 Node 8, analysis vs. test data.

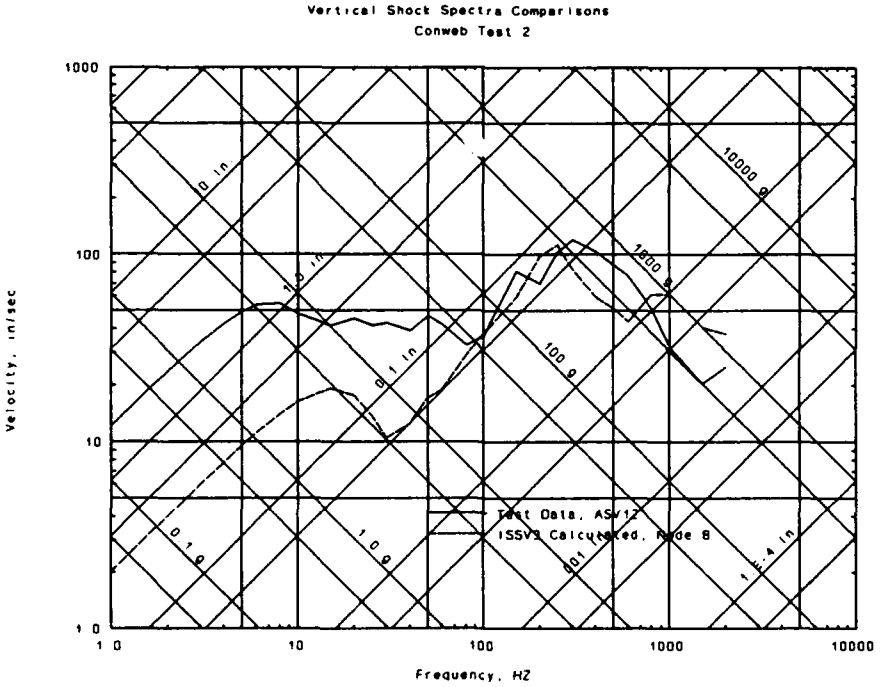

Figure 95. CONWEB 2, floor vertical shock spectra, ISSV3 Node 8, analysis vs. test data.

5.3.3 CONWEB 3 ANALYSIS.

CONWEB 3 was a test with the same structure as in CONWEB 1 and 4, the test wall had the same thickness, with an L/d ratio of 10. In CONWEB 3 a sand backfill was used. The finite-element grid for the ISSV3 in-structure analysis of CONWEB 3 is shown in Figure 50. This same grid was used for the calculation of CONWEB 1 and 4, with modifications to the backfill properties. Section properties used were shown previously in Table 8, and backfill properties were shown in Table 1.

CONWEB 3 analysis results are presented in Figure 96 to Figure 117. As in CONWEB 1, comparison of the interface pressures once again shows that the calculated time of arrival (t_a) of the load at the face of the structure lags the actual value by about 4 msec. Again, the shape and magnitude of the calculated interface stress at the center of the wall (Figure 97) compare favorably with the test data. Figure 96 shows the interface pressure measured on the lower part of the test wall and illustrates an interesting effect of the dynamic loading of buried structures in sands. This effect, known as soil arching, results from the redistribution of interface loads from the center of a loaded span to the supports. The current free-field model in ISSV3 does not include this effect, but this should have only minor impact on the overall in-structure shock response.

As before, all the data comparisons for structural response also lag by about 4 msec due to the loading t_a. Comparisons to test data of calculated acceleration, velocity, deflection histories, and shock spectra are shown in Figure 98 to Figure 117. Horizontal acceleration, velocity, and deflection histories were reproduced reasonably well by the ISSV3 analysis. There is no evidence of the underprediction of late time velocity in this sand backfill test. This lends credence to the hypothesis that the late-time velocity underpredictions in CONWEB 1 and 2 were due to flow effects in the clay backfill.

As in CONWEB 2, the front wall response (Figure 98 to Figure 101) shows an overprediction of velocity and deflection response. Given that the acceleration history compares very well at this location, the overprediction of velocity and deflection implies that the model of the front wall is softer than the actual wall. On the whole, however, the calculated horizontal in-

structure shock response compares favorably with test data throughout the structure.

CONWEB 3 vertical acceleration, velocity and deflection histories were also reproduced reasonably well by the ISSV3 analysis. The magnitudes of the vertical velocities and deflections were even smaller than in CONWEB 1 and 2, causing the uncertainties in measurement of late-time motions to have an even larger relative effect. Given the uncertainties of these measurements, the magnitudes calculated for vertical velocity and deflection by ISSV3 are reasonable.

Shock spectra were generated from the velocity histories for each position in the structure. These spectra show a good correlation between the calculated values and spectra generated for test data. Rigid-body deflection as seen on the low-frequency portion of the spectra was not underpredicted for this sand backfill test as it was for clay backfill tests in CONWEB 1 and 2. This indicates that the underprediction in CONWEB 1 and 2 was due to the problem with the modeling late time-flow effects of the clay backfill.

As discussed above, the front wall response was slightly overpredicted, a result that implies that the wall model was softer than the actual wall. The modeling of the front wall as a one-way slab neglecting all two-way effects could account for this relatively minor effect. The fact that this phenomenon occurred with this thin test wall implies that the difference may not be due to the relative importance of shear response for the thick vs. thin wall as was hypothesized in the CONWEB 2 discussion.

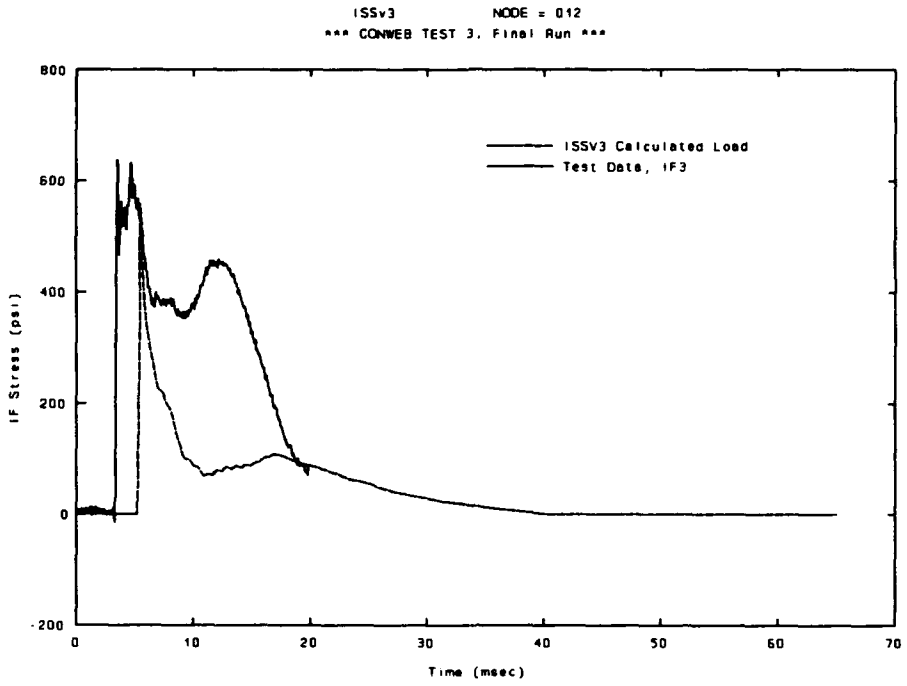

Figure 96. CONWEB 3, lower wall interface pressure load, ISSV3 Node 12, analysis vs. test data.

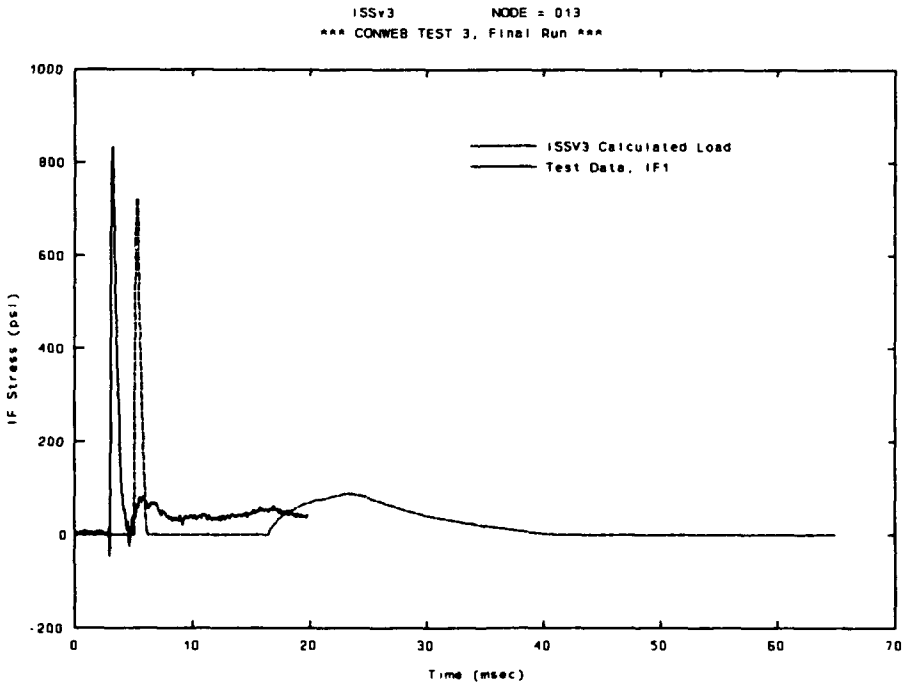

Figure 97. CONWEB 3, midwall interface pressure load, ISSV3 Node 13, analysis vs. test data.

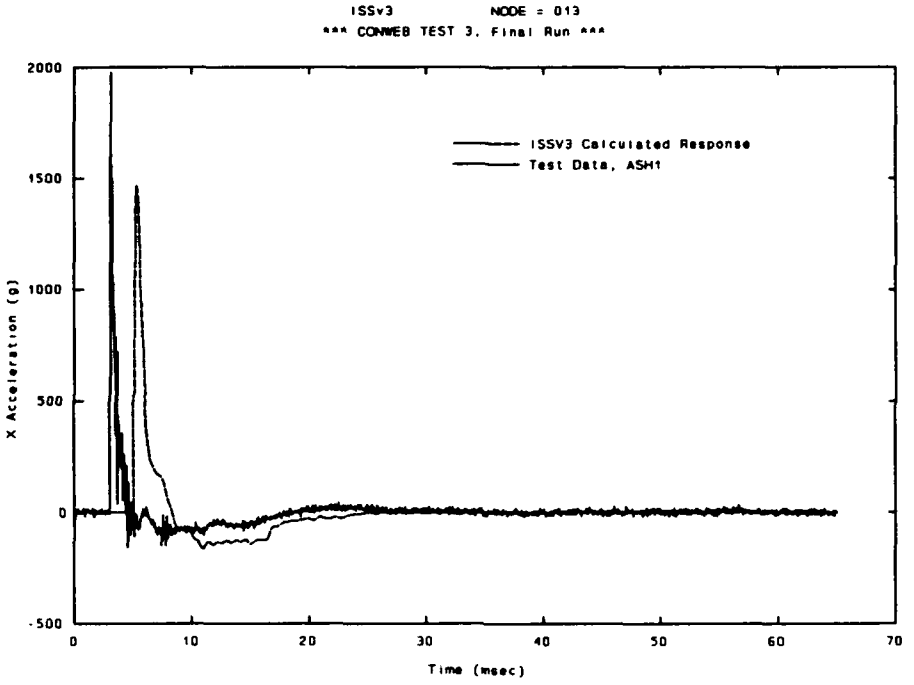

Figure 98. CONWEB 3, midwall horizontal acceleration, ISSV3 Node 13, analysis vs. test data.

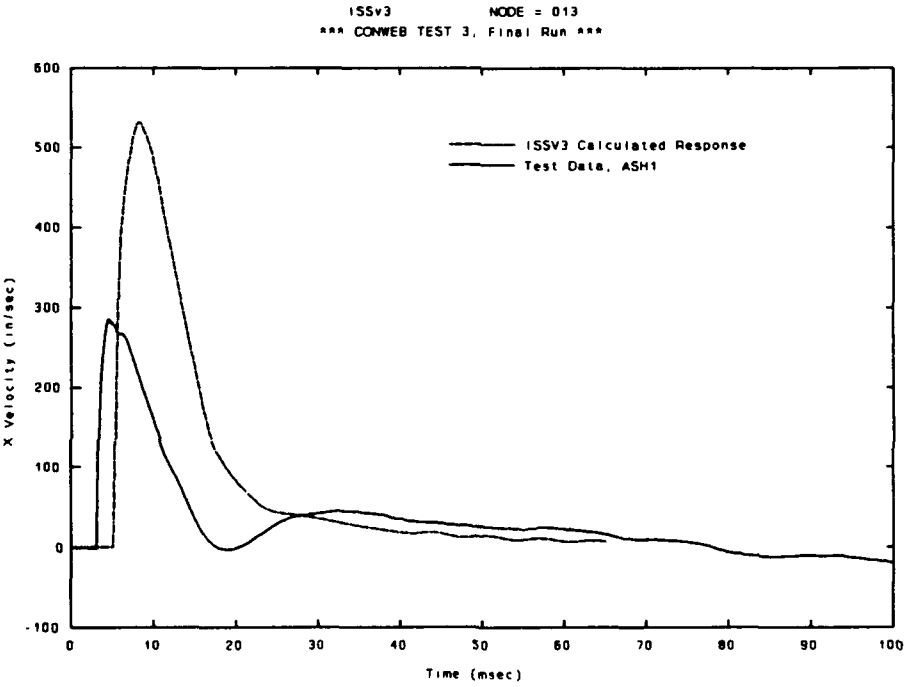

Figure 99. CONWEB 3, midwall horizontal velocity, ISSV3 Node 13, analysis vs. test data.

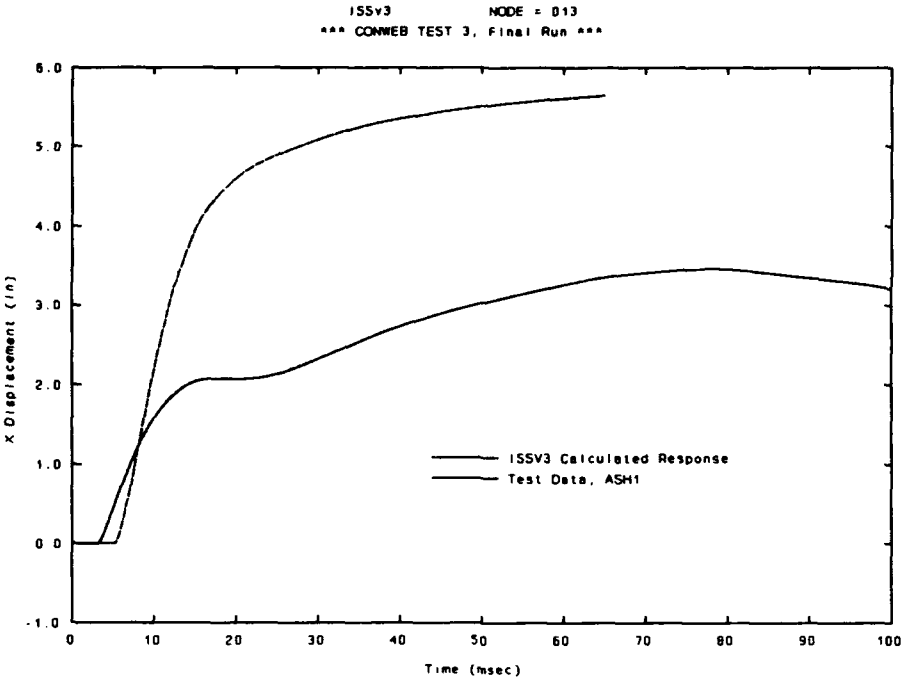

Figure 100. CONWEB 3, midwall horizontal deflection, ISSV3 Node 13, analysis vs. test data.

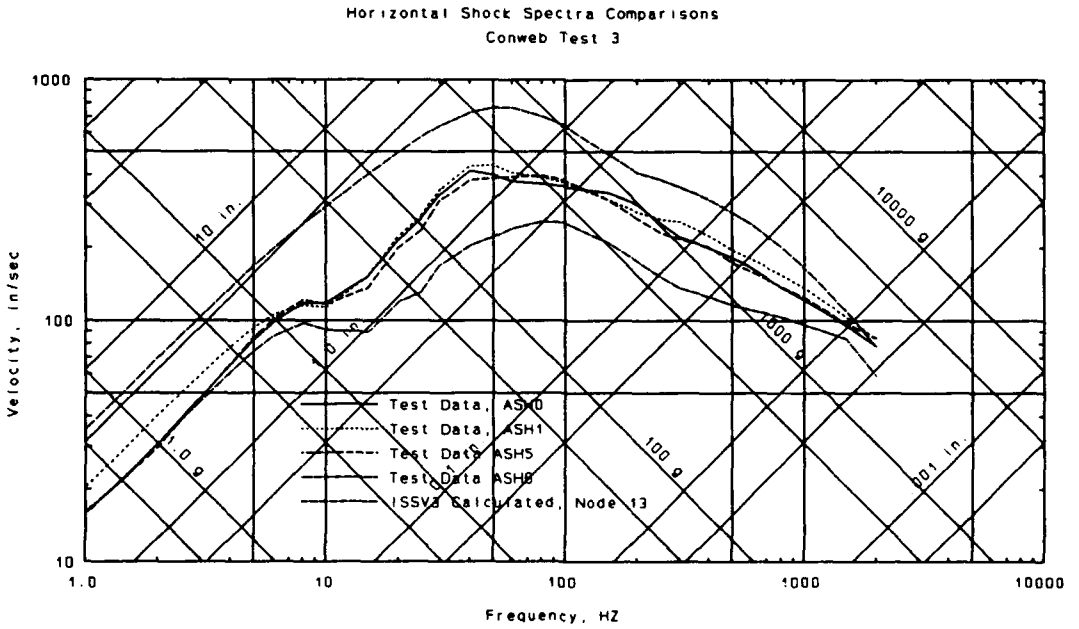

Figure 101. CONWEB 3, midwall horizontal shock Spectra, ISSV3 Node 13, analysis vs. test data.

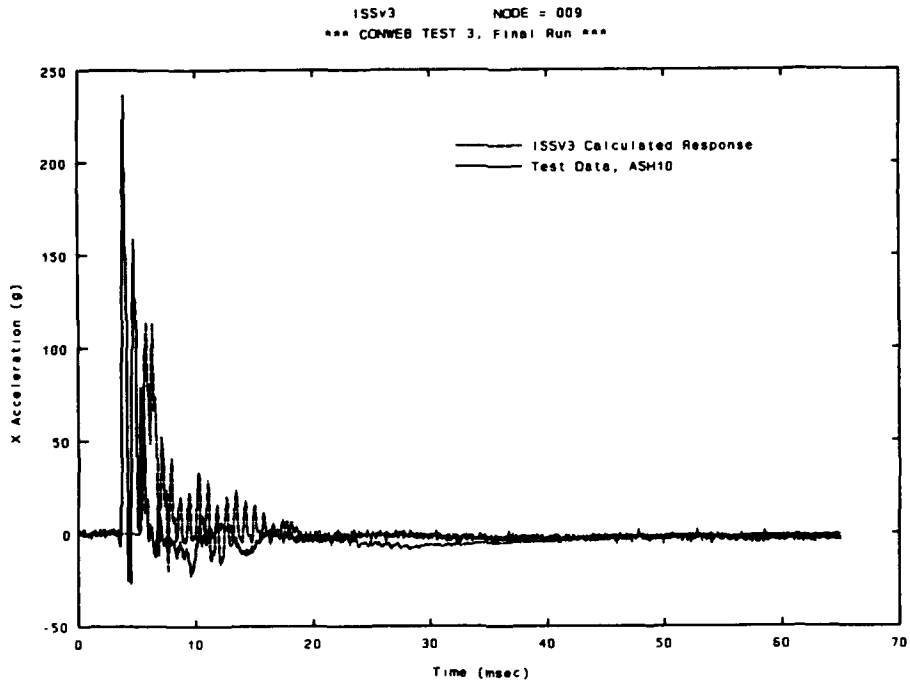

Figure 102. CONWEB 3, midfloor horizontal acceleration, ISSV3 Node 9, analysis vs. test data.

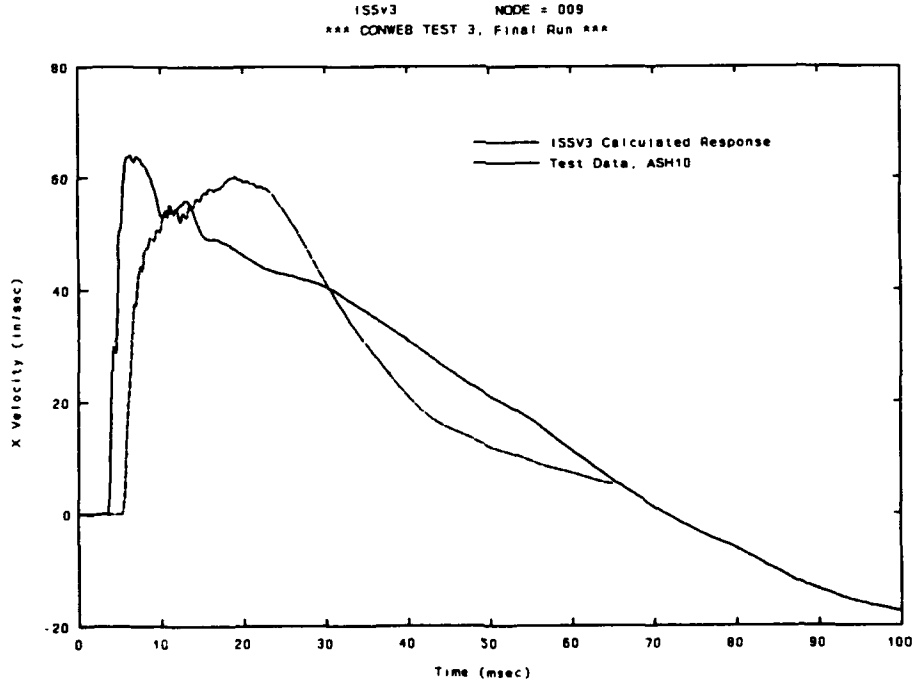

Figure 103. CONWEB 3, midfloor horizontal velocity, ISSV3 Node 9, analysis vs. test data.

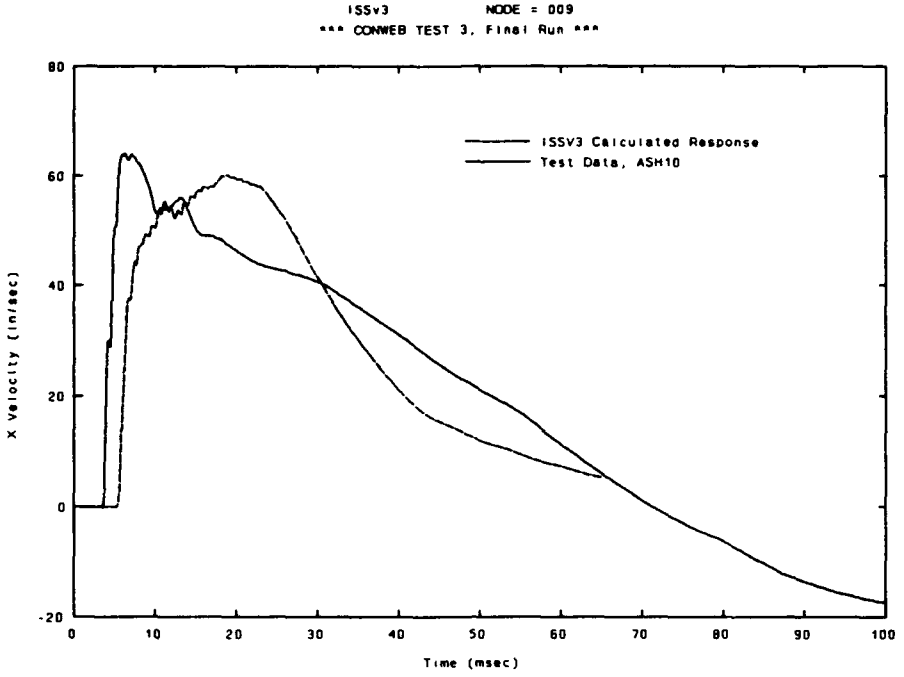

Figure 104. CONWEB 3, midfloor horizontal deflection, ISSV3 Node 9, analysis vs. test data.

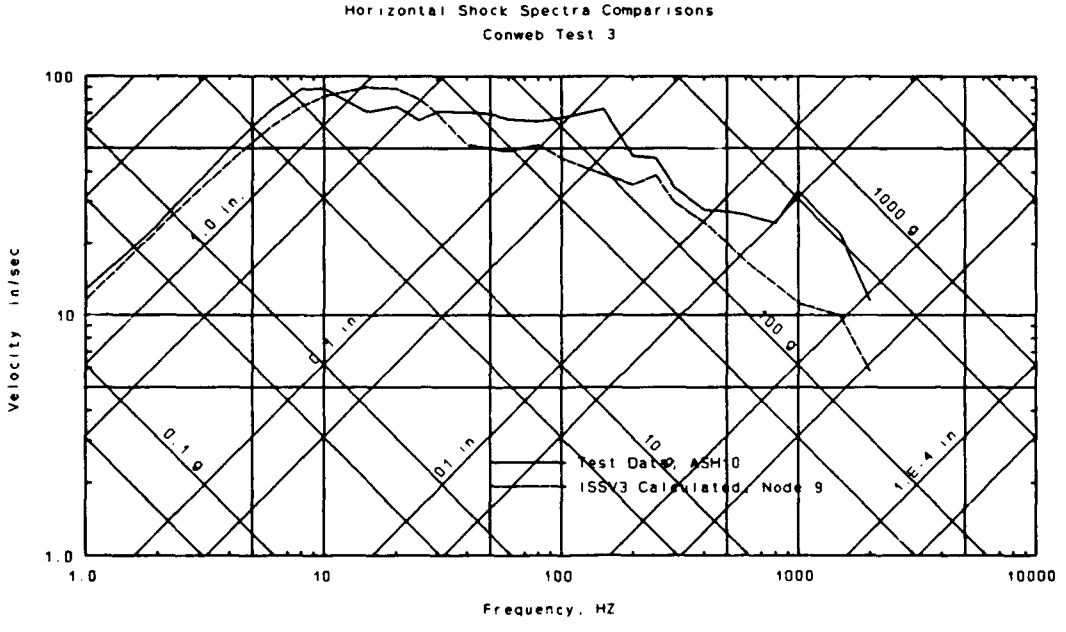

Figure 105. CONWEB 3, midfloor horizontal shock spectra, ISSV3 Node 9, analysis vs. test data.

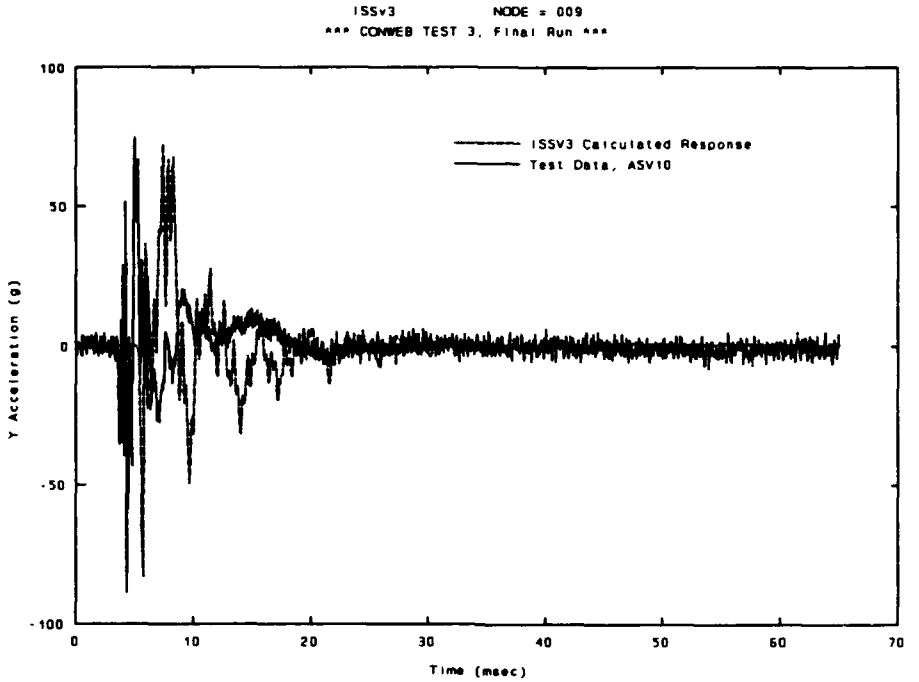

Figure 106. CONWEB 3, midfloor vertical acceleration, ISSV3 Node 9, analysis vs. test data.

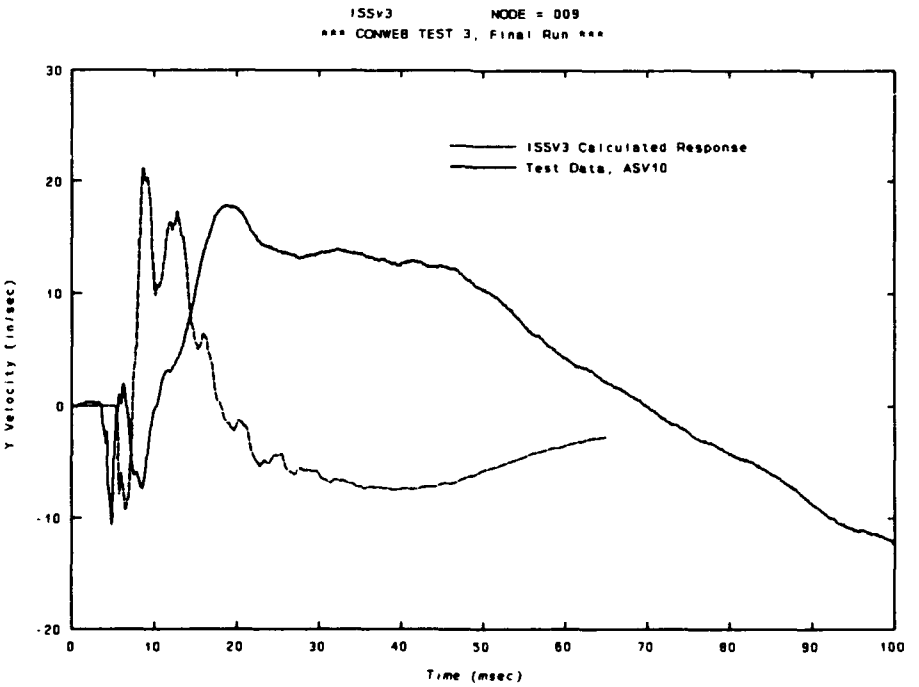

Figure 107. CONWEB 3, midfloor vertical velocity, ISSV3 Node 9, analysis vs. test data.

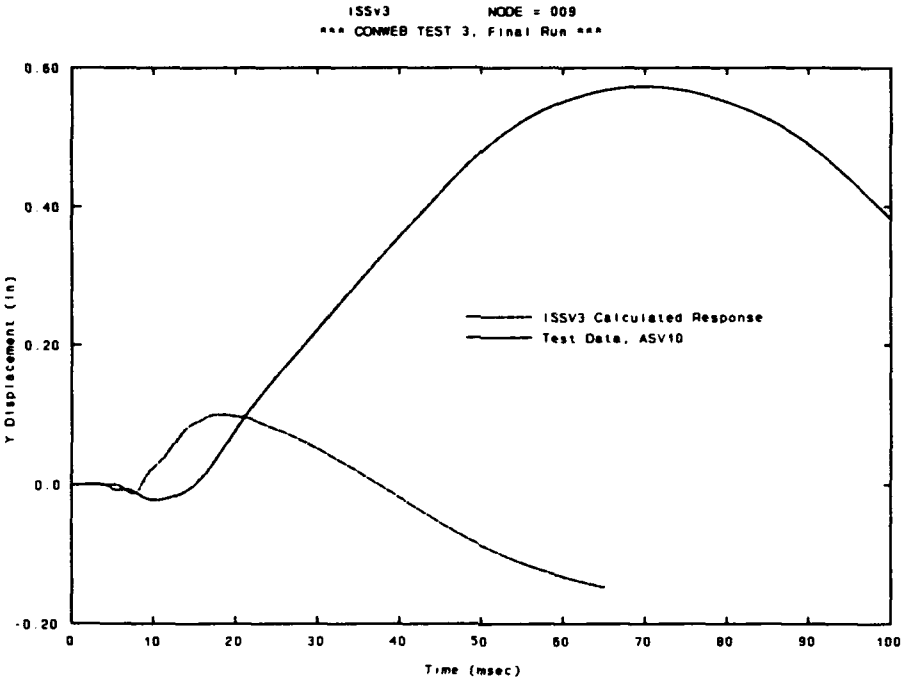

Figure 108. CONWEB 3, midfloor vertical deflection, ISSV3 Node 9, analysis vs. test data.

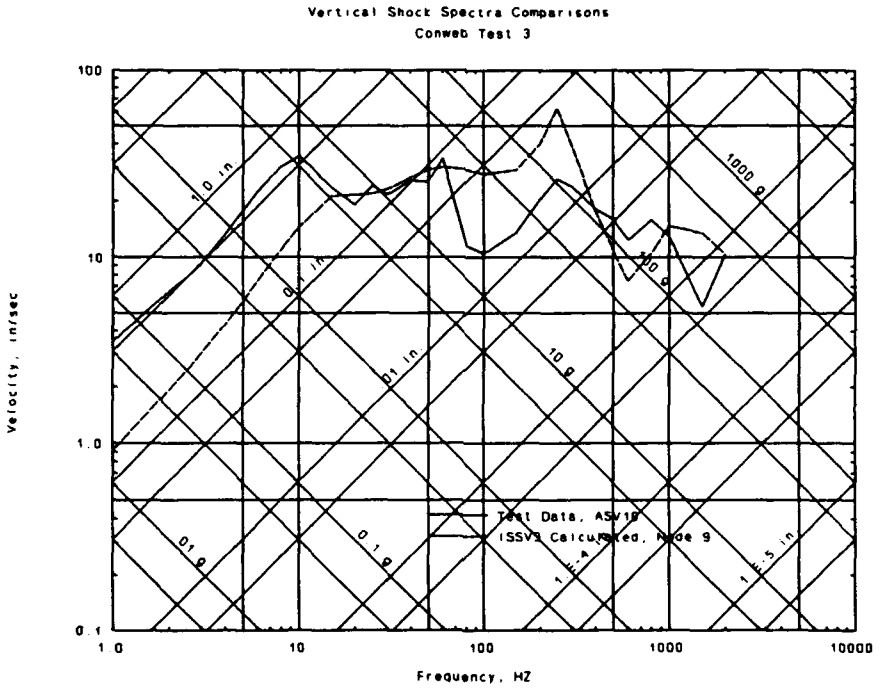

Figure 109. CONWEB 3, midfloor vertical shock spectra, ISSV3 Node 9, analysis vs. test data.

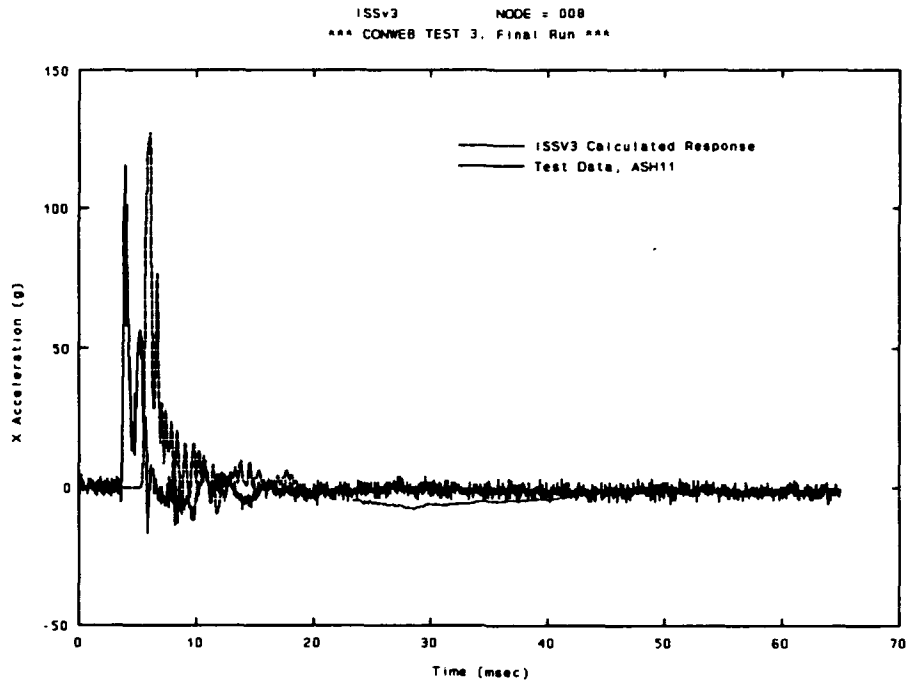

Figure 110. CONWEB 3, floor horizontal acceleration, ISSV3 Node 8, analysis vs. test data.

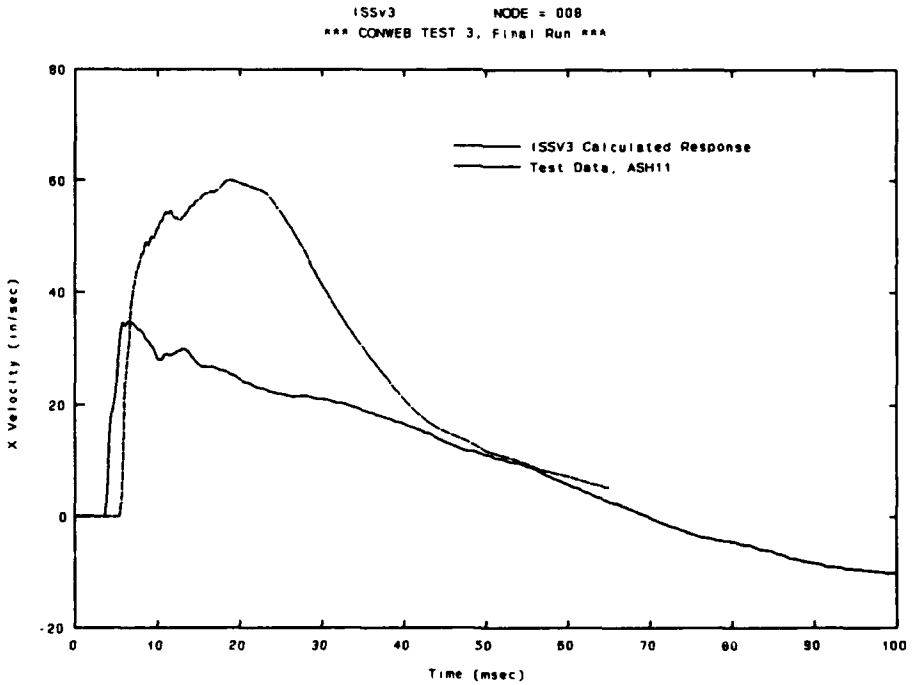

Figure 111. CONWEB 3, floor horizontal velocity, ISSV3 Node 8, analysis vs. test data.

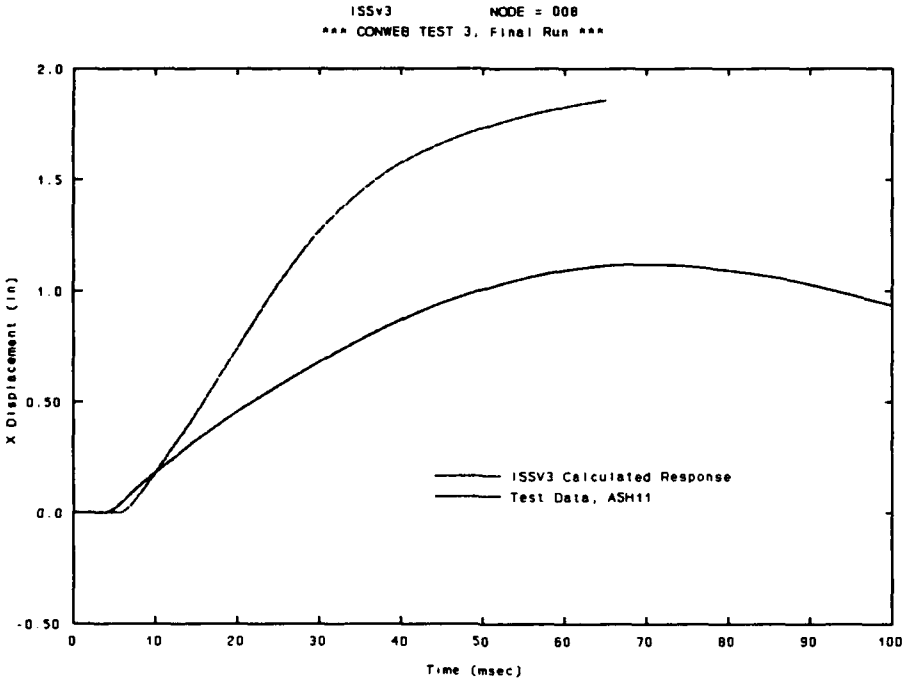

Figure 112. CONWEB 3, floor horizontal deflection, ISSV3 Node 8, analysis vs. test data.

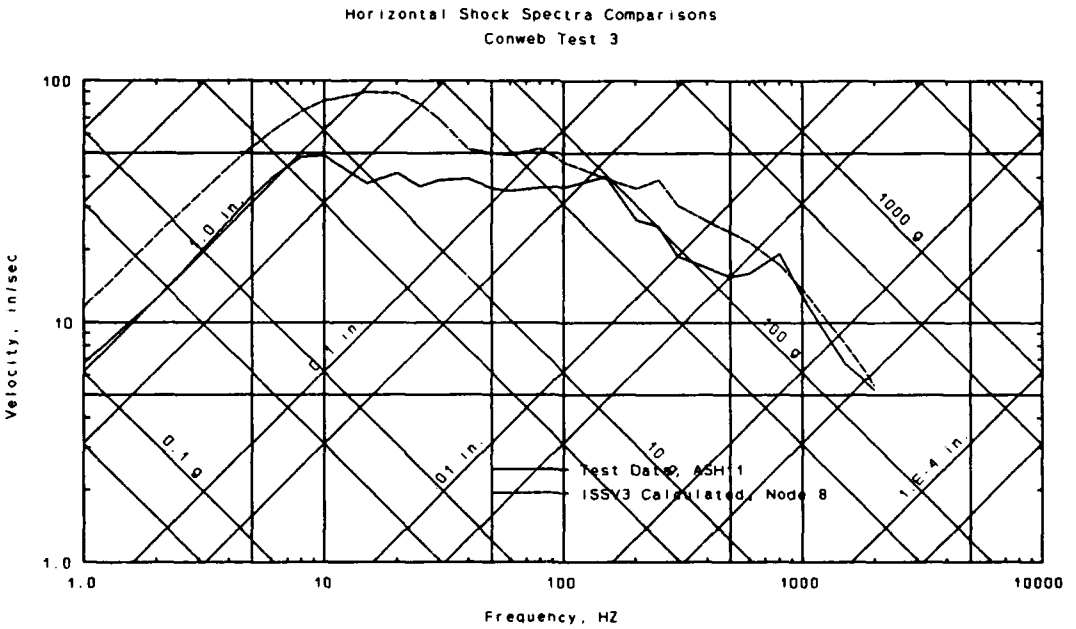

Figure 113. CONWEB 3, floor horizontal shock spectra, ISSV3 Node 8, analysis vs. test data.

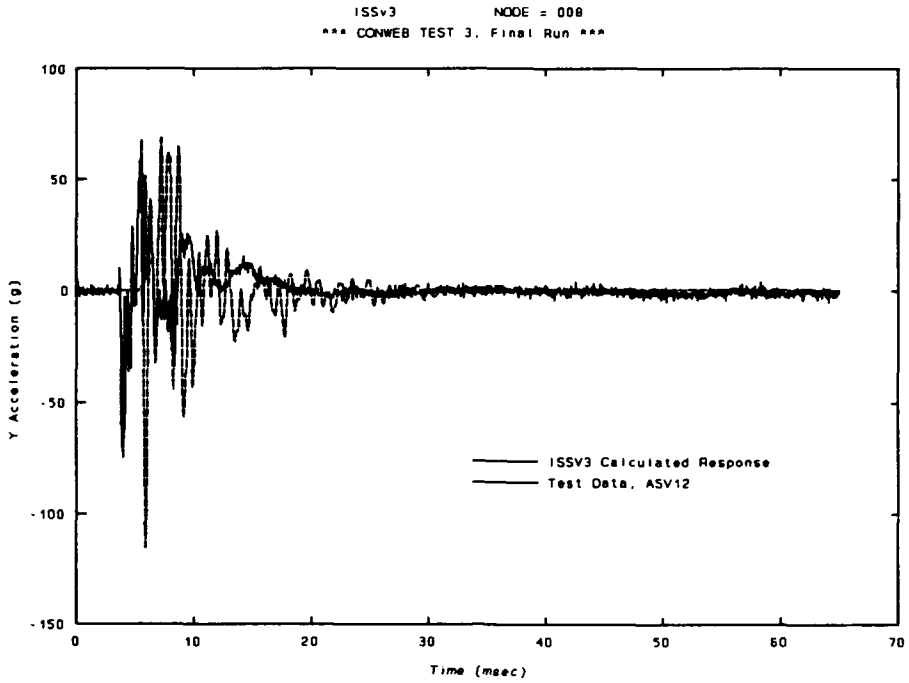

Figure 114. CONWEB 3, floor vertical acceleration, ISSV3 Node 8, analysis vs. test data.

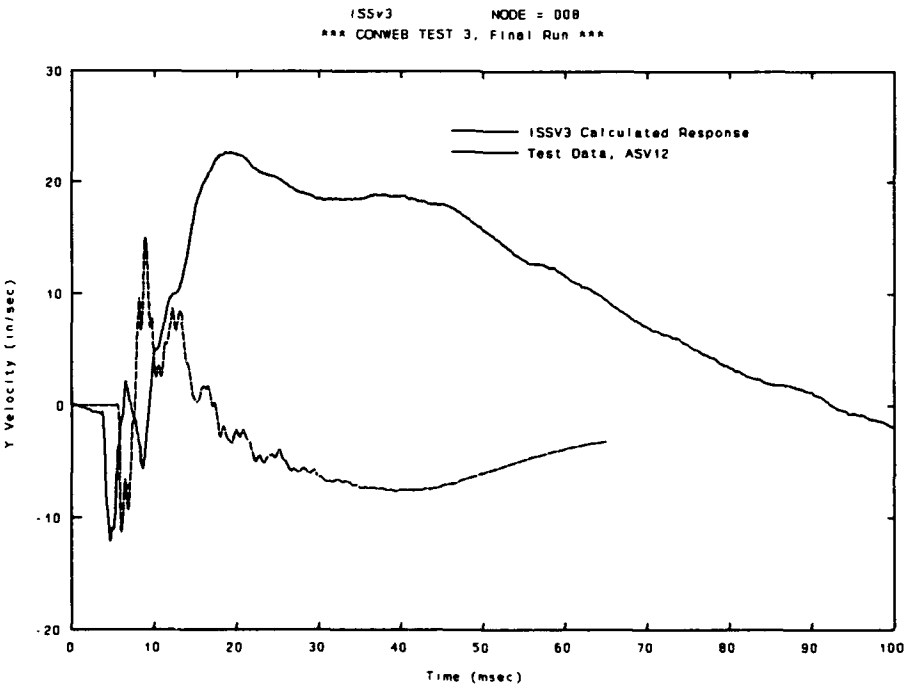

Figure 115. CONWEB 3, floor vertical velocity, ISSV3 Node 8, analysis vs. test data.

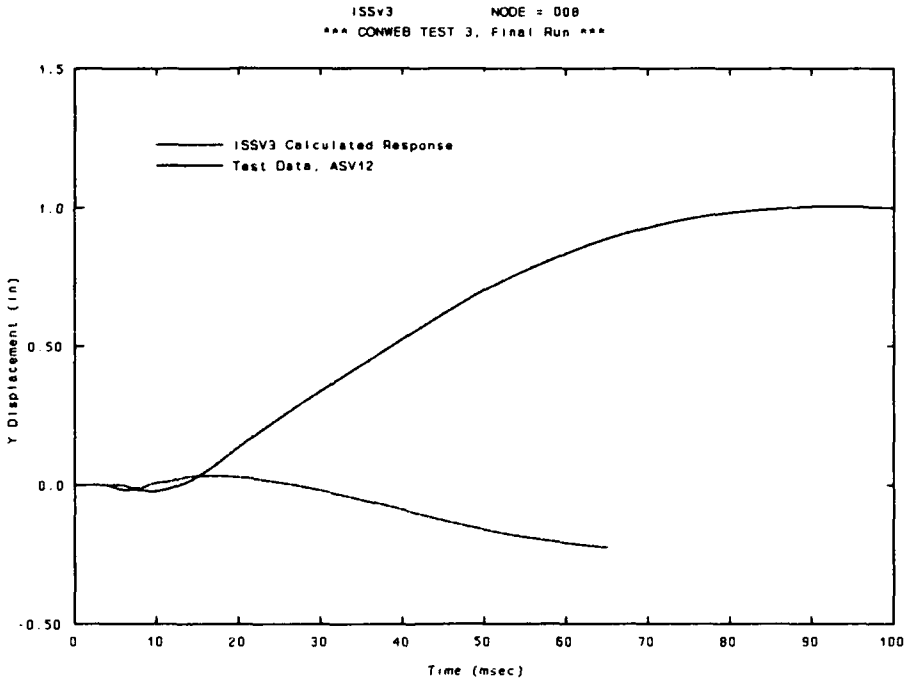

Figure 116 CONWEB 3, floor vertical deflection, ISSV3 Node 8, analysis vs. test data.

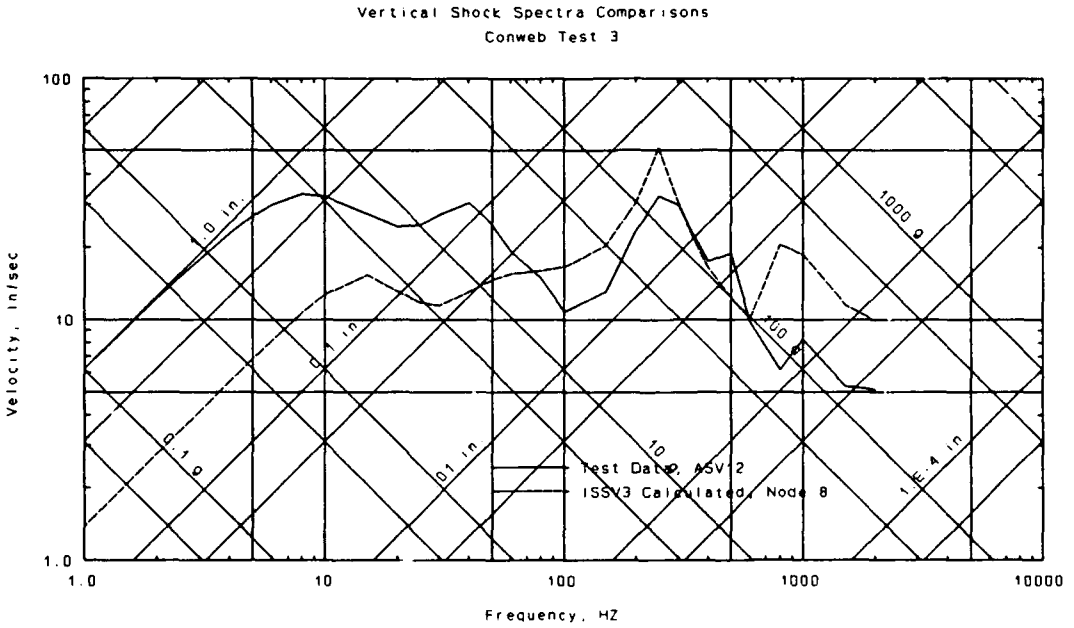

Figure 117. CONWEB 3, floor vertical shock spectra, ISSV3 Node 8, analysis vs. test data.

5.3.4 CONWEB 4 ANALYSIS.

CONWEB 4 was a test with the same structure as in CONWEB 1 and 3. The backfill in this test consisted of the in-situ soil in the test area, a very high seismic velocity, saturated gravely clay material. The test wall was the same thickness as in CONWEB 1 and 3, with an L/d ratio of 10. The finite-element grid for the ISSV3 in-structure analysis of CONWEB 4 is shown in Figure 50. This same grid was used for the calculation of CONWEB 1 and 3, with modifications to the backfill properties. Section properties used were shown above in Table 8; backfill properties were shown in Table 1.

Results from the CONWEB 4 analysis are shown in Figure 118 to Figure 139. As in CONWEB 1, examination of the interface pressure comparison once again shows that the calculated time of arrival (t_a) of the load at the face of the structure lags the actual value. However, the lag here is about 2 msec, versus about 4 msec in CONWEB 1. The shape and magnitude of the calculated interface stresses (Figure 118 and Figure 119) show a sharper higher peak stress than shown in the test data. However, the calculated interface stress compares reasonably well with the test data. As would be expected in a clay test, there is no evidence of the soil arching as was seen in the CONWEB 3 sand backfill test. Soil arching is a phenomenon associated with granular soils.

All the data comparisons for structural response also lag by about 2 msec due to the lag in loading t_a. Comparisons to test data of calculated acceleration, velocity, deflection histories, and shock spectra are shown in Figure 120 to Figure 139. Horizontal acceleration, velocity, and deflection histories were reproduced reasonably well by the ISSV3 analysis. As was seen in CONWEB 1 and 2, there is some evidence of the underprediction of late-time velocity in this test due to late-time flow effects in the clay backfill.

As in CONWEB 2 and 3, the front wall response (Figure 120 to Figure 123) shows an overprediction of velocity and deflection response. On the whole, however, the calculated horizontal in-structure shock response compares favorably with test data throughout the structure.

CONWEB 4 vertical acceleration, velocity, and deflection histories were also reproduced reasonably well by the ISSV3 analysis. The magnitudes of the vertical velocities and deflections were small as in CONWEB 1, 2, and 3; thus, the uncertainties in measurement of late-time motions have a large relative

effect. Given the uncertainties of these measurements, the magnitudes calculated for vertical velocity and deflection by ISSV3 are reasonable.

Shock spectra were generated from the velocity histories for each position in the structure. These spectra show a very good correlation between the calculated values and spectra generated for test data on the front wall. Horizontal rigid-body motion, as measured at node 9 in the center of the floor (Figure 127), was underpredicted when compared to test data spectra. This is the same gage (ASH10) that gave anomalous results in the prior analyses. Spectra generated at node 8 (Figure 135), 12 inches further back on the floor, show a very good correlation with data gathered at that point (gage ASH11). Given the heavy damage suffered by the structure in this test, gage failure at node 9 (ASH10) is quite possible.

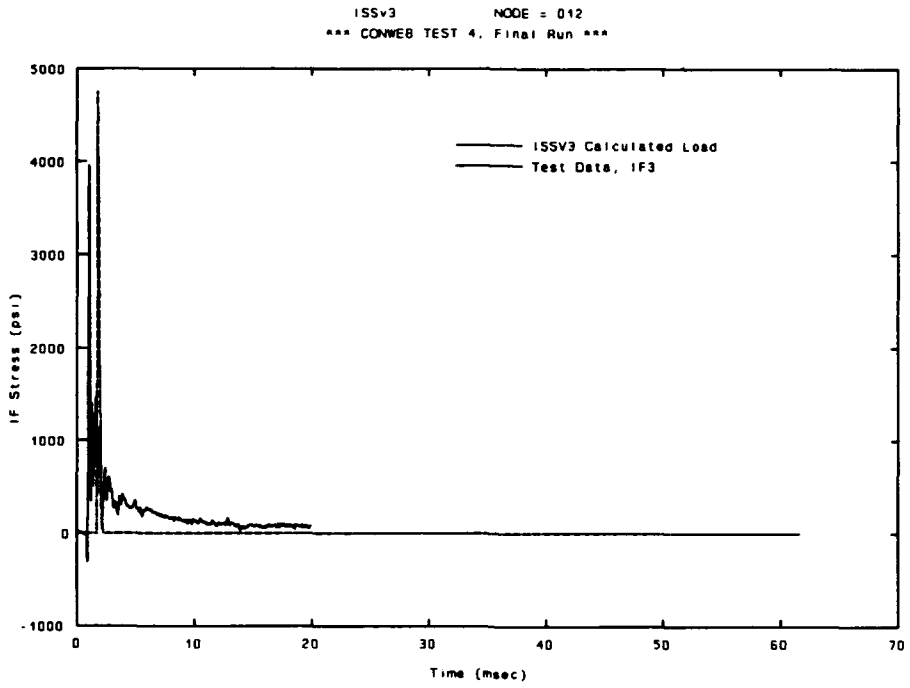

Figure 118. CONWEB 4, lower wall interface pressure load, ISSV3 Node 12, analysis vs. test data.

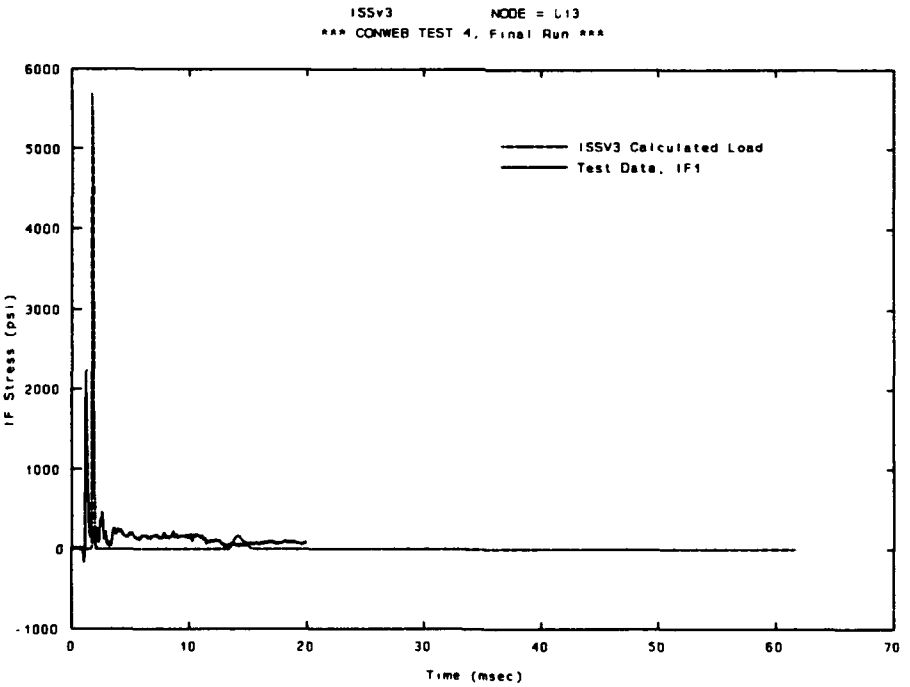

Figure 119. CONWEB 4, midwall interface pressure load, ISSV3 Node 13, analysis vs. test data.

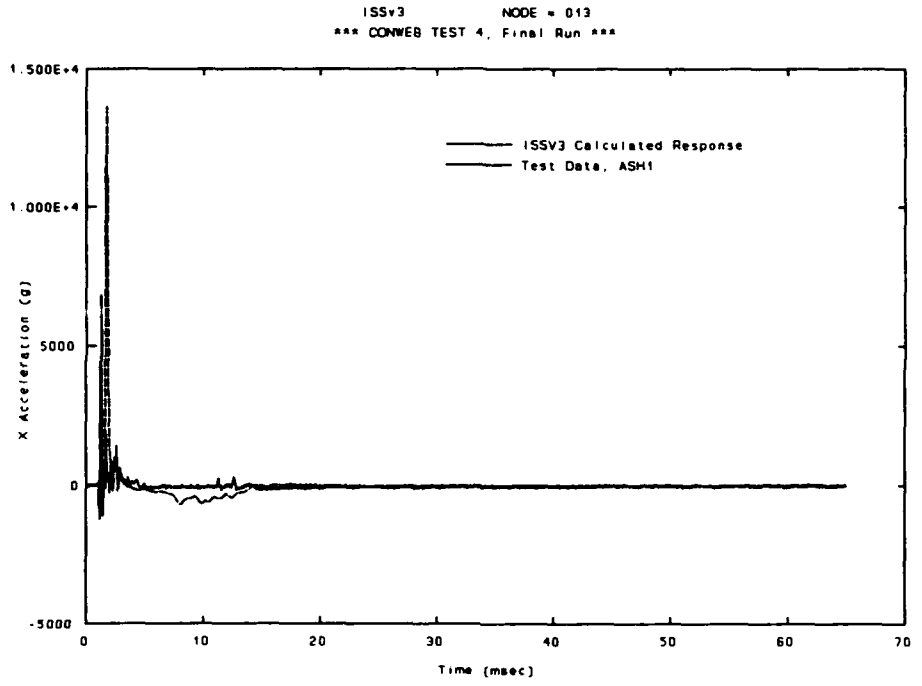

Figure 120. CONWEB 4, midwall horizontal acceleration, ISSV3 Node 13, analysis vs. test data.

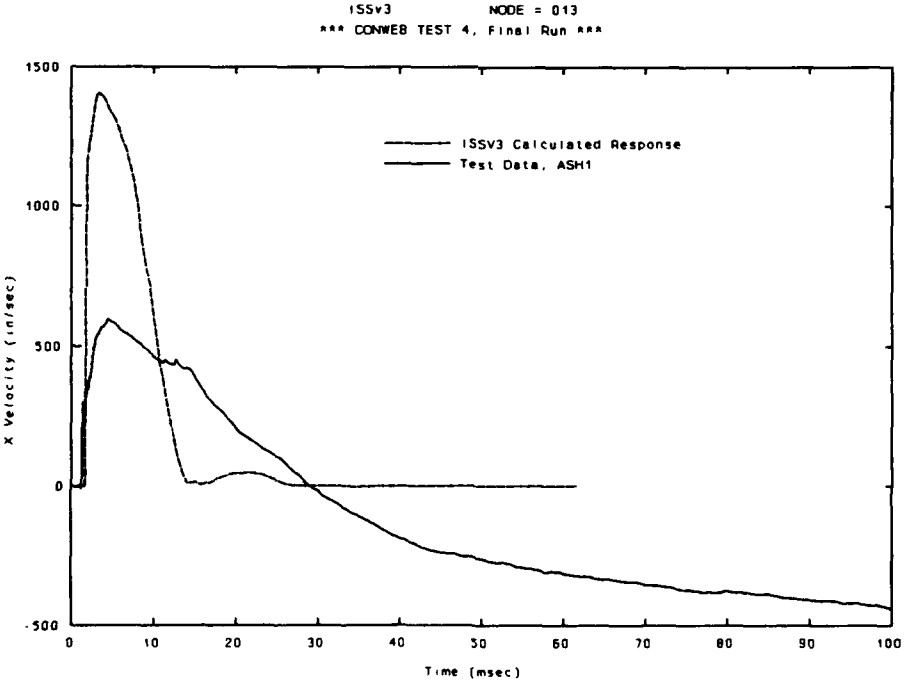

Figure 121. CONWEB 4, midwall horizontal velocity, ISSV3 Node 13, analysis vs. test data.

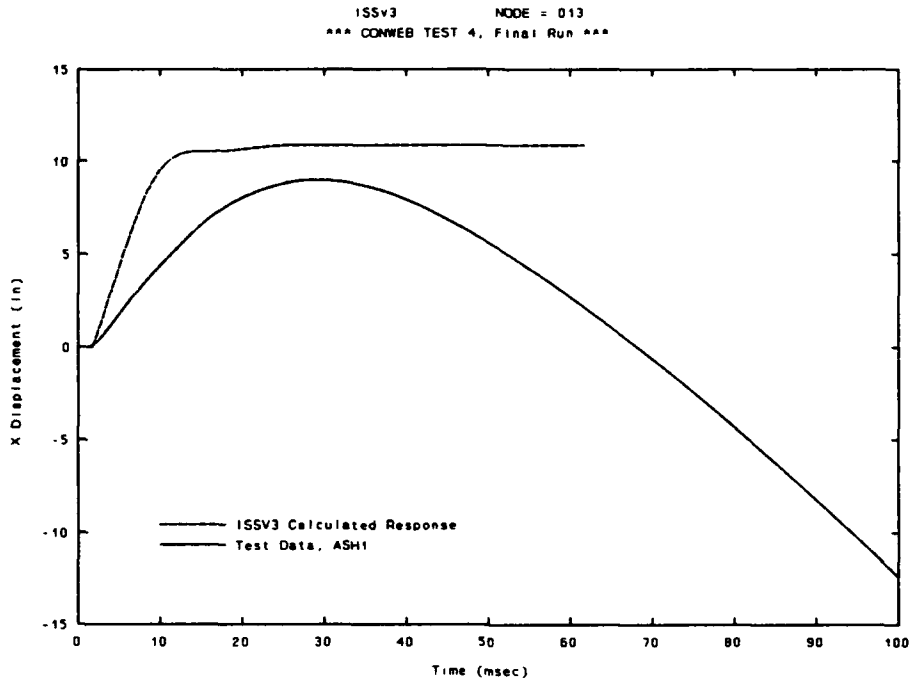

Figure 122. CONWEB 4, midwall horizontal deflection, ISSV3 Node 13, analysis vs. test data.

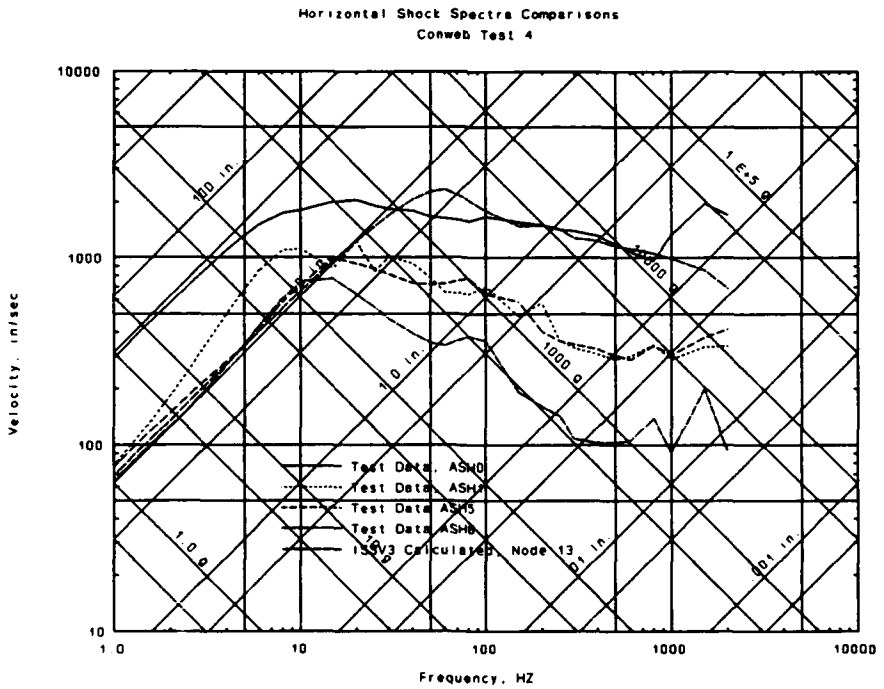

Figure 123. CONWEB 4, midwall horizontal shock spectra, ISSV3 Node 13, analysis vs. test data.

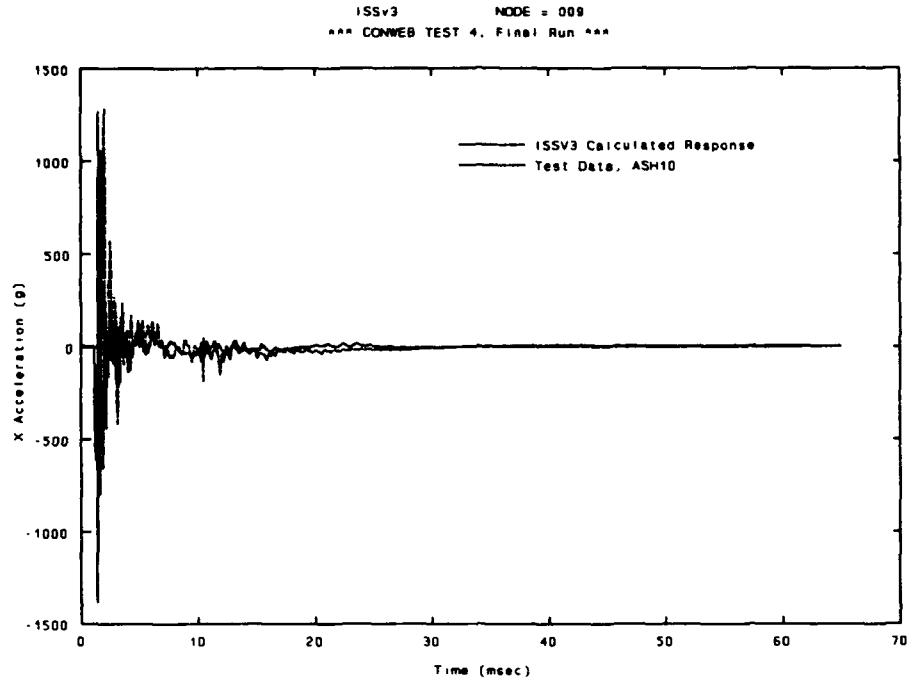

Figure 124. CONWEB 4, midfloor horizontal acceleration, ISSV3 Node 9, analysis vs. test data.

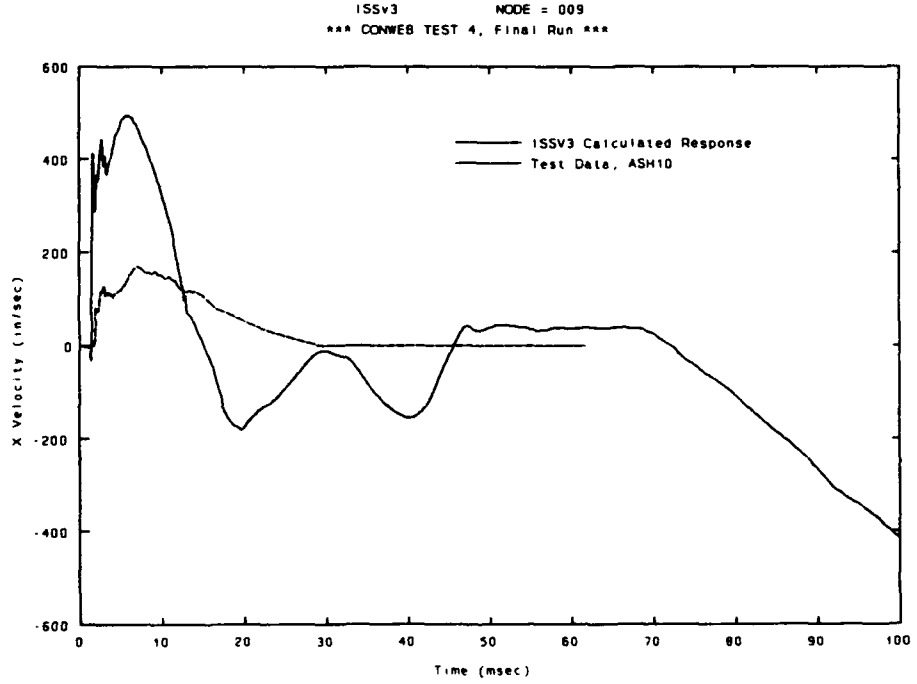

Figure 125. CONWEB 4, midfloor horizontal velocity, ISSV3 Node 9, analysis vs. test data.

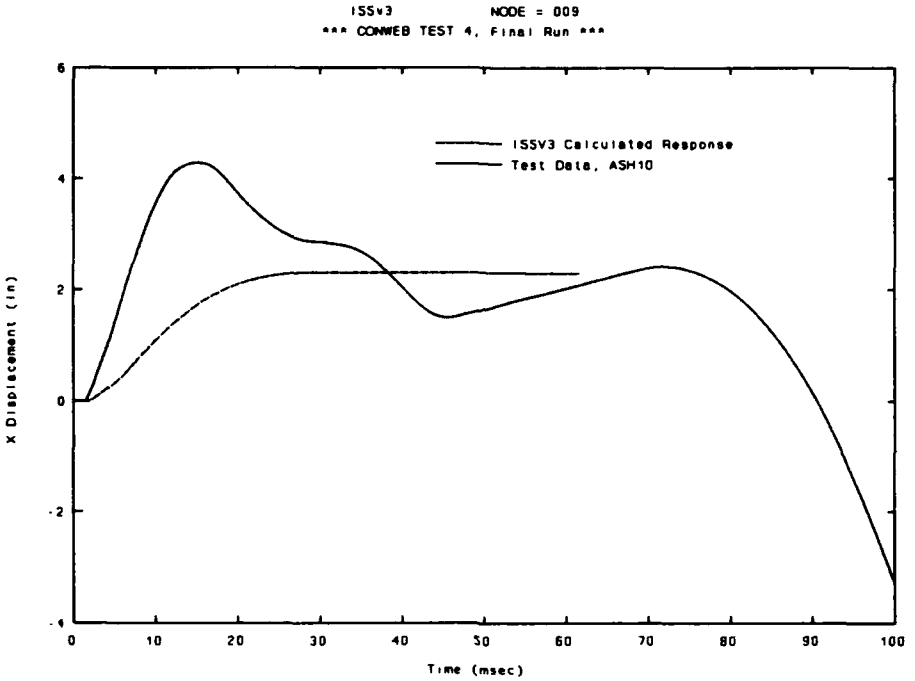

Figure 126. CONWEB 4, midfloor horizontal deflection, ISSV3 Node 9, analysis vs. test data.

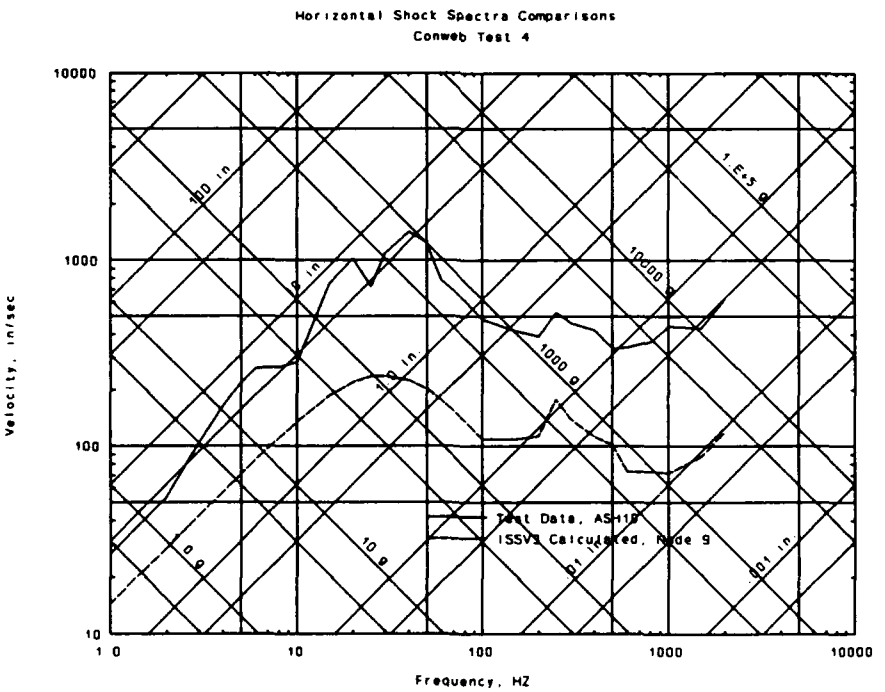

Figure 127. CONWEB 4, midfloor horizontal shock spectra, ISSV3 Node 9, analysis vs. test data.

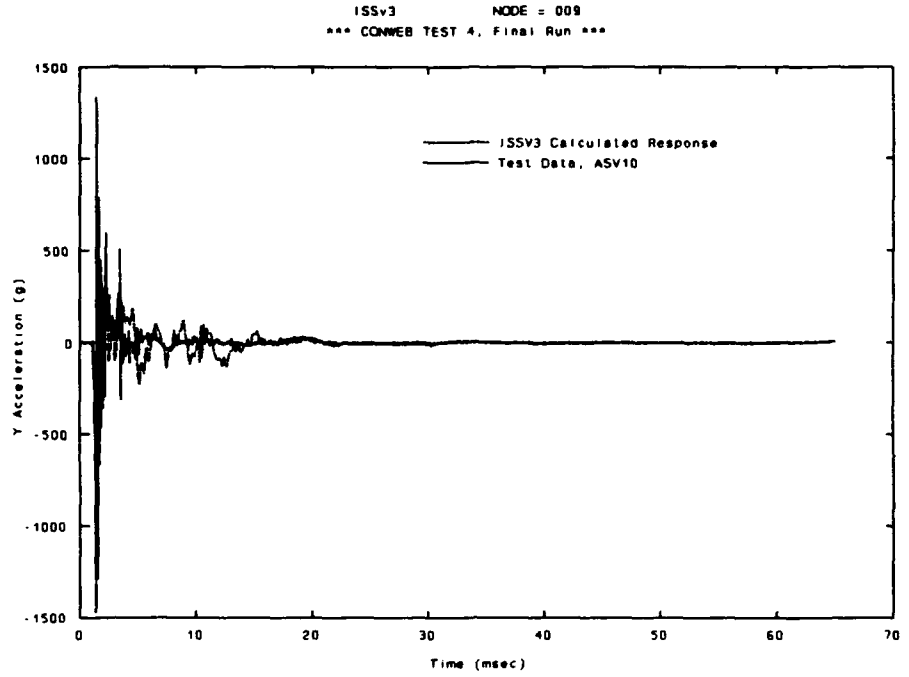

Figure 128. CONWEB 4, midfloor vertical acceleration, ISSV3 Node 9, analysis vs. test data.

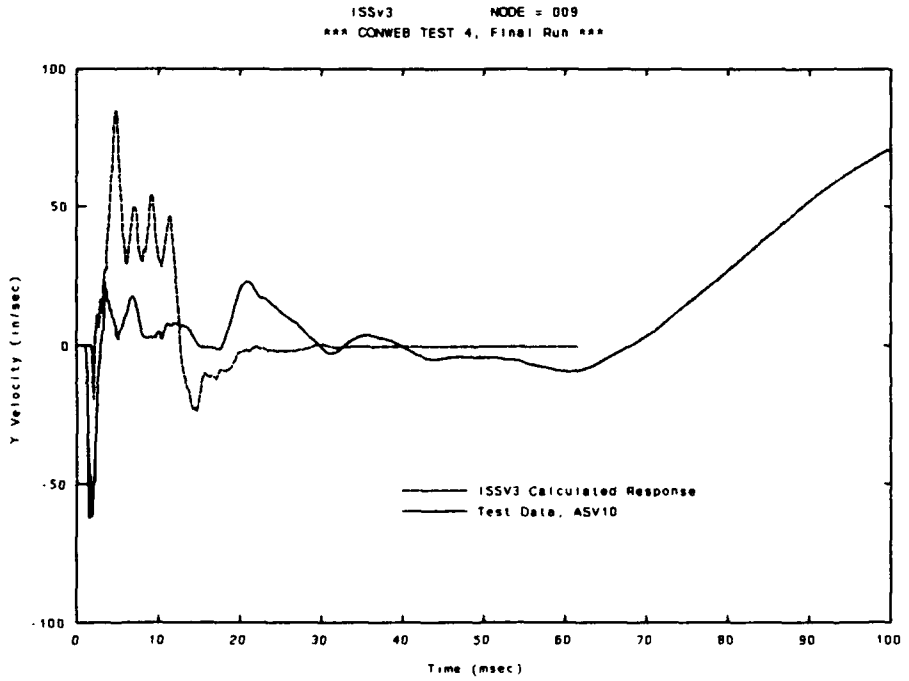

Figure 129. CONWEB 4, midfloor vertical velocity, ISSV3 Node 9, analysis vs. test data.

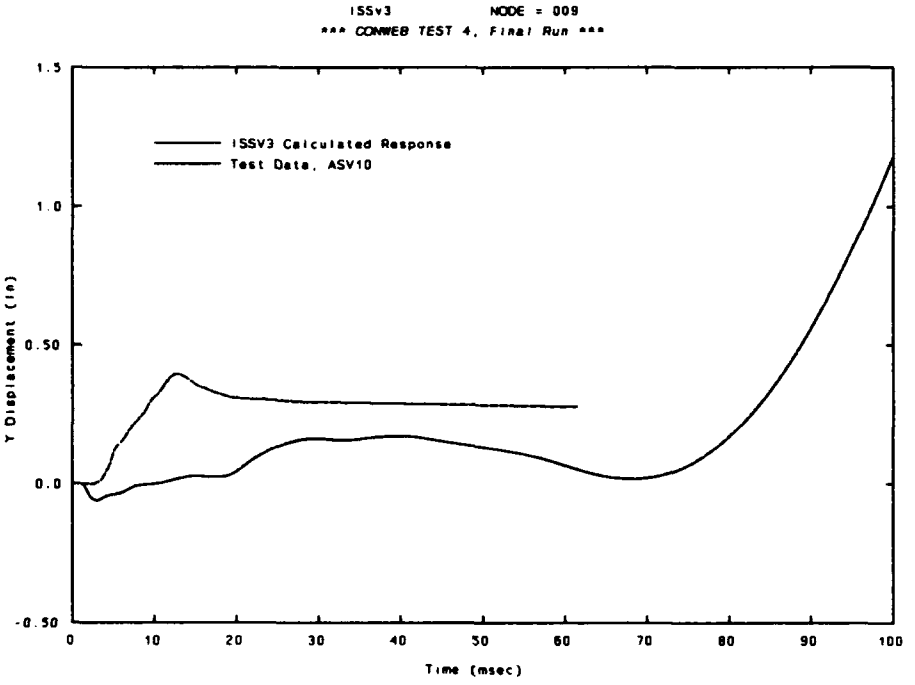

Figure 130. CONWEB 4, midfloor vertical deflection, ISSV3 Node 9, analysis vs. test data.

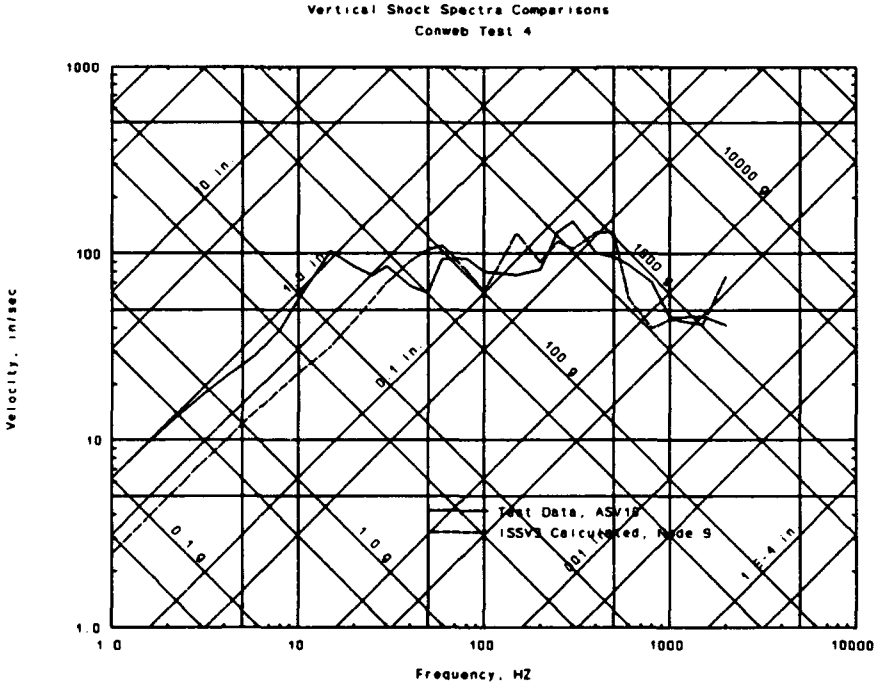

Figure 131. CONWEB 4, midfloor vertical shock spectra, ISSV3 Node 9, analysis vs. test data.

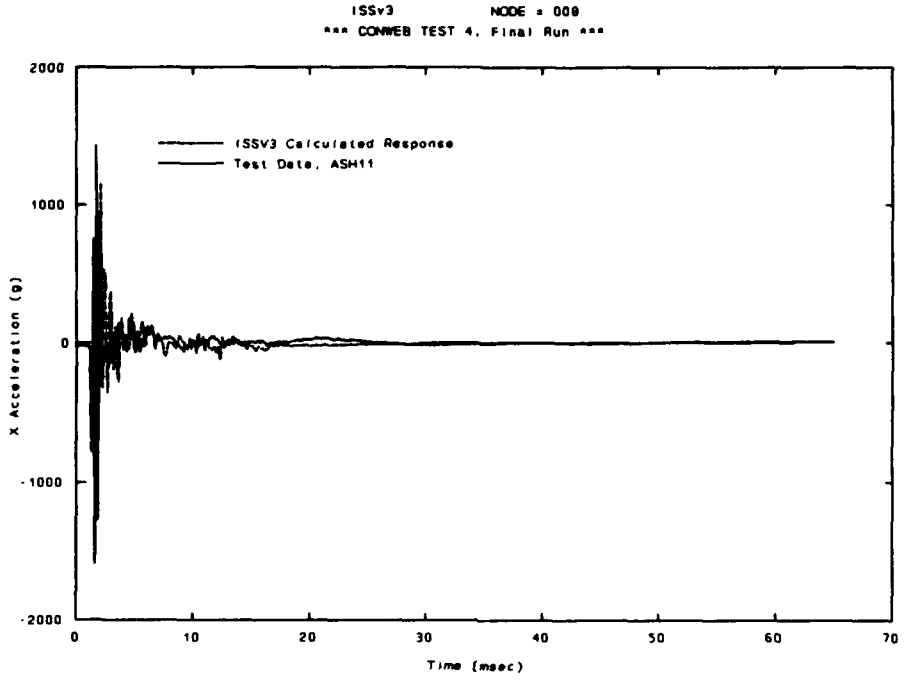

Figure 132. CONWEB 4, floor horizontal acceleration, ISSV3 Node 8, analysis vs. test data.

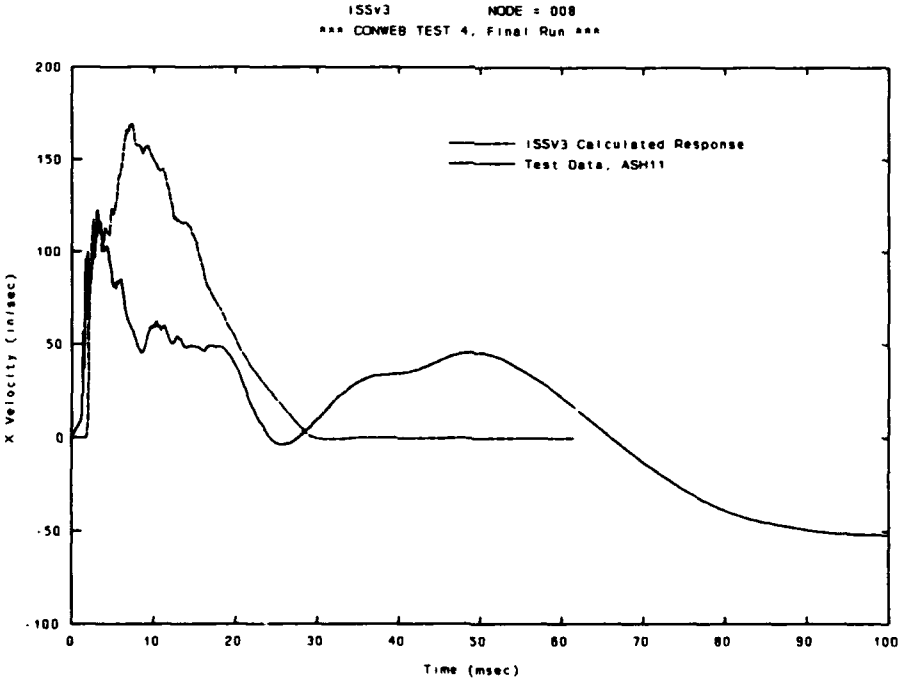

Figure 133. CONWEB 4, floor horizontal velocity, ISSV3 Node 8, analysis vs. test data.

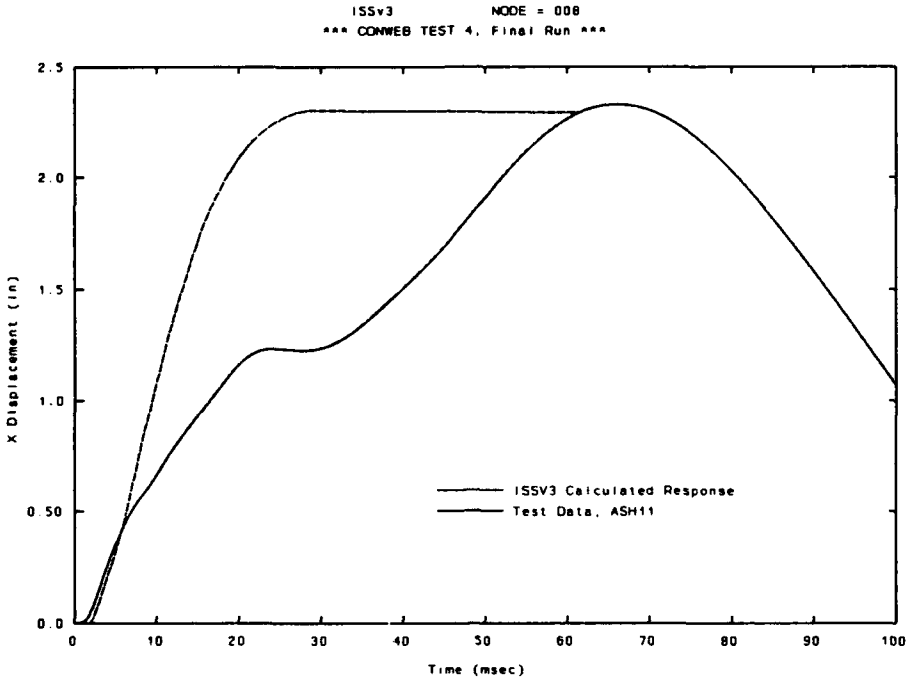

Figure 134. CONWEB 4, floor horizontal deflection, ISSV3 Node 8, analysis vs. test data.

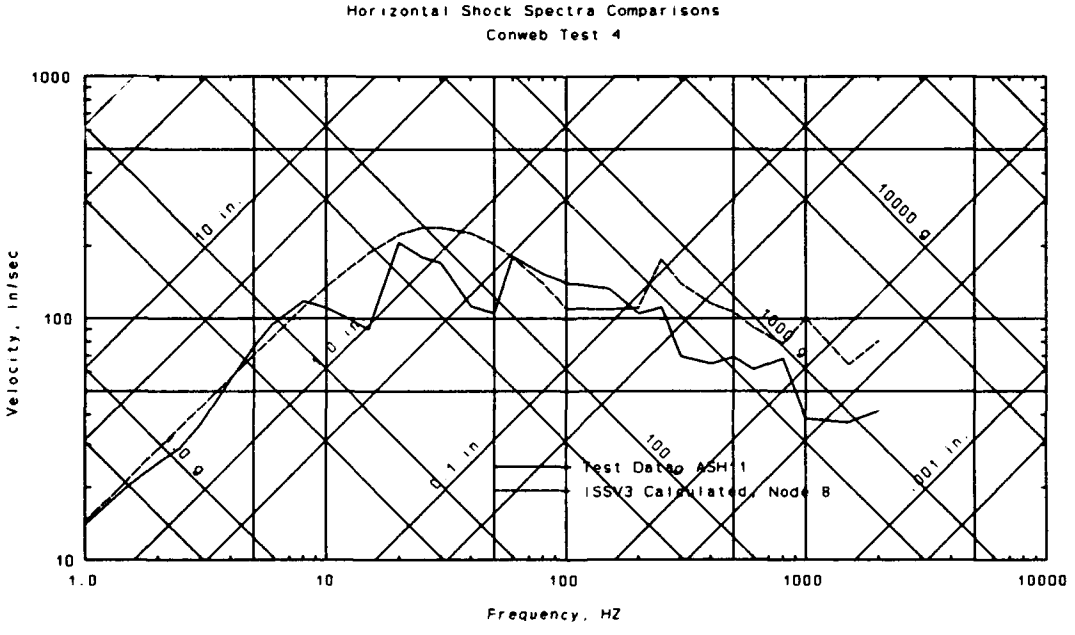

Figure 135. CONWEB 4, floor horizontal shock spectra, ISSV3 Node 8, analysis vs. test data.

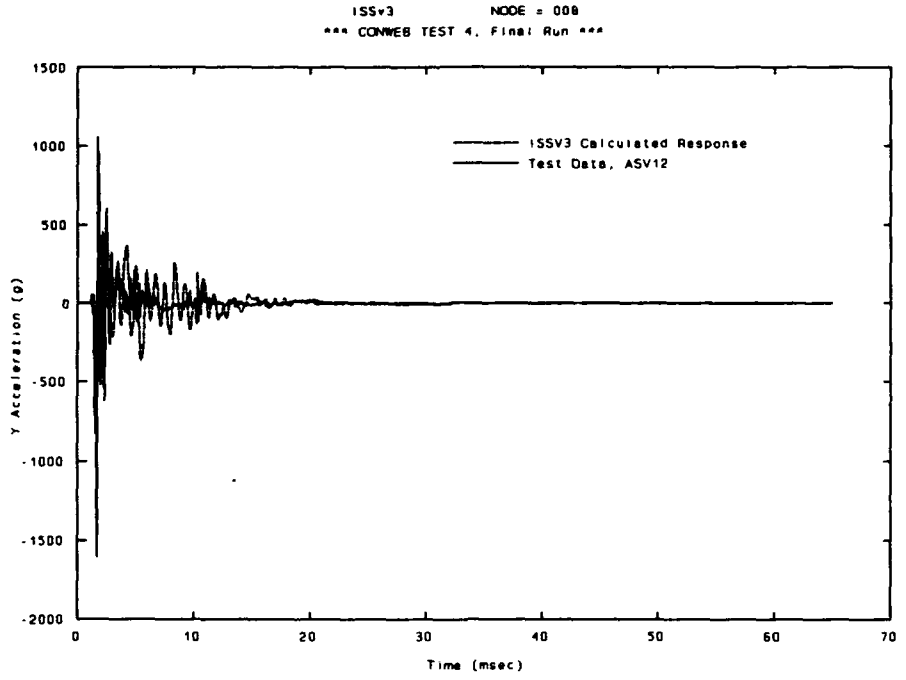

Figure 136. CONWEB 4, floor vertical acceleration, ISSV3 Node 8, analysis vs. test data.

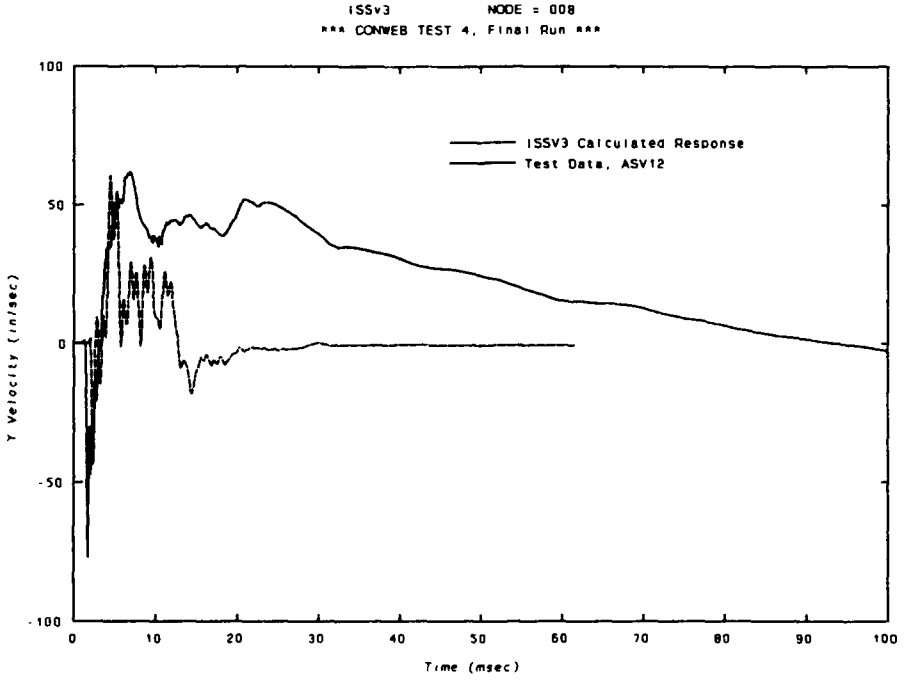

Figure 137. CONWEB 4, floor vertical velocity, ISSV3 Node 8, analysis vs. test data.

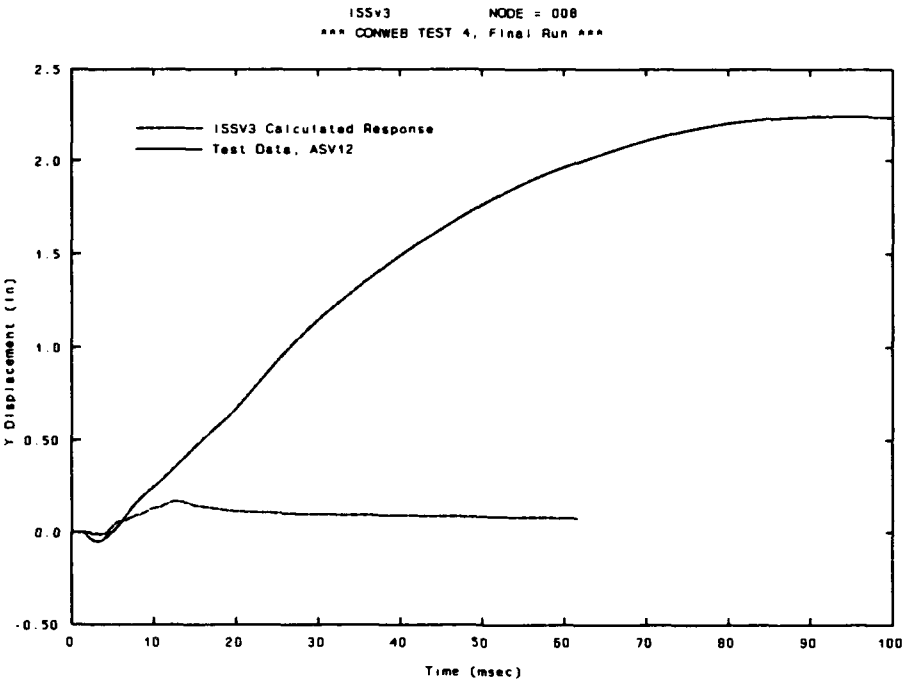

Figure 138. CONWEB 4, floor vertical deflection, ISSV3 Node 8, analysis vs. test data.

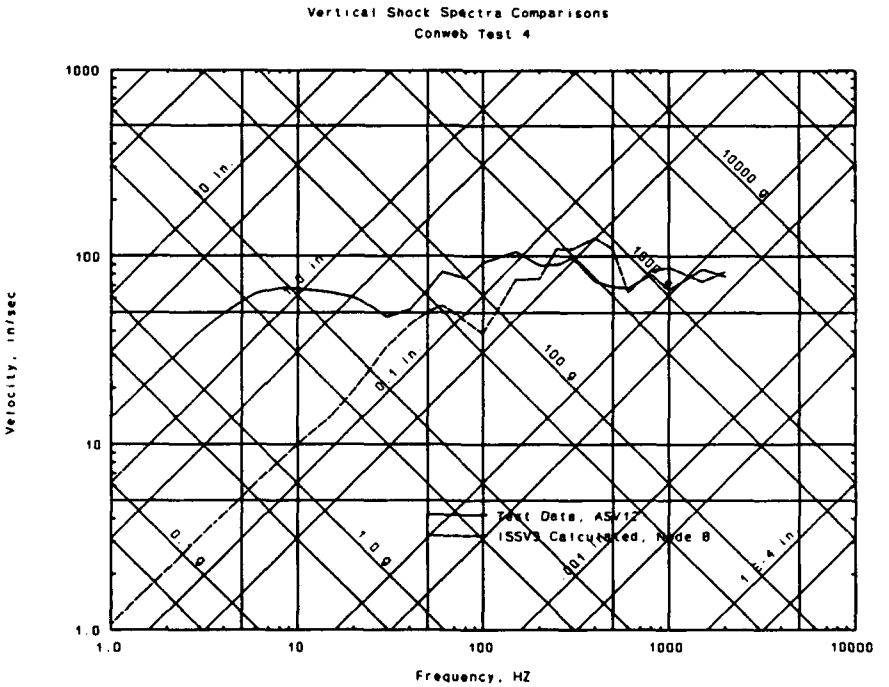

Figure 139. CONWEB 4, floor vertical shock spectra, ISSV3 Node 8, analysis vs. test data.

5.4 ISSV3 ANALYSIS SUMMARY.

The initial evaluation of ISSV3 as an in-structure shock analysis technique is favorable. Calculation of all four CONWEB tests with very dissimilar backfill materials gave reasonable results. The acceleration records generated had forms and magnitudes quite similar to test data. Comparisons of velocity and deflection records were somewhat hampered due to the difficulty of measuring low-level, late-time accelerations in dynamic tests. However, available data compared favorably with the ISSV3-generated velocity and deflection histories. Shock spectra generated from the ISSV3 velocity histories also compared very well with spectra derived from test data.

It is acknowledged that the current free-field model in ISSV3 needs to be improved. Late-time velocities are sometimes underpredicted due to flow effects in clay backfill. Also, other research by Hayes [1] and [10] has indicated that the characterization of backfill by seismic velocity, density, and attenuation coefficient may be overly simplistic. In spite of these problems in the free-field models, the interface loads generated by ISSV3 for the CONWEB tests were reasonable.

The single greatest strength of the ISSV3 program brought to light in the analysis of the CONWEB test series is the speed of the calculation. All of the calculations required less than four minutes to run on a 386, 20-MHz personal computer. This is a marked improvement over the four to sixteen hour run times for this application of the STABLE program.

SECTION 6
COMPARISON OF ANALYSIS TECHNIQUES

With the success of the initial evaluation of the ISSV3 program as an in-structure shock analysis tool, it is interesting to compare the program's results with the other available tools. Figure 140 to Figure 151 show direct comparisons of the shock spectra generated from the CONWEB test series data and all of the means of analysis investigated. The average front wall response is compared to the TM5 855-1 method, the SDOF wall analysis, the STABLE results (for CONWEB 2), and the ISSV3 results. The shock response on the floor of each structure is compared to the TM5 855-1 method, the rigid-body motion SDOF analysis, the STABLE results (for CONWEB 2), and the ISSV3 results. In every case, the results of the ISSV3 analysis are at least as accurate as the other techniques. With planned improvements in the free-field model, these comparisons are expected to be even better for later versions of the program.

It is important to note that the simplified in-structure shock methods investigated here are limited in a way that ISSV3 is not. The TM5 855-1 method and the rigid-body SDOF analysis are best suited to simple, small structures. There is no fundamental reason why ISSV3 can not be applied to the fast and accurate in-structure shock analysis of larger, complicated, multifloor, multibay structures.

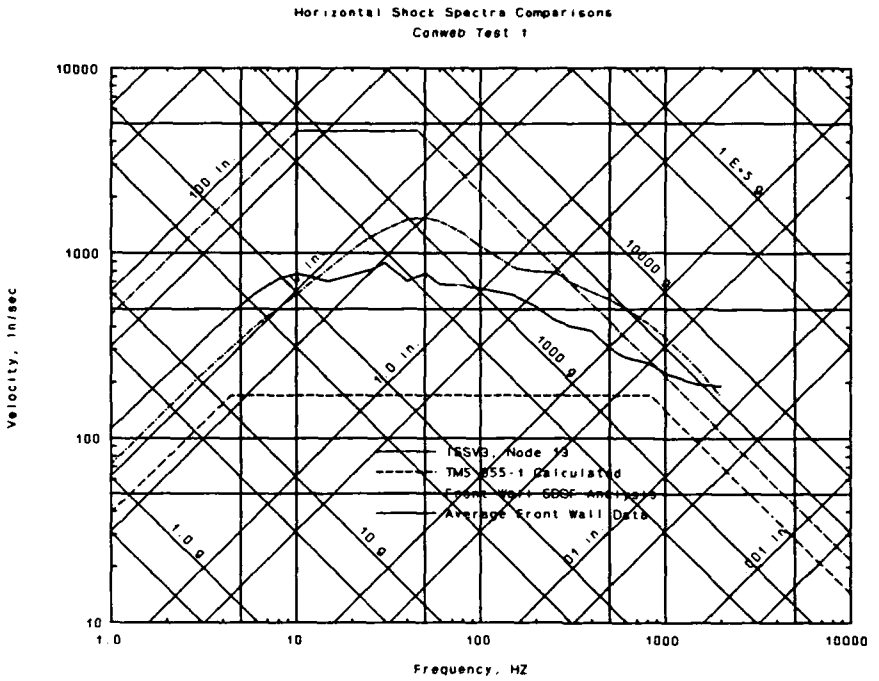

Figure 140. CONWEB 1, midwall horizontal shock spectra, ISSV3 Node 13, comparison of analysis techniques.

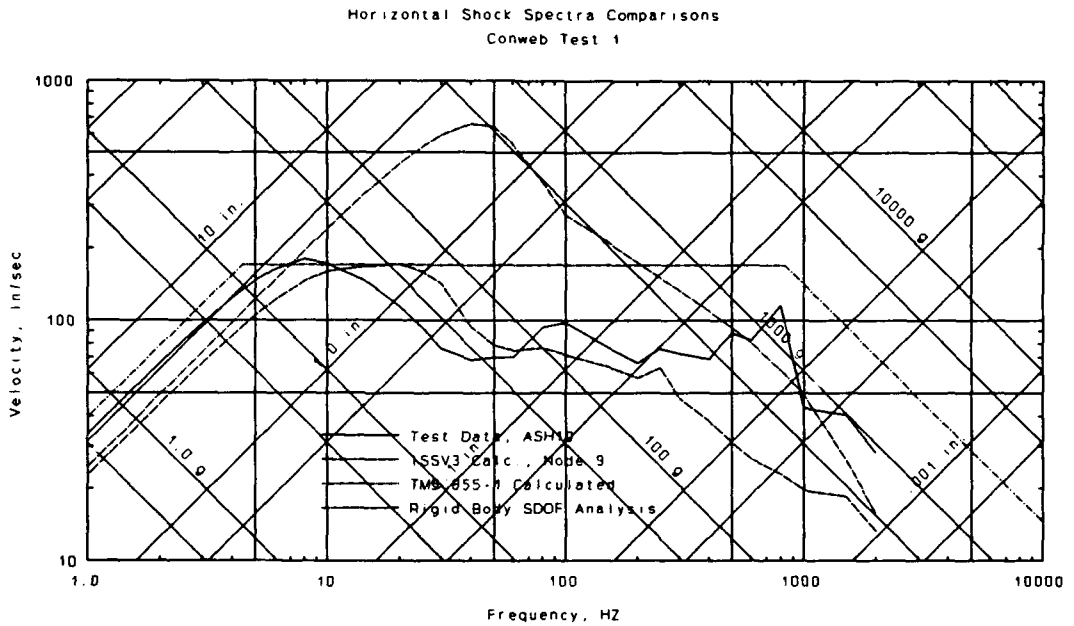

Figure 141. CONWEB 1, midfloor horizontal shock spectra, ISSV3 Node 9, comparison of analysis techniques.

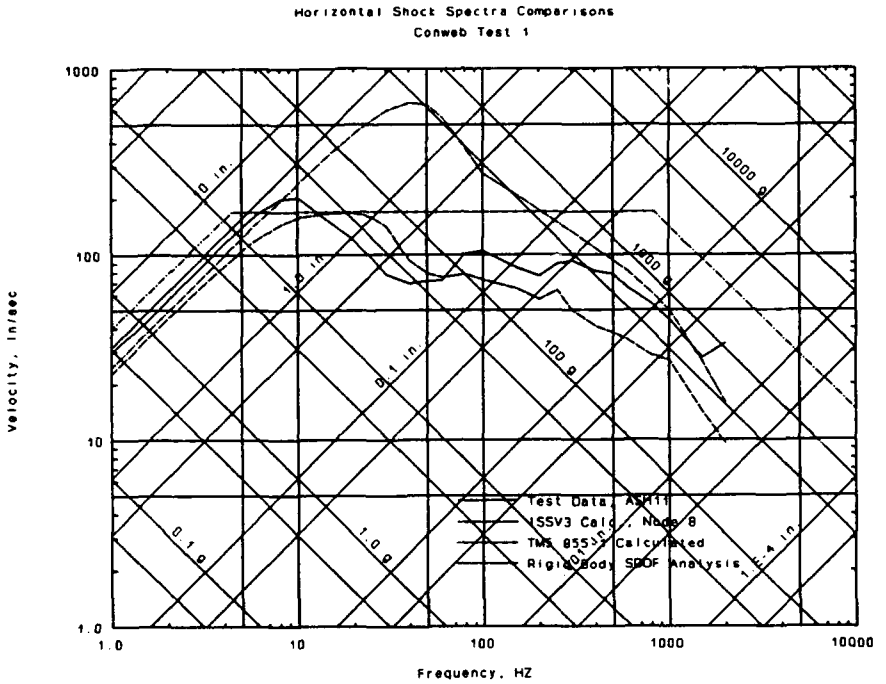

Figure 142. CONWEB 1, floor horizontal shock spectra, ISSV3 Node 8, comparison of analysis techniques.

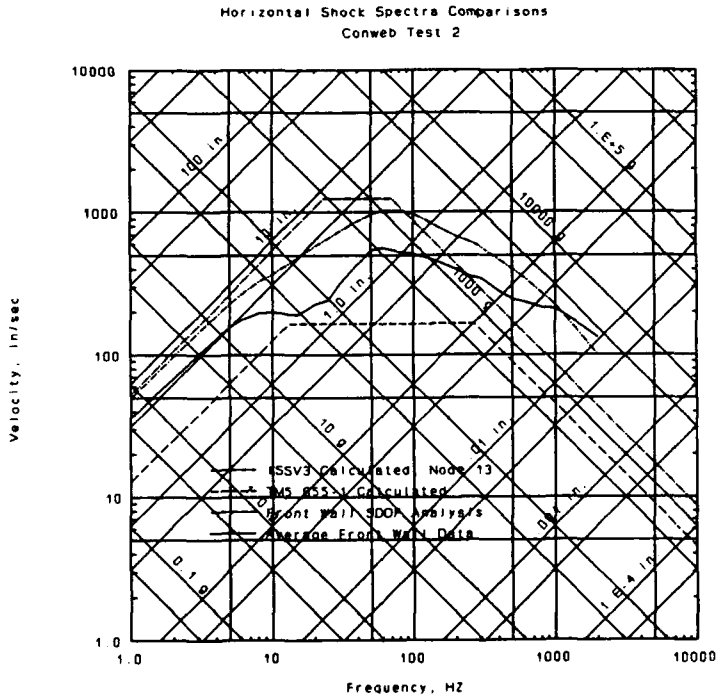

Figure 143. CONWEB 2, midwall horizontal shock spectra, ISSV3 Node 13, comparison of analysis techniques.

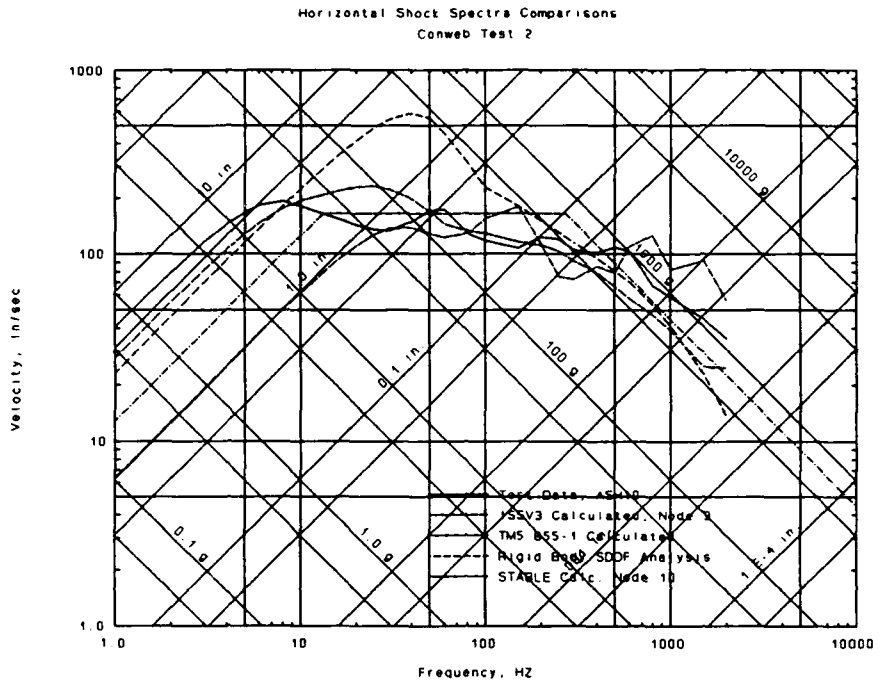

Figure 144. CONWEB 2, midfloor horizontal shock spectra, ISSV3 Node 9, comparison of analysis techniques.

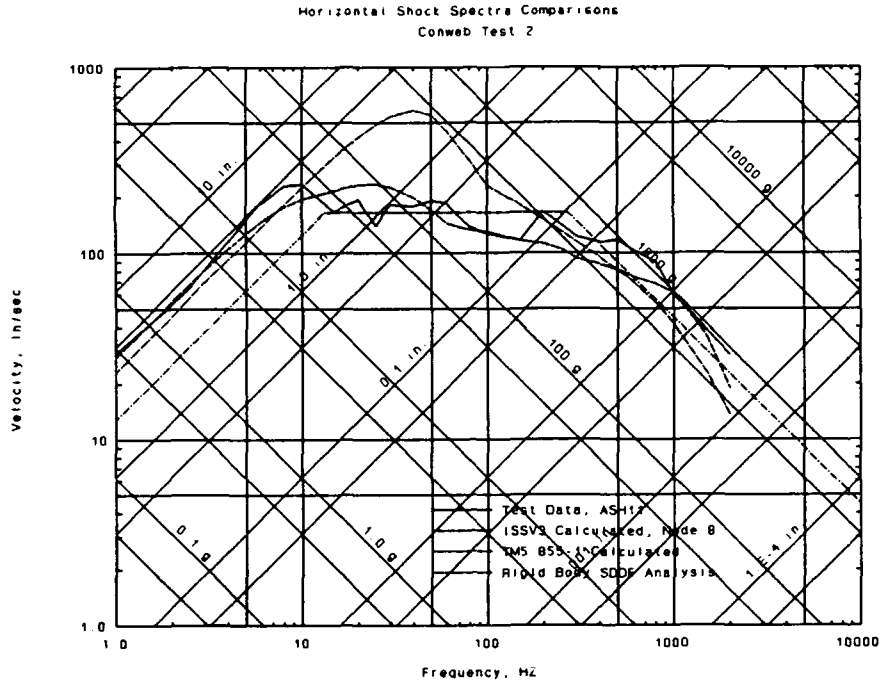

Figure 145. CONWEB 2, floor horizontal shock spectra, ISSV3 Node 8, comparison of analysis techniques.

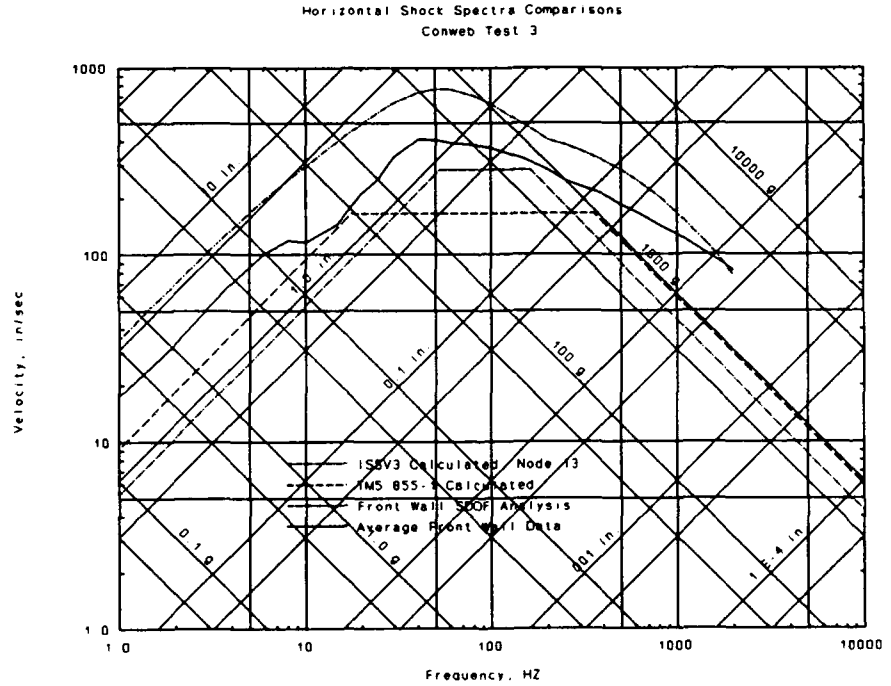

Figure 146. CONWEB 3, midwall horizontal shock spectra, ISSV3 Node 13, comparison of analysis techniques.

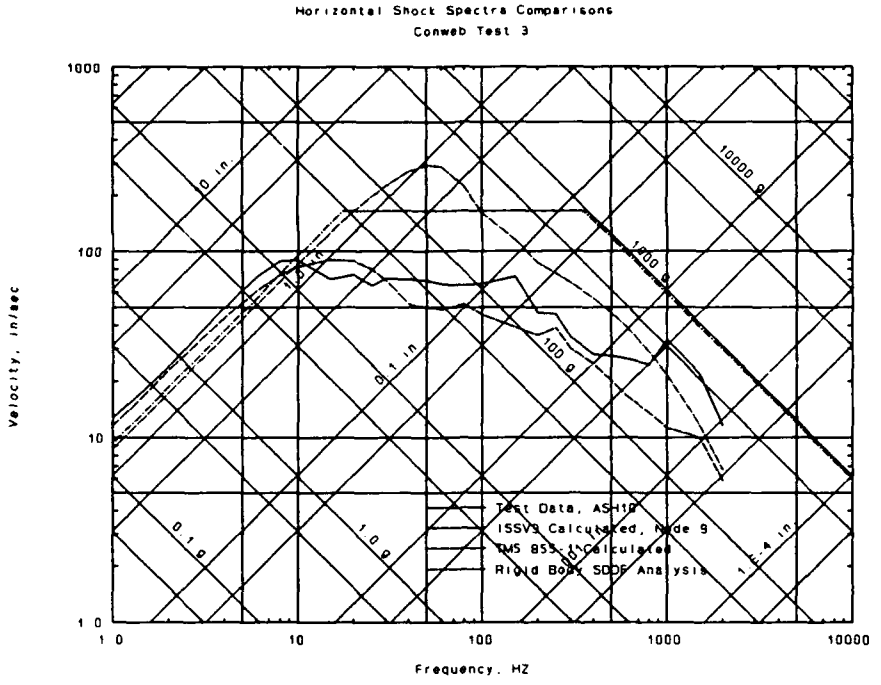

Figure 147. CONWEB 3, midfloor horizontal shock spectra, ISSV3 Node 9, comparison of analysis techniques.

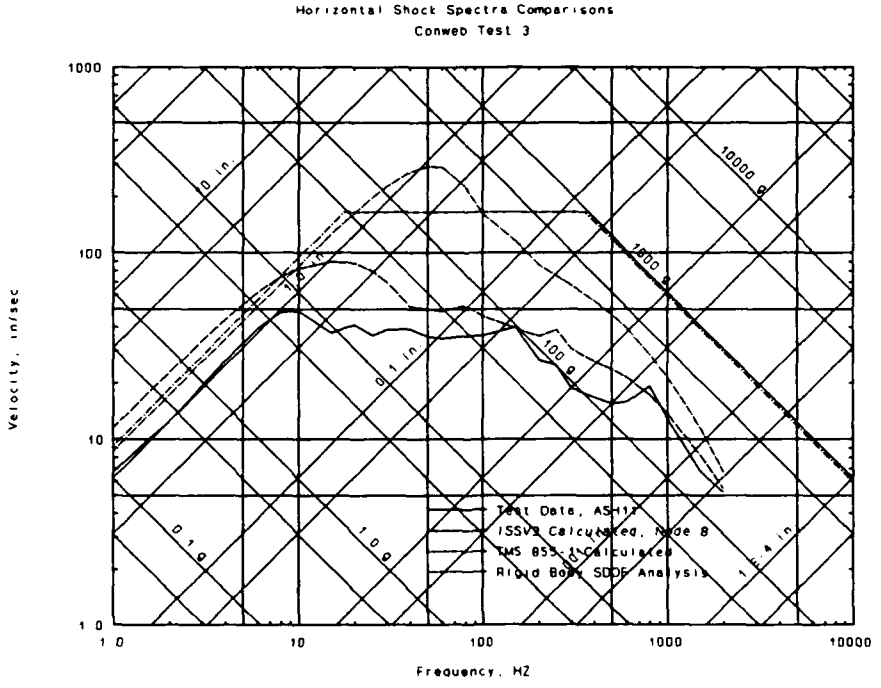

Figure 148. CONWEB 3, floor horizontal shock spectra, ISSV3 Node 8, comparison of analysis techniques.

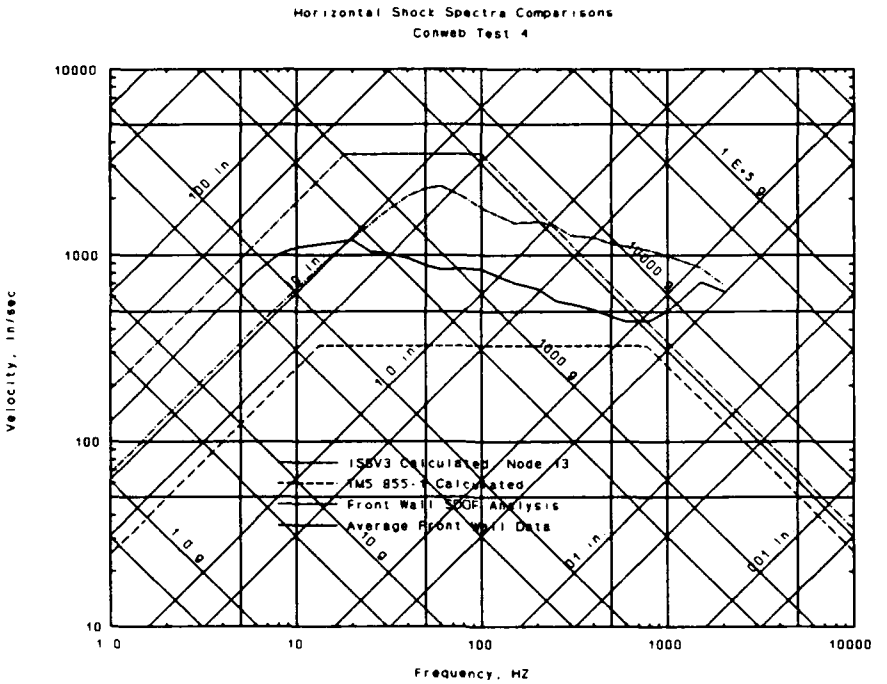

Figure 149. CONWEB 4, midwall horizontal shock spectra, ISSV3 Node 13, comparison of analysis techniques.

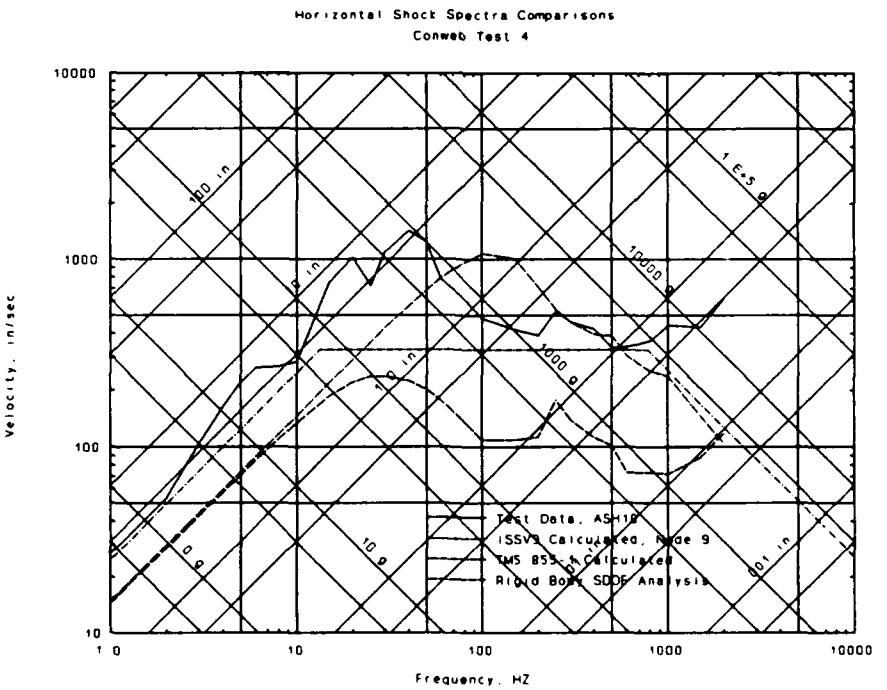

Figure 150. CONWEB 4, midfloor horizontal shock spectra, ISSV3 Node 9, comparison of analysis techniques.

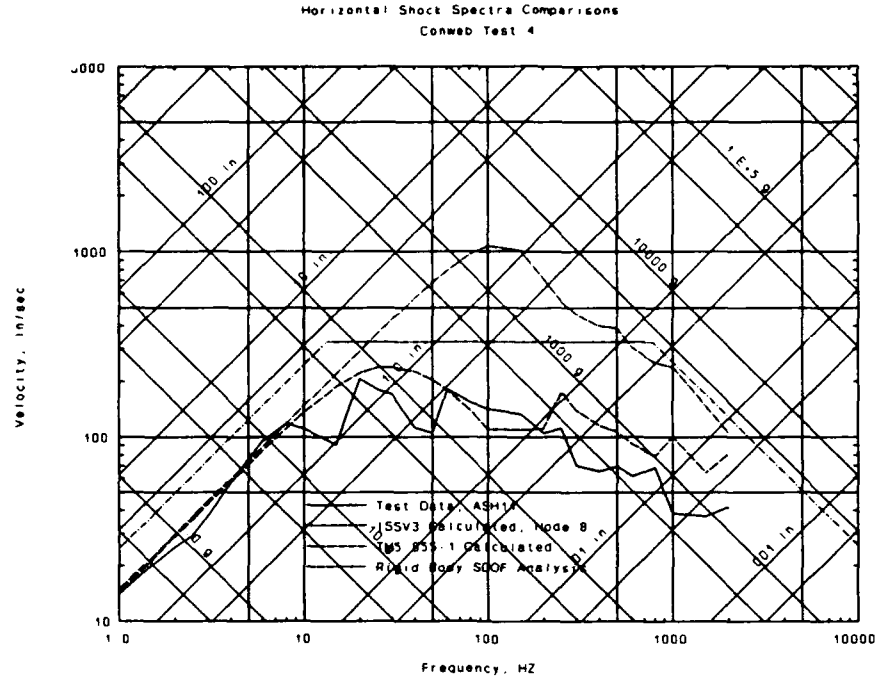

Figure 151. CONWEB 4, floor horizontal shock spectra, ISSV3 Node 8, comparison of analysis techniques.

SECTION 7
SUMMARY AND CONCLUSIONS

7.1 SUMMARY.

The semi-empirical calculational procedure in TM5 855-1 was shown to give reasonable estimates of the in-structure shock responses of the first three CONWEB tests. Inconsistences in the gage response in CONWEB 4 hampered comparisons for this test, but results appeared to be reasonable. The greatest weakness of this procedure is that it was developed for simple box-like structures. The assumptions that must be made to apply this procedure to more complicated structures have not been thoroughly evaluated. Great caution should be used in the application of such an empirically derived method to situations outside of those actually tested.

The results of the wall SDOF analyses were relatively inconsistent due to difficulty in developing reasonable loads to apply to the SDOF model. The loads used here were developed using the procedures in TM5 855-1 [2]. It is felt that these procedures do not adequately model structure-media interaction (SMI). There is current research at WES to address these deficiencies in SMI modeling.

The rigid-body SDOF analysis gave reasonable predictions of peak deflections and accelerations for CONWEB 1, 2, and 3. Peak velocities were overpredicted for these same tests. The same seemed to be true of CONWEB 4 when comparisons were made to horizontal acceleration gage ASH11. However, CONWEB 4 predictions in comparison with gage ASH10 were low for deflection and acceleration and reasonable for velocity. Underprediction of CONWEB 4 in comparison with gage ASH10 occurred in all of the analysis procedures used, perhaps lending credence to the possibility of testing or gage problems. It was hypothesized that the consistent overprediction of peak spectral velocity in the rigid-body SDOF analysis was due to problems in modeling structure media interaction. Overloading the structure with impulse leads to over-prediction of velocity. This should also lead to an overprediction of deflection. The fact that deflection predictions are reasonable, indicates a compensating overrestraint of the model. The Poisson's Ratios assumed for this analysis were on the high end of suggested values and this could easily account for this overrestraint. Taken together, all this illustrates the

difficulty of analyzing the complex response of a buried structure using a simple SDOF model. It should be noted, however, that the velocity predictions were conservative.

The evaluation of STABLE as an in-structure shock analysis technique led to the rejection of this program from further consideration. This rejection was not based on the problem of high frequency noise in the acceleration records that plagued this analysis. Favorable comparisons of the calculations results to CONWEB 2 test data indicate that the program is capable of handling this type of application. Modification of the program to eliminate the problem of high frequency noise in the acceleration records is quite possible and could perhaps be as simple as the inclusion of additional damping terms. The basis for the rejection of the application of STABLE to in-structure analysis is excessive run times on the target computer. The fine grid analysis required approximately 16 hours to complete on a 20 MHz, 386 personal computer. Excessive run times for STABLE are directly related to its formulation as an implicit finite-element analysis program. Modifications are possible that could increase the computational efficiency of STABLE, but it is felt that such modifications could not overcome such a fundamental limitation.

The initial evaluation of ISSV3 as an in-structure shock analysis technique was favorable. Calculation of all four CONWEB tests with very different backfill materials gave very reasonable results. The acceleration records generated had forms and magnitudes quite similar to test data. Comparisons of velocity and deflection records were somewhat hampered due to the difficulty of measuring low-level, late-time accelerations in dynamic tests. However, available data compared favorably with the ISSV3-generated velocity and deflection histories. Shock spectra generated from the ISSV3 velocity histories also compared very well with spectra derived from test data.

It is acknowledged that the current free-field model in ISSV3 needs to be improved. Late-time velocities are sometimes underpredicted due to flow effects in clay backfill. Also, other research by Hayes [1] and [10] has indicated that the characterization of backfill by seismic velocity, density, and attenuation coefficient may be overly simplistic. In spite of these problems in the free-field models, the interface loads generated by ISSV3 for the CONWEB tests were reasonable.

The single greatest strength of the ISSV3 program brought to light in the analysis of the CONWEB test series is the speed of the calculation. All of the calculations required less than four minutes to run on a 386, 20-MHz personal computer. This compares very favorably to the four to sixteen hour run times for this application of the STABLE program.

With the success of the initial evaluation of the ISSV3 program as an in-structure shock analysis tool, a comparison was made of the program's results with the other available tools. A direct comparison was made of the shock spectra generated from the CONWEB test series data and all of the means of analysis investigated. The average front wall response was compared to the TM5 855-1 method, the SDOF wall analysis, the STABLE results (for CONWEB 2), and the ISSV3 results. The shock response on the floor of each structure was compared to the TM5 855-1 method, the rigid-body motion SDOF analysis, the STABLE results (for CONWEB 2), and the ISSV3 results. In every case, the results of the ISSV3 analysis were at least as accurate as the other techniques. With planned improvements in the free-field model, these comparisons are expected to be even better for later versions of the program.

It is important to note that the simplified in-structure shock methods investigated here are limited in a way that ISSV3 is not. The TM5 855-1 method and the SDOF analyses are best limited to simple, small structures. There is no fundamental reason why ISSV3 can not be applied to the fast and accurate in-structure shock analysis of larger, complicated, multifloor, multibay structures.

7.2 CONCLUSIONS.

ISSV3 has been shown to be the best in-structure shock analysis tool examined. Extensive comparisons of the results of the in-structure shock analysis of the CONWEB test series, using several available methods, show that ISSV3 is fast, accurate, and easy to use. The speed with which ISSV3 can analyze a given problem will allow the user the flexibility to quickly complete numerous in-structure shock calculations. This should encourage a designer to include in-structure shock considerations in the early design phase of a protective facility.

Future work is planned to improve the current free-field model in ISSV3. Improvements in the SMI model are also being considered pending the

results of current research at WES. Further analysis effort is required to validate the ISSV3 program for use on multifloor, multibay buried structures as well as aboveground structures.

SECTION 8

LIST OF REFERENCES

1. Hayes, P. G. 1989. "Backfill Effects on Response of Buried Reinforced Concrete Slabs;" Technical Report SL-89-18, U.S. Army Engineer Waterways Experiment Station, Vicksburg, Mississippi.

2. Headquarters, Department of the Army. 1986. "Fundamentals of Protective Design for Conventional Weapons," Technical Manual 5-855-1, Washington D.C.

3. Jones, P. S., Hetherington, J. G., and Coltharp, D. R. 1988. "Response of Masonry Structures to Blast Loads;" Proceedings from Corps of Engineers Structural Engineering Conference, St. Louis, Missouri.

4. Campbell, S. D., and Bryant, L. M. 1989. "STABLE Computer Program, Version 2.0, User's Manual;" Report No. J650-89-008/1506, JAYCOR, Vicksburg, Mississippi.

5. Walker, R. E., Drake, J. L., Boyt, W. L., and Slawson, T. R. 1990. "Development of an Improved In-Structure Shock Model;" Applied Research Associates, Inc., Southern Division, Vicksburg, Mississippi.

6. Clough, R. W., and Penzien, J. 1974. Dynamics of Structures, McGraw-Hill, Inc.

7. Biggs, J. M. 1964. Introduction to Structural Dynamics, McGraw-Hill, Inc.

8. Newmark, N. M., and Rosenblueth, E. 1971. Fundamentals of Earthquake Engineering, Prentice-Hall, Inc.

9. Baker, W. E. 1973. Explosions in Air, Wilfred E. Baker.

10. Hayes, P. G. 1990. "Experimental Verification of Theoretical Response Calculations for Buried RC Slabs;" A Thesis, Submitted to the Faculty of Mississippi State University, in Partial Fulfillment of the Requirements for the Degree of Master of Science in Engineering Mechanics Department of Aerospace Engineering, Mississippi State, Mississippi.

11. Whitman, R. V., and Richart, F. E. 1967. "Design Procedures for Dynamically Loaded Foundations;" Journal of the Soil Mechanics and Foundations Division, Vol 93, No. SM6, American Society of Civil Engineers, pp 169-191.

12. Bowles, J. E. 1977. Foundation Analysis and Design, McGraw-Hill, Inc.

13. Bryant, L. M., and Campbell, S. D. 1989. "STABLE Computer Program, Version 2.0, Final Formulation Report;" Report No. J650-89-010/1506, JAYCOR, Vicksburg, Mississippi.

14. Campbell, S. D., Smith, J. L., and Flathau, W. J. 1989. "Validation of STABLE Computer to Predict In-Structure Shock;" Report No. J650-89-010/1519, JAYCOR, Vicksburg, Mississippi.

15. Bathe, K., and Wilson, W. L. 1976. Numerical Methods in Finite Element Analysis, Prentice-Hall, Inc.

16. Headquarters, Department of the Army. 1969. "Structures to Resist the Effects of Accidental Explosions," Technical Manual 5-1300, Washington D.C.

DISTRIBUTION LIST

DNA-TR-91-89

DEPARTMENT OF DEFENSE

ASSISTANT TO THE SECRETARY OF DEFENSE
ATTN: EXECUTIVE ASSISTANT

DEFENSE INTELLIGENCE AGENCY
ATTN: DB-6
ATTN: DB-6E2 D SUNSHINE
ATTN: DT-2A G WEBER

DEFENSE NUCLEAR AGENCY
ATTN: SPSD
ATTN: SPWE C GALLOWAY
ATTN: TDTR
2 CYS ATTN: TITL

DEFENSE TECHNICAL INFORMATION CENTER
2 CYS ATTN: DTIC/FDAB

FIELD COMMAND DEFENSE NUCLEAR AGENCY
ATTN: FCNM
2 CYS ATTN: FCTT W SUMMA

STRATEGIC AND THEATER NUCLEAR FORCES
ATTN: DR E SEVIN

THE JOINT STAFF
ATTN: JAD/SFD
ATTN: J8 NUCLEAR FORCE ANALYSIS DIV

DEPARTMENT OF THE ARMY

DEP CH OF STAFF FOR OPS & PLANS
ATTN: DAMO-NCZ

HARRY DIAMOND LABORATORIES
ATTN: SLCHD-NW-P-CORRIGAN

U S ARMY ATMOSPHERIC SCIENCES LAB
ATTN: SLCAS-AR-M R SUTHERLAND

U S ARMY BALLISTIC RESEARCH LAB
ATTN: SLCBR-SS-T
ATTN: SLCBR-TB-B G BULMASH)

U S ARMY ENGR WATERWAYS EXPER STATION
ATTN: C WELCH CEWES-SE-R
ATTN: D RICKMAN CEWES-SE-R
ATTN: E JACKSON CEWES-SD-R
ATTN: F DALLRIVA CEWES-SS-R
ATTN: J BALSARA CEWES-SS-R
2 CYS ATTN: R C DOVE

U S ARMY NUCLEAR & CHEMICAL AGENCY
ATTN: MONA-NU

U S ARMY NUCLEAR EFFECTS LABORATORY
ATTN: ATAA-TDC R BENSON

DEPARTMENT OF THE NAVY

NAVAL RESEARCH LABORATORY
ATTN: CODE 2627
ATTN: CODE 4770 G COOPERSTEIN
ATTN: CODE 7920 A WILLIAMS

NAVAL SURFACE WARFARE CENTER
ATTN: K42 L VALGE

NAVAL WEAPONS EVALUATION FACILITY
ATTN: CLASSIFIED LIBRARY

OFFICE OF CHIEF OF NAVAL OPERATIONS
ATTN: OP 654

DEPARTMENT OF THE AIR FORCE

AERONAUTICAL SYSTEMS DIVISION
ATTN: ASD/ENSSS H GRIFFIS

AIR UNIVERSITY LIBRARY
ATTN: AUL-LSE

BALLISTICS MISSLE ORGANIZATION
ATTN: ASMS
ATTN: MYE

FOREIGN TECHNOLOGY DIVISION
ATTN: SDMDA S SPRING

HQ USAF/XOXFS
ATTN: AFXOOTS

PHILLIPS LABORATORY SPACE AND MISSILES
ATTN: HO R DUFFNER
ATTN: NTA A SHARP
ATTN: NTCA
ATTN: NTED J RENICK
ATTN: NTES

WRIGHT RESEARCH & DEVELOPMENT CENTER
ATTN: WRDC/MLBT W F ANSPACH

DEPARTMENT OF ENERGY

LAWRENCE LIVERMORE NATIONAL LAB
ATTN: L-262 PAUL GUDIKSEN
ATTN: L-439 J KELLER
ATTN: L-81 R PERRETT
ATTN: L-85 P CHRZANOWSKI

LOS ALAMOS NATIONAL LABORATORY
ATTN: A S MASON
ATTN: J NORMAN
ATTN: R W SELDEN
ATTN: R W WHITAKER
ATTN: B SHAFER

SANDIA NATIONAL LABORATORIES
ATTN: A CHABAI DIV 9311

U.S. DEPARTMENT OF ENERGY
OFFICE OF MILITARY APPLICATIONS
ATTN: OMA/DP-225

OTHER GOVERNMENT

CENTRAL INTELLIGENCE AGENCY
ATTN: OSWR/NED
ATTN: OSWR S WALLENHORST

DEPARTMENT OF DEFENSE CONTRACTORS

AEROSPACE CORP
ATTN: H BLAES
ATTN: L SELZER
ATTN: P RAUSCH

AEROTHERM CORP
ATTN: C NARDO

APPLIED RESEARCH ASSOCIATES, INC
ATTN: J KEEFER

APTEK, INC
ATTN: T MEAGHER

BOEING TECHNICAL & MANAGEMENT SVCS, INC
ATTN: D ECKBLAD

CALIFORNIA RESEARCH & TECHNOLOGY, INC
ATTN: J THOMSEN

CALSPAN CORP
ATTN: M DUNN
ATTN: M HOLDEN

CARPENTER RESEARCH CORP
ATTN: H J CARPENTER

G B LABORATORY, INC
ATTN: G BURGHART

GENERAL ATOMICS, INC
ATTN: CHARLES CHARMAN

GENERAL ELECTRIC CO
ATTN: B MAGUIRE

GENERAL RESEARCH CORP
ATTN: W ADLER

H & H CONSULTANTS, INC
ATTN: W HALL

HERCULES, INC
ATTN: P MCALLISTER

HORIZONS TECHNOLOGY, INC
ATTN: W T KREISS

INSTITUTE FOR DEFENSE ANALYSES
ATTN: CLASSIFIED LIBRARY
ATTN: E BAUER

JAYCOR
ATTN: W FLATHAU

KAMAN SCIENCES CORP
ATTN: R RUETENIK
ATTN: T STAGLIANO

KAMAN SCIENCES CORP
ATTN: F SHELTON
ATTN: LIBRARY B KINSLOW

KAMAN SCIENCES CORP
ATTN: D MOFFETT
ATTN: DASIAC

KAMAN SCIENCES CORPORATION
ATTN: DASIAC

LACHEL AND ASSOCIATES, INC
ATTN: J BECK

LOCKHEED MISSILES & SPACE CO, INC
ATTN: P J SCHNEIDER
ATTN: R K JAMISON
ATTN: T J KELIHER

LOGICON R & D ASSOCIATES
ATTN: R ROSS
ATTN: T A MAZZOLA

LOGICON R & D ASSOCIATES
ATTN: G GANONG

LOGICON R & D ASSOCIATES
ATTN: J WEBSTER

PACIFIC-SIERRA RESEARCH CORP
ATTN: R SMALL

RAND CORP
ATTN: LIBRARY

S-CUBED
ATTN: C NEEDHAM

SCIENCE APPLICATIONS INTL CORP
ATTN: J STODDARD

SCIENCE APPLICATIONS INTL CORP
ATTN: D BACON
ATTN: J COCKAYNE
ATTN: P VERSTEEGEN
ATTN: W LAYSON

SCIENCE APPLICATIONS INTL CORP
ATTN: A LAGINOLLI
ATTN: A MARKLLUCI
ATTN: J SONTOWSKI

SCIENCE APPLICATIONS INTL CORP
ATTN: J MANSHIP

SOUTHERN RESEARCH INSTITUTE
ATTN: C PEARS

SRI INTERNATIONAL
ATTN: DR B S HOLMES
ATTN: M SANAI

TECH REPS, INC
ATTN: F MCMULLAN

THE TITAN CORPORATION
ATTN: K KREYENHAGEN

TOYON RESEARCH CORP
ATTN: J CUNNINGHAM

TRW INC
ATTN: A ZIMMERMAN
ATTN: M SEIZEW

WEIDLINGER ASSOC, INC
ATTN: DARREN TENNANT
ATTN: H LEVINE

WEIDLINGER ASSOCIATES, INC
ATTN: M BARON